Norwegian University
of Life Sciences

Master's Thesis 2020 60 ECTS

Department of Chemistry, Biotechnology and Food Science (IKBM)

Searching for a redox partner for bacterial lytic polysaccharide monooxygenases

Camilla Jellestad Demmene

Masters in Biotechnology

Searching for a redox partner for bacterial lytic polysaccharide monooxygenases

Master thesis

Camilla Jellestad Demmene

Protein Engineering and Proteomics Group

Department of Chemistry, Biotechnology and Food Science

The Norwegian University of Life Sciences

2020

ACKNOWLEDGEMENTS

The present work was carried out at the Department of Chemistry, Biotechnology and Food Science at the Norwegian University of Life Sciences with Prof. Vincent Eijsink, Dr. Zarah Forsberg and Dr. Tina Rise Tuveng as supervisors.

First, I would like to thank Zarah Forsberg and Tina Rise Tuveng for their invaluable help throughout this work. They have taken the time to answer all my questions with patience and great understanding. Your comments and feedback have been immensely appreciated. I am convinced that I had the most able-minded, skillful, kind and supportive supervisors I could have wished for.

I would also like to express my gratitude to Vincent Eijsink, first of all for allowing me the opportunity to write for the Protein Engineering and Proteomics (PEP) group. Secondly, for all the time he has used to give me intelligent, insightful and inspiring comments and feedback. I am very grateful.

Thanks to the entire PEP group for welcoming me with open arms and for lending a helping hand whenever I needed it.

I would like to thank my family for always supporting me and believing in me. I would especially like to thank my sister, for being the one member of my family that understand what I'm actually doing, for being my "outsider biotechnologist brain" and bouncing ideas with me, and for sometimes acting as the grammar-police.

Lastly, I would like to thank Siri, Nina and the rest of the "Garrulous Grouses". Thank you for being there for me no matter what. A smarter, funnier, kinder, more quick-witted, passionate and compassionate group of friends could not exist, and I love you all.

Ås, June 1st, 2020

Camilla Jellestad Demmene

ABSTRACT

Biomass is considered a vast resource for supplying sustainable and renewable energy. Lignocellulose is the most abundant source of biomass found on earth and utilization of this energy source is studied around the world. Enzymatic degradation is a promising approach to produce fuels, chemicals and materials from lignocellulosic biomass. A wide array of biomass-degrading enzymes can be found in nature, e.g. in white- and brown rot fungi, or in bacteria such as *Cellvibrio japonicus*. The discovery of lytic polysaccharide monooxygenases (LPMOs) has been of tremendous importance in understanding and utilizing biomass degradation processes. LPMOs are oxidative mono-copper enzymes that degrade glycosidic bonds in recalcitrant polysaccharides such as cellulose and chitin. The LPMOs require an initial reduction of the copper active site and a dioxygen co-substrate (e.g. O_2 or H_2O_2) before catalysis can occur. In vitro studies commonly use reducing agents such as ascorbic acid to facilitate this reduction. In fungi, several redox enzymes that can directly interact with and reduce the LPMO active site have been described. In addition, several of those redox partner enzymes can also produce and supply the LPMO with H_2O_2. However, for bacterial LPMOs no similar redox partners have been identified so far, although a few potential candidates have been suggested.

This study examines the potential redox ability of two such candidates, hereinafter called LPMO activating protein A and B (LapA and LapB), from the marine bacterium *Saccharophagus degradans*. These proteins were tested for their potential ability to drive the LPMO from the same organism, called *Sd*LPMO10A. In addition, this novel tri-modular LPMO was subjected to functional characterization where it was shown to be a C1-oxidizing, cellulose-active enzyme with optimal activity at 60 °C. The apparent melting temperature of the copper-loaded enzyme was measured to 57 °C and 47 °C when the copper was removed from the active site. The C-terminal carbohydrate-binding domain was shown to bind cellulose, but the internal domain is still of unknown function and calls for further characterization.

LapA and LapB are also multi-modular enzymes which have similar sequence- and domain organization as two proteins that has been shown to be co-expressed with LPMOs and are important for optimal growth on cellulose in the bacterium *Cellvibrio japonicus*. Like *Sd*LPMO10A, LapA bound to cellulose, but LapB did not show any binding which may be a result of incorrect folding during a denaturation/refolding process. Initial activity tests of LapA and LapB to drive *Sd*LPMO10A did not result in desired oxidative LPMO activity during the tested conditions.

There are many factors which have yet to be explored, the main being to investigate the occurrence of a potent redox cofactor present in LapA and LapB. For the time being, LapA and LapB remain potential candidates for bacterial redox partners of LPMOs.

SAMMENDRAG

Biomasse blir ansett som en viktig kilde til bærekraftig og fornybar energi. Lignocellulose er den største kilden til biomasse som finnes på planeten, og bruk av denne energikilden blir studert verden rundt. Enzymatisk nedbryting er en lovende tilnærming for å produsere drivstoff, kjemikalier og andre materialer fra lignocellulose. I naturen finnes mange enzymer som deltar i nedbryting av biomasse. Oppdagelsen av lytisk polysakkarid monooksygenaser (LPMOer) har vært svært viktig for forståelsen og nyttegjøringen av enzymatisk nedbryting på biomasse. LPMOer er enzymer som bryter glykosidbånd i polysakkarider som er utfordrende å bryte ned, slik som cellulose og kitin. For å aktivere LPMOer kreves en reduksjon av kobber i det aktive setet, samt dioksygen som ko-substrat (f.eks. O_2 or H_2O_2). *In-vitro* studier bruker vanligvis reduktanter som askorbinsyre for å oppnå denne aktiverende reduksjonen. I sopp finnes det flere redoks-enzymer som kan interagere direkte med det aktive setet i LPMOer. I tillegg kan flere av disse redokspartner-enzymene også produsere H_2O_2 som LPMOer kan nyttiggjøre seg av. I bakterier finnes det fortsatt ingen kjente redokspartnere som kan redusere det aktive setet og produsere H_2O_2 for LPMOer, selv om det finnes flere enzymer som potensielt kan utføre disse oppgavene.

Denne studien utforsker potensialet for to av disse enzymene fra den marine bakterien *Saccharophagus degradans*, videre kalt LapA og LapB, til å utføre reduksjonen av det aktive setet. Disse proteinene ble testet for deres evne til å fungere som redokspartnere ved å bruke LPMOen fra den samme type bakterie, kalt *Sd*LPMO10A. Karakterisering av *Sd*LPMO10A viste at det er et C1-oksiderende, cellulose-aktivt enzym med optimumstemperatur på 60 °C, Antatt smeltepunktet ble bestemt til 57 °C med kobber i det aktive setet, mens antatt smeltepunkt uten kobber i det aktive setet ble bestemt til 47 °C. Domenet i C-terminal ende av enzymet, antatt å være karbohydrat-bindene, viste binding til cellulose, mens det indre domenet er fortsatt ukjent, og bør karakteriseres videre.

LapA og LapB er også multi-modulære enzymer som har liknende sekvens- og domenekarakteristika som proteiner som blir uttrykt sammen med LPMOene i *Cellvibrio japonicus*, og som er viktige for denne organismens vekst på cellulose. Som for *Sd*LPMO10A viste også LapA binding til cellulose, mens LapB ikke viste binding, hvilket kan være et resultat av ukorrekt folding under forsøket på å denaturere og refolde proteinet. De første aktivitetstestene for LapA og LapBs redoks-aktivitet på *Sd*LPMO10A viste ikke de ønskede resultatene for oksidasjons-aktivitet fra *Sd*LPMO10A.

Det er allikevel foreløpig mange faktorer å ta i betraktning som enda ikke er utforsket, hovedsakelig å undersøke om LapA og LapB inneholder en kraftig nok kofaktor til å redusere LPMOer. Det kan fortsatt konkluderes med at LapA og LapB enda ikke kan utelukkes som potensielle bakterielle redoks-partnere for LPMOer.

ABBREVIATIONS

BSA	- Bovine serum albumin
dCTP	- Deoxycytidine triphosphate
DEAE	- Diethylaminoethyl
DHB	- 2,5-Dihydroxybenzoic acid
DTT	- Dithiothreitol
DP	- Degree of polymerization
ETDA	- Ethylenediamine tetraacetic acid
HPAEC	- High-performance anion-exchange chromatography
ICS	- Ion chromatography system
IPTG	- Isopropyl ß-D-1-thiogalactopyranoside
IEX	- Ion exchange chromatography
LIC	- Ligation independent cloning
LPMO	- Lytic polysaccharide monooxygenase
MALDI-ToF MS	- Matrix-assisted laser desorption ionization- time of flight mass spectrometry
NEBuffer	- New England Biolabs buffer
PCR	- Polymerase chain reaction
PPE	- Periplasmic extract
PQQ	- Pyrroloquinoline quinone
SEC	- Size exclusion chromatography
SOC	- Super Optimal broth with Catabolite repression
TMHMM	- Transmembrane hidden Markov model

TABLE OF CONTENT

1. INTRODUCTION

Unsustainable use of resources, dangerous pollution and high levels of emissions have caught the world's attention. Global climate changes are threatening our way of life. A drastic reform is needed if we wish to maintain any semblance of our current lifestyles going into the future. The increasing awareness of these issues is causing discussions of a "green shift" and increasing amounts of time and money is invested into finding sustainable ways to obtain materials, food, energy and fuel. Many companies and researchers around the world devote time, effort and funds to uncovering resources that are accessible in an economic and ecologically sustainable way. A resource showing great potential is biomass.

Biomass is a renewable natural resource with the potential to, in some areas, replace the usage of fossil resources (Cherubini, 2010). The many different types of biomass offer a multitude of characteristics, which can be important in production of a variety of products. Use of fossil resources for fuel releases large quantities of carbon dioxide, a greenhouse gas that is one of the key drivers of the global climate change. When using biomass for production of biofuels, the net release of carbon dioxide is considered lower than for fossil fuels. This is due to biomass production demanding CO_2 input. Emitted CO_2 levels from biofuel production and -consumption are estimated to potentially approach that of biomass production input (Cheng, 2017; Lynd et al., 1991). In this case, all emissions can be considered part of the carbon cycle, which means that biomass can be a carbon-neutral alternative.

Moreover, plastics produced from fossil resources are a large burden to many ecosystems, not only due to greenhouse gas emissions during production, but also, according to the UN, by causing the death of over 1 million sea birds and 100 000 mammals and sea turtles each year (Leahy, 2004; UNESCO, 2017). By using biomass to produce bio-based plastics, the negative effects of the fossil-based plastics can be reduced, mainly by reducing CO_2 emissions, thus creating a more circular economy (Brodin et al., 2017). Moreover, even though not all bio-based products are biodegradable, many of them are, and this can reduce the risk of death from obstruction or indigestion caused by plastic in for instance birds (Brodin et al., 2017; Pierce et al., 2004). In fact, bio-based biodegradable plastics already exist on the market and are used in various materials, from textiles, such as crop covers, to plastic containers, and even as part of fertilizers (Luyt & Malik, 2019).

In addition to significant environmental gain, the use of biomass as a starting material to produce the abovementioned products also reduces the involved risk regarding supply. Biomass

is found abundantly and can be reproduced. For example cellulose has a global production of about 1.5 x10^{12} tons per year (Rojas, 2016). Fossil resources are formed over millions of years, which means that the supply is limited to current availability, and with modern consumption rates, these sources will be depleted not too far into the future (Shafiee & Topal, 2009). Biomass can also be used to produce a multitude of pharmacological products, such as in certain bandages, and for drug delivery (Rojas, 2016; Shi et al., 2014; Shokri & Adibkia, 2013). It is also used in food packaging and cosmetics. In addition, biomass can be used directly as food, and other types of non-digestible biomass can be used as preservatives and thickeners for other food products (Barikani et al., 2014). All these utilization areas strongly indicate the extensive and important impacts that the use of biomass-based products can have for society.

Cellulose and chitin are the two most abundant forms of biomass on the planet (Barikani et al., 2014; Rojas, 2016). Chitin is an insoluble polysaccharide consisting of *N*-acetyl-D-glucosamine residues linked with β-1,4-glycosidic bonds (**Figure 1A**). Chitin is abundant in Nature, where it is found in e.g. insect exoskeletons and crustacean shells, with only cellulose being a more abundant natural, renewable resource (Barikani et al., 2014).

Cellulose is found and produced in plants and can constitute as much as over 90 % of the weight in some species, like cotton (Rojas, 2016). Cellulose is a polysaccharide where the monomeric unit is D-glucopyranose. The units are β-1,4-linked and rotated 180 degrees relative to each other, making the dimer, cellobiose, the repeating unit (**Figure 1A**). Cellulose chains, varying from 1000 to 30 000 monomers, aggregate into microfibrils that are stabilized trough inter- and intramolecular hydrogen bonds and van der Waal forces (**Figure 1B**). These bonds make the inner core of microfibrils highly organized (i.e. crystalline), while the fibril surface shows less structural order (i.e. sub-crystalline to amorphous). Altogether, the feature of the fibril makes cellulose highly resistant to chemical and enzymatic hydrolysis. Besides in plants, cellulose can also be found in bacteria, algae, fungi and animals. Whereas bacterial cellulose is typically crystalline and relatively pure, plant cellulose is more complex as it is mixed with lignin and hemicelluloses in the plant cell wall (Rojas, 2016).

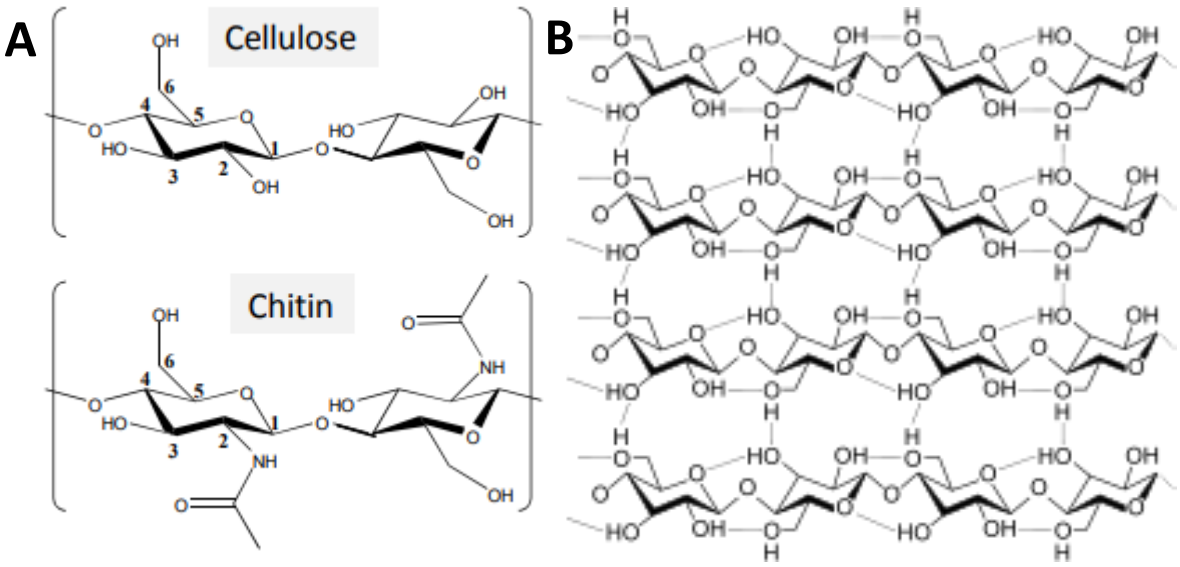

Figure 1: A) Repeating units of cellulose and chitin shown in brackets, with carbons for the first monomer marked 1 to 6 (C1-C6) according to IUPAC nomenclature and Fischer projection of carbohydrates (when non-cyclic). The figure was adapted from (Cardoso et al., 2017). B) Cellulose structure; intra- and intermolecular hydrogen bonds stabilize a crystalline structure.

With cellulose and chitin being the foremost and second most abundant natural polymers on the planet, respectively, their commercial uses can have great impact on the bioeconomy. Modified derivatives of cellulose can be used as biosensor (amino-cellulose), pharmaceutical coating or bioadhesive (cellulose esters or ethers), in gels for drug-delivery or as food and cosmetic thickeners (carboxymethyl cellulose), along with many other potential applications (Rojas, 2016; Shi et al., 2014; Shokri & Adibkia, 2013). Chitin is also used in food, e.g. for packaging and as a preservative, in cosmetics and drug delivery, as well as in purification membranes for water, as photopaper, and more (Barikani et al., 2014).

Next to applications of these polysaccharides in their polymeric forms, there is great interest in converting them to their monosugars ("saccharification"), in particular for cellulose. The resulting sugars (glucose in the case of cellulose) can be used in fermentation processes to produce fuels, such as ethanol, or other useful products.

1.1. DEGRADATION OF LIGNOCELLULOSIC BIOMASS

The dry matter of plants is called lignocellulosic biomass, and it is the most abundant biomass on earth, with 10-50 billion tons being produced annually (Abdel-Hamid et al., 2013; Zhao et al., 2012). Lignocellulosic biomass has a very recalcitrant structure due to the complexity of plant cell walls (Zhao et al., 2012). Plant cell walls and their complex structure are very important to the plant. They help participate in signaling between cells, protection against

pathogens, shaping of cells and keeping plants rigid (Bacic et al., 1988; Carpita & Gibeaut, 1993; Sørensen et al., 2010). The cell walls are carbohydrate-rich structures with complex mixes of different fibers (Bacic et al., 1988; Sørensen et al., 2010). The primary cell wall consists mostly of proteins and polysaccharides, with cellulose, hemicellulose and pectin being the major polysaccharide groups (Loix et al., 2017). Cellulose often occurs as crystalline microfibrils that are connected by hemicelluloses such as xylan or β-glucans, as well as by varying types of pectin (**Figure 2**) (Bacic et al., 1988; Loix et al., 2017; Rojas, 2016). The secondary cell wall is similar to the primary wall, but additionally contains lignin between the carbohydrates, causing it to have even higher complexity and rigidity (Loix et al., 2017). Due to this complex structure, there is a need for advanced methods to be able to efficiently and inexpensively utilize lignocellulosic biomass. In this respect, enzymatic treatment technologies for polysaccharide degradation are particularly important.

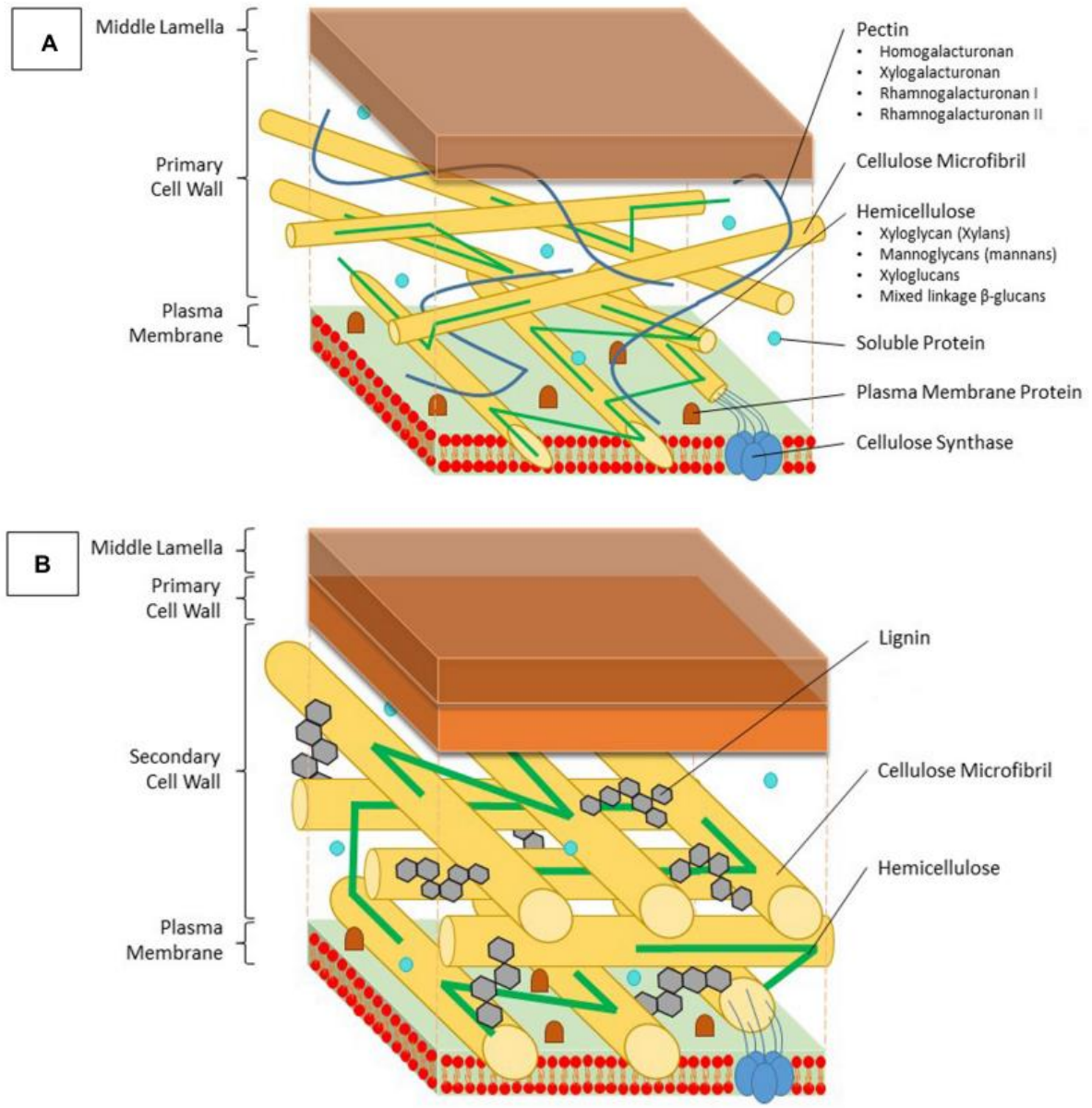

Figure 2: Model of lignocellulosic composition of the A) primary and B) secondary cell walls of plant cells. Cellulose microfibrils (yellow cylinders) and hemicellulose (green lines) can be found in both layers. Pectin (blue lines) is mainly found in the primary wall, while lignin (grey hexagons) is a component mostly incorporated in the secondary cell wall. The figure was taken from (Loix et al., 2017).

For utilizing lignocellulosic biomass, breakdown of the recalcitrant cell wall structure is essential. In industry, lignin and hemicellulose are usually removed first, using pretreatment methods such as steam pretreatment, and mechanical or chemical pulping (Chandra et al., 2016; Öhgren et al., 2005). After this, enzymatic degradation is often utilized for degradation of the cellulose to reach the final product of glucose.

In Nature, a multitude of organisms produce enzymes which can participate in degradation of lignocellulose. Fungi are the major lignocellulose degraders (Sánchez, 2009). For example,

brown-rot fungi can modify lignin so that they can depolymerize cellulose, while white-rot fungi can also degrade lignin (Sánchez, 2009). There are also many bacterial species which can degrade lignocellulose, e.g. some species in the *Clostridium* genus and the *Cellvibrio* genus, and the soil bacteria *Sporocytophaga myxococcoides* and *Thermobifida fusca* (Berg et al., 1972a; Berg et al., 1972b; de Souza, 2013; Tuveng et al., 2016; Wilson, 2004). Some families of anaerobic fungi and bacteria can degrade cellulose by using membrane-associated extracellular enzyme complexes containing hydrolytic enzymes. These enzyme complexes are called cellulosomes and may contain a variety of cellulases and hemicellulases (Malherbe & Cloete, 2002; Schwarz, 2001). These enzymes may contain non-catalytic carbohydrate binding modules (CBMs) that increase enzyme efficiency by promoting binding to the substrate (Black et al., 1996; Ferreira et al., 1993).

The most common method of enzymatic degradation performed by bacterial and fungal species are free enzyme systems, which means that multiple enzymes are released into the extracellular environment for degradation of biomass surrounding the organisms (Lopes et al., 2018). In free enzyme systems, many enzymes work synergistically for maximal degradation of the biomass, which means that these systems can have great potential for industrial biomass conversion processes (Lopes et al., 2018; Van Dyk & Pletschke, 2012). Synergistic cooperation between enzymes means that, when working in tandem they give product yields that are higher than the sum of the yields obtained when using the individual enzymes (Van Dyk & Pletschke, 2012). For instance, during cellulose degradation, multiple cellulases work synergistically to yield monomeric glucose (Rojas, 2016; Sánchez, 2009; Van Dyk & Pletschke, 2012).

Glycoside hydrolases comprise the largest class of enzymes in the carbohydrate-active enzyme (CAZy; http://www.cazy.org/) database with more than 130 families (Mewis et al., 2016), which are grouped together based sequence similarities and that all have the ability to hydrolyze glycosidic bonds (Garvey et al., 2013). Cellulases, i.e. enzymes with the ability to degrade cellulose occur in several of these sequenced-based families. Cellulases can be divided into three major groups: cellobiohydrolases, endoglucanases and β-glucosidases. These enzymes catalyze many different reactions. For example, cellobiohydrolases can work from either the reducing or the non-reducing end of the cellulose chain, cleaving off monomers or dimers (Sánchez, 2009; Van Dyk & Pletschke, 2012), while endoglucanases can cleave cellulose further in on the strands, leaving products with chain-lengths of three-six glucose units (Fierobe et al., 1993; Mansfield et al., 1999). β-glucosidase can act on cellobiose and other soluble cellodextrins produced by e.g. endoglucanases, degrading them into monomeric glucose units

(Bisaria & Ghose, 1981). However, many of these cellulase reactions often require lytic polysaccharide monooxygenases (LPMOs) to contribute to cellulose degradation.

The discovery of LPMOs has been very important for the efficiency of biomass degradation. Since most naturally occurring biomass contains a mix of polysaccharides, and many of these polysaccharides are complex or crystalline in structure, they are challenging to degrade. LPMOs are enzymes that cleave glycosidic bonds in the most recalcitrant polysaccharides (Vaaje-Kolstad et al., 2010). The majority of LPMOs are only active on insoluble substrates (Vaaje-Kolstad et al., 2017) and thus act on substrates that few other enzymes can attack. The products of LPMOs, on the other hand, are more accessible poly- and oligosaccharides of varying sizes (Westereng et al., 2016), which other biodegrading enzymes can access. For example, cellobiohydrolases can work from either the reducing or the non-reducing end of the cellulose chain, but not on the rest of the surface of crystalline cellulose (Sánchez, 2009; Van Dyk & Pletschke, 2012). For these enzymes, LPMO activity can generate additional starting points, making the substrate more accessible. LPMOs are also thought to make the substrate more amorphous, which means that endoglucanases can more easily access the cellulose strands (Forsberg et al., 2016). Therefore, LPMOs significantly increase polysaccharide degradation when used for industrial purposes, which gives them great economic and ecological value.

1.2. DISCOVERY AND CLASSIFICATION OF LPMOs

The first LPMO to be characterized was CBP21 (chitin binding protein, 21 kDa) from *Serratia marcescens*. Although CBP21 was shown to be essential for chitin degradation, it was first classified as a CBM (family 33) in the CAZy database (Vaaje-Kolstad et al., 2005) and assumed not to have a catalytic function. Five years later, in 2010, it was shown that CBP21 was in fact an enzyme with a novel oxidative mechanism (Vaaje-Kolstad et al., 2010). Other enzymes with similar activity on cellulosic biomass were first placed in a family called GH61 (glycoside hydrolase 61), due to detection of low endoglucanase activity in an early study (Saloheimo et al., 1997). However, it has later been shown that GH61s are, like CBP21, oxidative enzymes, which are active on cellulosic substrates (Quinlan et al., 2011). Therefore, both these groups of enzymes were designated a new enzyme class in the CAZy database, named “Auxiliary Activities” (AA). This class now contains multiple LPMO families, as well as some families of other cell wall degrading enzyme (Levasseur et al., 2013).

The AA class consists of different enzyme families that are all considered important for cell wall degradation and that catalyze redox chemistry (Levasseur et al., 2013). The enzymes in the AA class are therefore considered one class, not based on a specific reaction mechanism or substrate, but based on their common ability to degrade recalcitrant cell wall components (Levasseur et al., 2013). Currently, there are seven LPMO-containing AA families; AA9 and AA10 (Levasseur et al., 2013), AA11 (Hemsworth et al., 2014), AA13 (Lo Leggio et al., 2015), AA14 (Couturier et al., 2018), AA15 (Sabbadin et al., 2018), and AA16 (Filiatrault-Chastel et al., 2019). These families are spread across all domains of life. While AA9, AA11, AA13 and AA16 are strictly fungal, AA10s can be found in both bacteria, fungi, viruses and archaea, and AA15s have been found in eukaryotic organisms (e.g. insects and algae) and viruses (Zhou et al., 2019). The fact that LPMOs can be found in such a wide variety of life, is an indication of the importance of this class of enzymes.

LPMOs act on various substrates which, to some degree, is related to families and phylogeny. The most common substrates are crystalline cellulose and chitin. Most AA9s have activity on cellulose and family AA11 have activity on chitin, while families AA10 and AA15 contain enzymes in both categories (Levasseur et al., 2013; Sabbadin et al., 2018; Vaaje-Kolstad et al., 2010). Family AA16 also has cellulose activity (Filiatrault-Chastel et al., 2019). Some LPMOs have been observed to act on hemicelluloses like xylan, soluble polysaccharides like xyloglucan and glucomannan, and oligosaccharides (Frandsen et al., 2016; Isaksen et al., 2014; Tandrup et al., 2018). For instance, xylan-degrading LPMOs are found in families AA9 and AA14 (Couturier et al., 2018). In the AA13-family one can find activity on starch (Tandrup et al., 2018).

The most common LPMO substrates, cellulose and chitin, have crystalline structures, which very few enzymes can access without some form of de-crystallization event occurring. The flat surface surrounding the active site of LPMOs allows for direct interaction with the surfaces of these crystalline substrates (**Figure 3**), which is why LPMOs can attack very recalcitrant polysaccharides (Bissaro et al., 2018).

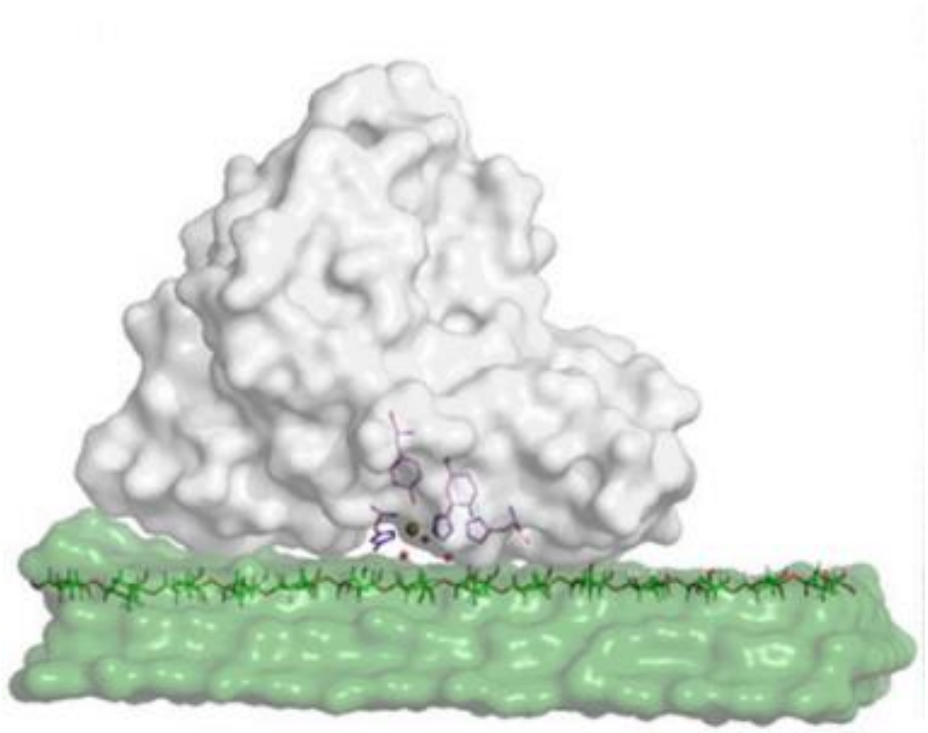

Figure 3: 3D illustration of the *Thermoascus aurantiacus* LPMO (grey) interacting with the surface of crystalline cellulose (green). The active site of the LPMO as well as one chain of cellulose are shown as stick-figures. The figure was adapted from (Kim et al., 2014).

1.3. STRUCTURE AND FUNCTION OF LPMOs

Despite the low sequence similarities among LPMOs from different AA families, the overall fold is conserved. The core is built up by two β-sandwiches made up of anti-parallel strands. Loops of varying lengths and a varying number of short helices connect the strands. These loops show pronounced variations that affect the substrate-recognizing surfaces of the proteins. In particular, the long "L2" region, is highly variable and presumably an important determinant of substrate specificity and regioselectivity (**Figure 4A**)(Vaaje-Kolstad et al., 2017; Wu et al., 2013).

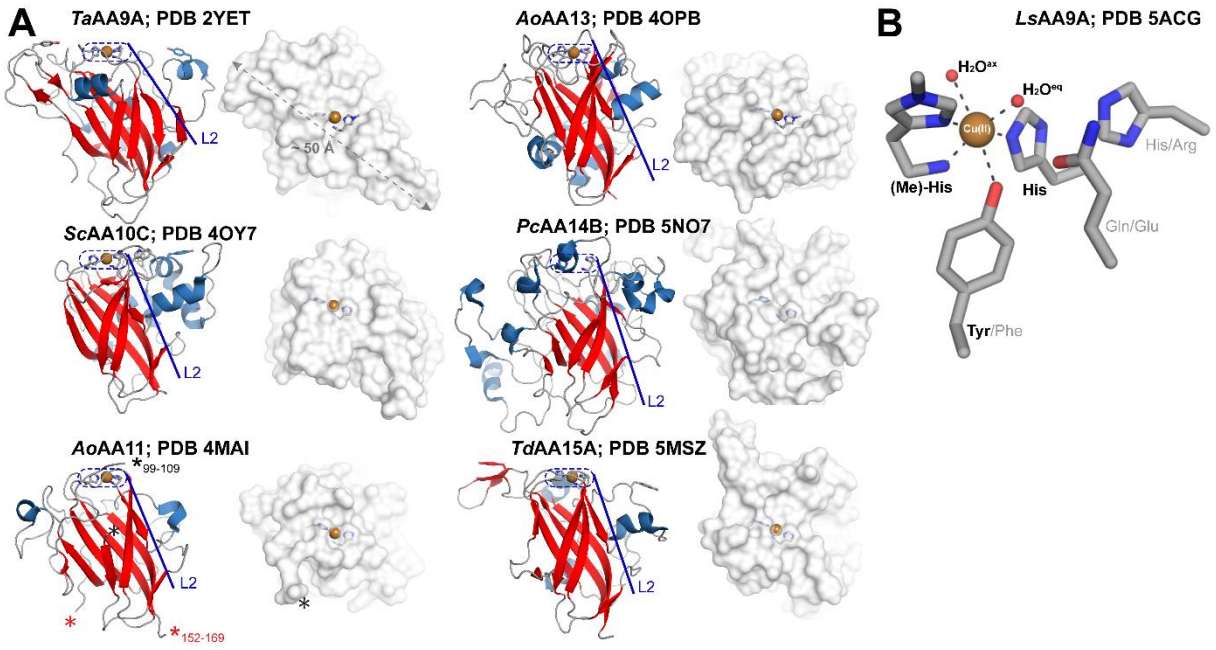

Figure 4: A) Domain structures and surface views for six LPMO families. The β-sandwhiches are shown in red. L2 regions are shown above/to the right side of the blue lines, and show varying structure for the different families. B) Coordination of copper molecule in the active site by two histidines (one is methylated), and one tyrosine. Light grey labels indicate amino acids that are part of the second coordination sphere of this LPMO. The figure was adapted from (Forsberg, 2020).

The active sites of LPMOs show strong similarities across evolutionary and phylogenetic origins. In general, one side of LPMOs has a flat surface area containing two centered histidines which are fully conserved in all LPMOs. The two histidines bind a single copper ion in what is called a histidine brace (**Figure 4B**). The copper ion is coordinated by three nitrogen ligands provided from the histidine residues, one of which is the N-terminal residue. The second coordination sphere, which comprises residues close to the copper site that do not directly interact with the copper, but that may help shape the active site and assist in coordinating the co-substrate, varies between the different LPMO families and within some of the LPMO families. The substrate-binding surface area varies in size and shape. AA9s generally have flat substrate-binding surfaces with solvent exposed aromatic residues such as tyrosine or tryptophan. These residues are believed to stack with the glucose units of cellulose (**Figure 5**) (Li et al., 2012; Wu et al., 2013). The AA10s have largely hydrophilic substrate-interacting surfaces with normally only one surface-exposed aromatic residue oriented in such a way that it can participate in stacking interactions (Vaaje-Kolstad et al., 2017).

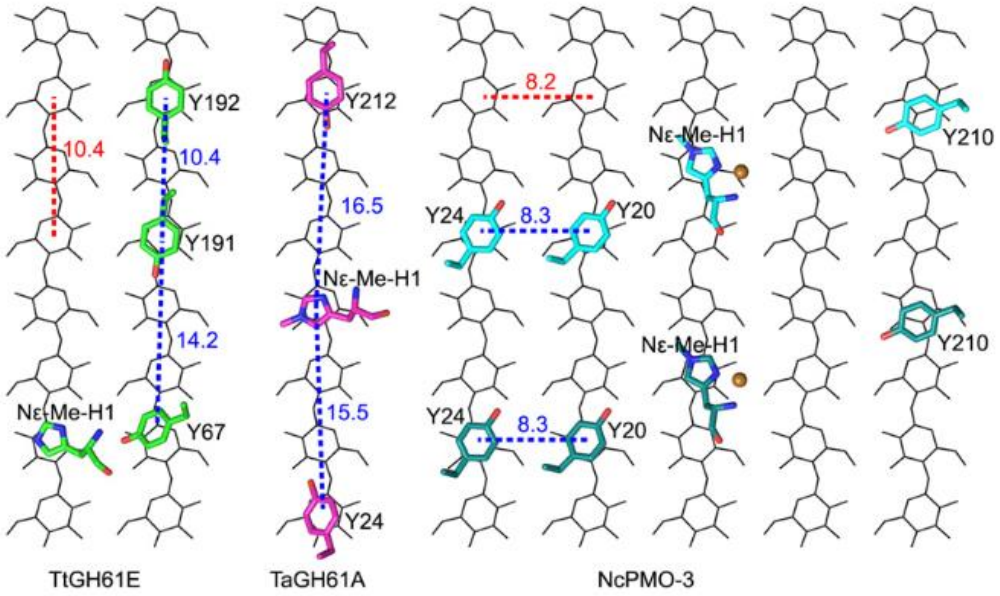

Figure 5: Stacking of aromatic residues on cellulose shown for three AA9 LPMOs, from *Thielavia terrestris* (*Tt*LPMO9E), *Thermoascus aurantiacus* (*Ta*LPMO9A) and *Neurospora crassa* (*Nc*LPMO9D). Two alternative binding scenarios are shown for *Nc*LPMO9D, which occur based on movement along the chains by an odd number of pyranose units. The side chains of aromatic residues and histidines are shown in color, while the black lines represent the cellulose chains. The stacking of the aromatic residues leads to positioning of the active site (here represented by the N-terminal histidines). The figure was adapted from (Li et al., 2012).

1.4. THE REACTION MECHANISM OF LPMOs

LPMOs catalyze cleavage of glycosidic bonds in crystalline structures. For cellulose active LPMOs, there are three types of regioselectivities, meaning some can only oxidize either the C1 or C4 carbon in cellulose, while other show less specificity and can oxidize both the C1 and C4 carbon (Bissaro et al., 2018).

The oxidizing event is initiated after reduction of the copper in the active site from Cu^{2+} (oxidized state) to Cu^{+} (reduced state). Following this reduction, the LPMO can perform oxidation of the substrate using a dioxygen co-substrate (i.e. O_2 or H_2O_2; see **Figure 6**):

O_2 as co-substrate (monooxygenase reaction): Until recently, the LPMO reaction has been thought to be completely dependent on O_2 (Kjaergaard et al., 2014; Vaaje-Kolstad et al., 2010; Walton & Davies, 2016). Subsequent to reduction of the copper in the active site (i.e. LPMO-Cu(II)→LPMO-Cu(I)) the LPMO activates molecular oxygen. The oxygen atom not bound to the LPMO is then split off as a water molecule by accepting two protons and one electron. The remaining oxygen abstracts a hydrogen from the substrate, after which the resulting hydroxyl

group reacts with the substrate radical in a "rebound" reaction. The resulting hydroxylation of the substrate leads to bond destabilization and cleavage, leaving the copper in the active site in an oxidized state. When using O_2 as substrate, stochiometric amounts of reductant are needed to re-reduce the LPMO in between catalytic events and to deliver electrons to each reaction cycle (Bissaro et al., 2018). Reduced LPMOs that are not bound to substrate have also been found to function as oxidases, meaning they can reduce O_2, leading to production of H_2O_2 (Kittl et al., 2012).

H_2O_2 as co-substrate (peroxygenase reaction): In 2017, Bissaro et al. assessed the possibility that H_2O_2 could act as a co-substrate of LPMOs (Bissaro et al., 2017). Such a peroxygenase reaction would only require a "priming" reduction of the LPMO, i.e. use of sub-stoichiometrically amounts of reductant, after which the enzyme could perform multiple catalytic cycles when supplied with H_2O_2. The reduced copper binds to H_2O_2 in the presence of substrate. A water molecule dissociates, leaving only oxygen bound to the copper. This oxygen then abstracts a hydrogen from the substrate, and the resulting hydroxyl group is transferred back to the substrate. The copper is left with +1 charge, which means that it is ready for another round of catalysis without another reduction. (Bissaro et al., 2017; Bissaro et al., 2018)

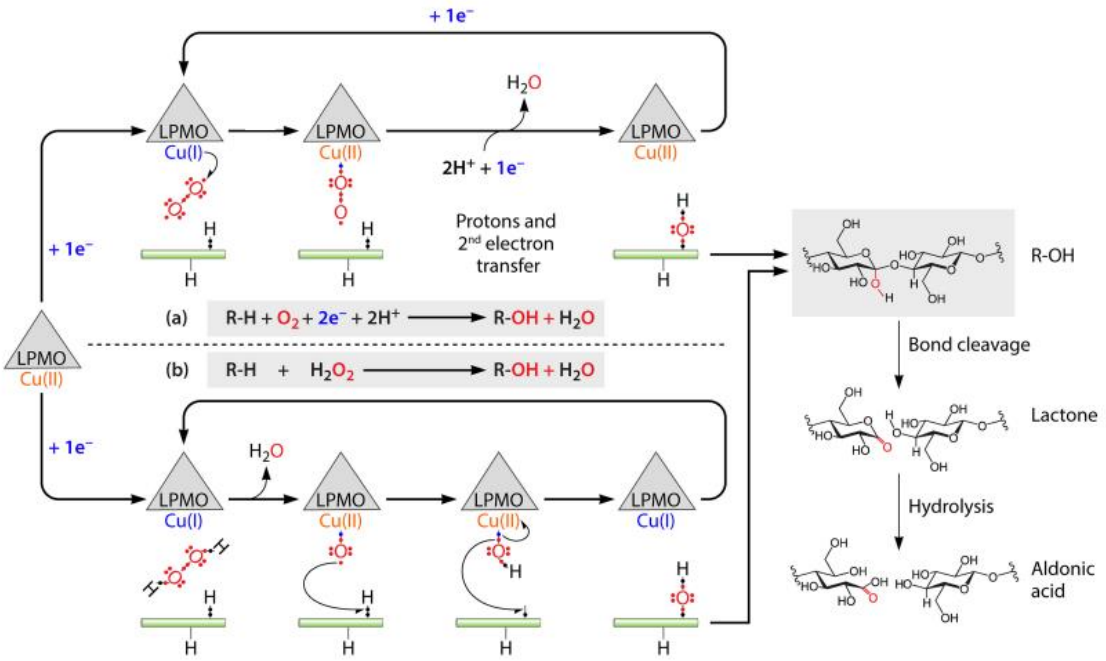

Figure 6: Possible reaction mechanism for an LPMO using molecular oxygen (a) or hydrogen peroxide (b) as co-substrate. Initial reduction, initiating both pathways, is shown to the far left, before the LPMO reacts with the co-substrate. For pathway (a), further supply of two protons and one electron is required. This is not needed in pathway

(b), since hydrogen peroxide already provides these factors. Independent of the mechanism, the LPMO reaction results in hydroxylation of a carbon in the glycosidic bond, which leads to bond destabilization and breakage. In this Figure C1-oxidation of a cellulose substrate is illustrated. The figure was adapted from (Bissaro et al., 2018).

Both pathways introduce a break in a crystalline cellulose strand, by hydroxylating either C1 or C4, which leads to bond cleavage (**Figure 6**, far right). The actual bond cleavage is thought to be a spontaneous elimination reaction (Beeson et al., 2012). This initially results in formation of a lactone (oxidation at the C1 carbon; **Figure 6**, lower right corner) or ketone (oxidation at the C4 carbon; **Figure 7**). These groups are spontaneously hydrated, where lactones result in aldonic acids, while the ketones result in gemdiols. (Bissaro et al., 2018; Eijsink et al., 2019)

Figure 7: Spontaneous hydrolysis of a ketone product of a C4-oxidizing LPMO reaction to a final gemdiol product. The figure was adapted from (Isaksen et al., 2014).

The efficiency of the monooxygenase and the peroxygenase activity differ significantly. When using H_2O_2 as a co-substrate, the reaction is two to three orders of magnitude faster than the monooxygenase reaction. The peroxygenase reaction also uses less reductant, since only "priming" reduction is needed for multiple rounds of catalysis, while the LPMO needs to be reduced after each cycle when using molecular oxygen as a co-substrate (Bissaro et al., 2018).

Damage to proteins due to reactions with oxidative species, called oxidative inactivation, is considered a serious issue when it comes to industrial application of enzymes, as it slows or halts reactions (Valderrama et al., 2002). Autocatalytic oxidative inactivation of LPMOs can occur for reactions with both hydrogen peroxide and molecular oxygen as co-substrate. However, it is believed that production of hydrogen peroxide or other reactive oxygen species, produced by reduced LPMOs that are not bound to the substrate, causes the inactivation in molecular oxygen-driven reactions. As shown by *Bissaro et. al.*, high amounts of hydrogen peroxide lead to inactivation of LPMOs that have been subjected to a priming reduction (Bissaro et al., 2017). The inactivation is due to oxidative modifications that occur in or near the active site. Modifications on the two copper-coordinating histidines is most prominent.

Bissaro et al. also showed that the inactivation is affected by the presence of the carbohydrate substrate. While LPMO reactions lacking substrate led to rapid enzyme inactivation, LPMOs in reactions with substrate showed a higher degree of enzyme stability (Bissaro et al., 2017).

1.5. KNOWN REDOX PARTNERS OF LPMOs

For the LPMOs to become active, there is a need for reduction of the copper ion in the active site. This reduction occurs when there is a reducing agent present in the reaction that can donate electrons. This electron donor is needed in all types of LPMO reactions (i.e. considering the monooxygenase and the peroxygenase reactions). There are many different types of molecules that can function as an electron donor. Small, organic molecules such as ascorbic acid and gallic acid can reduce the copper (Quinlan et al., 2011; Vaaje-Kolstad et al., 2010), and are often used as reductants in *in vitro* reactions. Lignin and lignin-derivatives comprise another group of molecules with electron donating abilities (Cannella et al., 2012; Dimarogona et al., 2012). Pigments used in photosynthesis may also drive LPMO reactions (Cannella et al., 2016), along with phenols found in plants and fungi (Frommhagen et al., 2016; Kracher et al., 2016). Due to the oxidative instability of LPMOs in reactions with high concentrations of H_2O_2, it is important to carefully dosage the reductant to the system. Therefore, continuous and controlled supply of H_2O_2 to LPMOs gives more stable LPMO reactions (Müller et al., 2018). Controlled supply of H_2O_2 can be provided by several redox enzymes, in particular oxidases that use O_2 as an electron acceptor. Today, several fungal enzymes have been shown to function as redox partners for LPMOs. Cellobiose dehydrogenase, pyranose dehydrogenase and glucose oxidase are examples of such redox partners (Bissaro et al., 2017; Bissaro et al., 2018; Langston et al., 2011; Phillips et al., 2011; Várnai et al., 2018).

1.5.1. CELLOBIOSE DEHYDROGENASE (CDH)

Cellobiose dehydrogenases (CDHs) are modular enzymes that are classified as both family AA3 (dehydrogenase domain) and AA8 (cytochrome domain). CDH has been shown to function as a natural redox partner for fungal AA9 LPMOs (Langston et al., 2011; Phillips et al., 2011). In white rot fungi, CDH is found to be secreted along with LPMOs (Hori et al., 2013; Wymelenberg et al., 2011). CDHs are large flavocytochromes, which means that they are flavin-dependent dehydrogenase enzymes containing an additional cytochrome domain. The cytochrome domain binds a heme b prosthetic group, and the dehydrogenase domain binds a flavin adenine dinucleotide (FAD). The two domains are connected by a flexible linker which

allows for some degree of motion between them (Breslmayr et al., 2020). For some CDHs, the dehydrogenase domain can also contain a C-terminal CBM (Zámocký et al., 2004). This allows for strong affinity to the cellulose surface (**Figure 8**) (Bissaro et al., 2018; Tan et al., 2015).

The dehydrogenase domain is the catalytic domain of the CDH, and the FAD works as a cofactor. CDH oxidizes cellobiose and other soluble oligosaccharides at the C1 position by accepting two electrons at the flavin adenine dinucleotide group ($FAD + 2e^- + 2H^+ \rightarrow FADH_2$) (Bissaro et al., 2018; Igarashi et al., 2002). Following this event, one of these electrons can be donated, by single electron transfer, from the flavin in the dehydrogenase domain to the heme b in the cytochrome domain(Igarashi et al., 2002). In turn, the cytochrome can directly interact and reduce the copper in the LPMO active site (Courtade et al., 2016). Molecular oxygen can also re-oxidize the flavin (and the heme) leading to the formation of H_2O_2. However, it has been shown that the reaction with molecular oxygen is much slower than cytochrome-mediated electron transfer with LPMOs, which means that reduction of molecular oxygen is not a hindrance for the copper reduction (Bissaro et al., 2018; Tan et al., 2015).

Indeed, when incubated with its substrate, in the absence of good electron acceptors, CDH has been found to produce H_2O_2. This product cannot be seen when an LPMO and its substrate are present in the reaction (Loose et al., 2016). Since hydrogen peroxide is a known co-substrate of LPMOs, this suggests that the LPMO consumes the hydrogen peroxide the CDH produces, strengthening the belief that cooperation between these two enzymes is significant (Bissaro et al., 2018; Loose et al., 2016) and may involve more than only reduction of the LPMO (Bissaro et al., 2017; Bissaro et al., 2018). This was substantiated by recent findings by *Kracher et al*., who presented a genetically enhanced CDH, called CDH_{oxy+}. This enzyme has a larger production rate of H_2O_2, and might therefore be able to supply LPMOs with both an initial reduction, as well as a cofactor (Kracher et al., 2019).

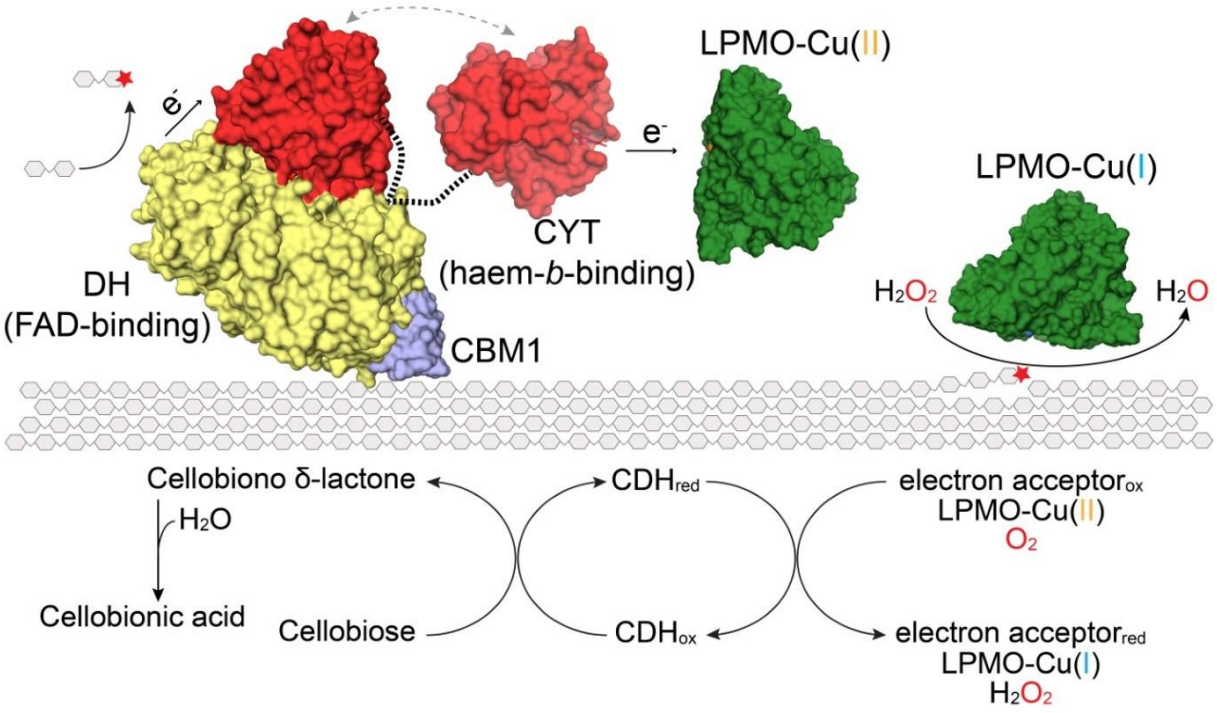

Figure 8: Illustration of the CDH/LPMO redox system for fungal cellulose oxidation. The CBM (blue) keeps CDH attached to the cellulose surface where LPMOs are active. The cytochrome (red), which is connected to the dehydrogenase domain (yellow) via a flexible linker (dashed lines), shows two conformations, a closed and an open form. In the reduced open form, the cytochrome domain can interact directly with the LPMO active site and reduce the copper. Subsequently, the reduced LPMO can cleave a glycosidic bond in the cellulose fiber. The dehydrogenase domain of CDH can produce H_2O_2 at a low rate, which may be used as a co-substrate by the LPMO. Illustration made by Zarah Forsberg (not published).

1.5.2. PYRANOSE DEHYDROGENASE (PDH)

Pyranose dehydrogenase (PDH) is another known redox partner of LPMOs. Compared to CDH, PDH is not a flavin, but a pyrroloquinoline quinone (PQQ)-dependent dehydrogenase that is found in the AA12 family. The PQQ-dependent pyranose dehydrogenase from the fungus *Coprinopsis cinerea* was the first characterized member of this family (Matsumura et al., 2014). This enzyme has a three-domain structure like three-domain CDHs, with an AA12 dehydrogenase domain, an N-terminal AA8 heme containing cytochrome and a C-terminal cellulose-binding module (CBM1) (Várnai et al., 2018).

Even though the dehydrogenase domain has a different cofactor, it carries out a reaction similar to CDHs (Várnai et al., 2018). PQQ-dependent PDH can oxidize substrates such as D-glucosone and L-fucose to 2-keto-D-gluconic acid and L-fuconic acid, respectively, and as for CDH, the oxidation occurs at the C1 position. As for CDHs, PQQ-dependent PDH is able to reduce LPMOs. Furthermore, addition of free PQQ to the LPMO/PDH reaction showed that PQQ may

act as a redox mediator between the two enzymes. However, it is currently less clear whether PDH produces H_2O_2 or not. (Várnai et al., 2018).

Considering that the CDHs can use oligosaccharides as substrate, they may generate C1-oxidized products that are similar to products produced by C1-oxdizing LPMOs and they may oxidize the products generated by C4-oxidizing LPMOs. For that reason, CDHs are not optimal for studying LPMO efficiency as one cannot distinguish between products that have been oxidized by the LPMO or the CDH. Since PDH does not use these oligosaccharides as substrate, this enzyme may be better suited for studying LPMO kinetics. The products of the PDH can be analyzed chromatographically, which means that both LPMO and PDH products can be analyzed in the same reaction (Várnai et al., 2018).

1.5.3. GLUCOSE OXIDASE (GOx)

Glucose oxidase (GOx) is an enzyme that oxidizes glucose to gluconic acid using O_2 as an electron acceptor with the consequential production of hydrogen peroxide. Like CDHs, this is also a FAD-dependent enzyme that belongs to the AA3 family of CAZymes. Compared to CDH and PDH, GOxs do not contain a cytochrome domain and can thereby not carry out the initial reduction needed to activate LPMOs. However, the oxidase activity and high reactivity with O_2 make GOx a good H_2O_2 producer. In combination with a priming amount of reductant (e.g. ascorbic acid), GOx can efficiently drive the LPMO reaction (Bissaro et al., 2017).

1.6. BACTERIAL REDOX PARTNERS

In bacteria no CDH-like redox enzyme has been yet been described and there are no obvious partners for LPMO activation in the current literature. However, a few potential candidates have been proposed. In Gram-negative *Cellvibrio japonicus*, two proteins have been suggested as potential redox partners for LPMOs. These proteins are named Cbp2D and Cbp2E and have been shown to be important for growth on cellulose (Gardner et al., 2014) as well as being co-secreted with LPMOs during growth om chitin (Tuveng et al., 2016). Both proteins contain a CBM2, which is a group of CBMs that has been shown to bind cellulose, chitin, and xylan (Black et al., 1995; Gilkes et al., 1988; Nakamura et al., 2008), which may be taken to suggest that these proteins are involved in cellulose turnover. Cbp2D and Cbp2E both contain so-called YceI-domains, which have been found to bind ubiquinone, a known redox mediator (also known as Coenzyme Q8), but can also bind other isoprenoid units such as octaprenyl pyrophosphate (Vincent et al., 2010). YceI-containing proteins exist in all types of organisms

where they have been reported to play essential roles in respiratory electron transport and may also have antioxidant activity (Nohl et al., 2001). However, a direct role in biomass degradation has not yet been shown. Cbp2D contains two cytochrome-domains (**Figure 9**), which, by analogy to fungal CDHs, could play a role in electron transport to LPMOs.

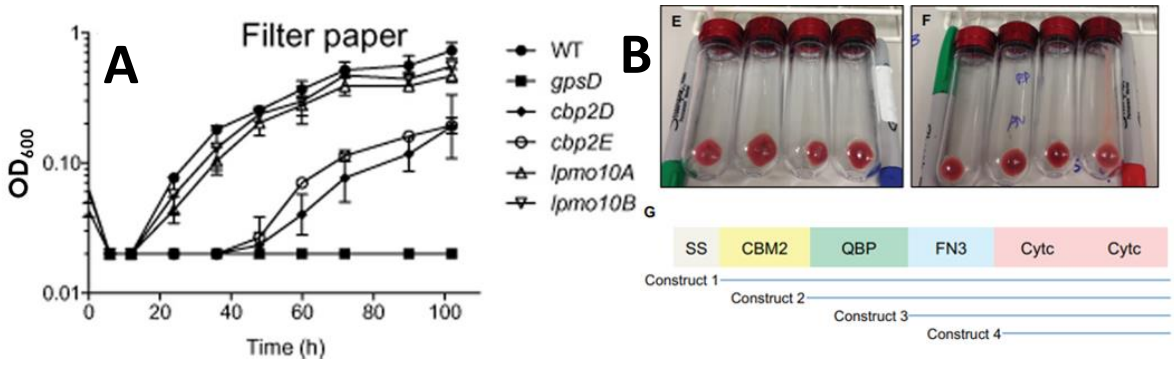

Figure 9: The impact of Cbp2D and Cbp2E on growth of *C. japonicus* on cellulose. A) Growth of strains with varying knock-out mutations showing that deletion of Cbp2D or Cbp2E leads to impaired growth. A strain with a knockout of a transporter for cellulose degrading enzymes (gpsD) was used as a negative control, since it has poor growth on cellulose. The Figure was adapted from (Gardner et al., 2014). B) Test-tubes showing pellets of lysed *Escherichia coli* (from periplasmic extraction) containing different constructs of Cbp2D. The red color indicates the cytochrome domains found in this protein, which is believed to be important should the enzyme function as a redox partner of LPMOs. The figure was adapted from the Supplementary information and article of (Gardner et al., 2014).

Even though there are suggestions as to potential bacterial redox partners for LPMOs, there are still no confirmed findings. A lack of proteomics data makes it hard to find the same connection between LPMOs and enzymatic redox partners in bacteria, as have been proven to exist in fungi. No known bacterial versions of the fungal CDHs, PDHs and GOxs have yet been found.

2. AIM OF THIS STUDY

The ultimate goal of this study was to find a potential bacterial counterpart to fungal CDH or PDH. To achieve this, finding proteins with similar characteristics is essential. The two *C. japonicus* proteins Cbp2D and 2E are, as described above, known to be important for growth on cellulose, and are co-secreted with the LPMOs (Tuveng et al., 2016). However, no in-depth biochemical characterization has been carried out for these proteins, in some part due to expression difficulties in the model organism *Escherichia coli* (Gardner et al., 2014).

Saccharophagus degradans is another Gram-negative bacterium. It is an aerobic, marine bacterium which can utilize complex carbohydrates (such as chitin, cellulose, starch, xylan and pectin) from many different sources, like marine algae or plants. The *S. degradans* genome contains one gene coding for an LPMO, named SdLPMO10A. It also contains two genes coding for proteins which show a strong similarity to Cbp2D and Cbp2E of *C. japonicus* (Taylor et al., 2006). The goal of this study was to express and purify these two proteins (encoded by genes here called *LapA* and *LapB*) and the LPMO from *S. degradans* in order to functionally characterize the enzymes. In subsequent steps the potential roles of the Cbp2D and Cbp2E homologues as redox partners for *Sd*LPMO10A were studied.

3. MATERIALS AND METHODS

3.1. MATERIALS

3.1.1. EQUIPMENT

Table 1 shows an overview of equipment and materials used to perform the methods described in section 3.2. The table lists analysis equipment, one-use plastic equipment and similar, along with the suppliers.

Table 1: The table shows equipment used during the laboratory work, such as analytical machines and centrifuges, along with the company which supplied the equipment.

Equipment	**Supplier**
10 000 mw cutoff centrifuge filters	Merck KGaA
1000 MWCO snakeskin, 3,7 ml/cm	ThermoFisher Scientific
Äkta pure chromatography system	Cytiva (Former GE Healthcare)
Äkta purifier chromatography system	Cytiva (Former GE Healthcare)
Amicon® Ultra-15 10K centrifuge filter tubes	Merck KGaA
Avanti™ J-25 centrifuge	Beckman Coulter Inc
Eppendorf Centrifuge 5425	Eppendorf
Eppendorf tubes	Eppendorf
Harbinger biotechnology system	PolyScience
Heat block	Grant Instruments (Cambridge) Ltd.
HiLoad 16/600 Superdex 75 pg column	Cytiva (Former GE Healthcare)
HiTrap™ DEAE column	Cytiva (Former GE Healthcare)
HisTrap™ HP column	Cytiva (Former GE Healthcare)
ICS-3000	ThermoFisher Scientific
ICS-5000	ThermoFisher Scientific
JA10 rotor	Beckman Coulter Inc
JA14 rotor	Beckman Coulter Inc
MALDI target plate	Bruker Daltonics
MALDI-ToF MS, UltrafleXtreme	Bruker Daltonics
Microfluidizer® high shear fluid processor	Microfluidics International Corporation
Microwave oven	Whirlpool Nordic AS
Millipore filter plate	Merck KGaA

Millipore pump	VWR International AS
Millipore well plate	ThermoFisher Scientific
Pipette tips	VWR International AS
PCR machine, SimpliAmp™ Thermal cycler	ThermoFisher Scientific
PCR tubes	Axygen, Inc.
PD midiTrap G-25 column	Cytiva (Former GE Healthcare)
Protein gel tub and power source	Bio-Rad Laboratories, Inc.
Quartz µCuvette® G1.0, 3 mm	Eppendorf
SDS-PAGE gel	Bio-Rad Laboratories, Inc.
Sonication water bath	Branson Ultrasonics Corporation
Spectrophotometer, BioPhotometer	Eppendorf
StepOnePlus™ Real-Time PCR System	ThermoFisher Scientific
Telstar AV-100 Vertical Laminar Flow Bench	Catalan Institute of Nanoscience and Nanotechnology
ThermoMixer	Eppendorf
Vacfuge Concentrator plus	Eppendorf
Water bath, Julabo	VWR International AS
ZipTips	Eppendorf

3.1.2. CHEMICALS

Table 2 lists chemicals used in the laboratory work, along with their suppliers.

Table 2: Table showing all chemical compounds used during the laboratory work, along with the company which distributes it.

Compound	**Distributor**
Acetic acid	Merck KGaA
Acetonitrile	Honeywell International
Agarose	Lonza Group
Agar powder	VWR International AS
Ammonium bicarbonate	Sigma-Aldrich Corporation
Ammonium sulphate	Acros Organics B.V.B.A.
Ampicillin (sodium salt)	Sigma-Aldrich Corporation
Antifoam	Sigma-Aldrich Corporation

Ascorbic acid	Sigma-Aldrich Corporation
Bacto Tryptone	Becton, Dickinson and Company
Bacto Yeast Extract	Becton, Dickinson and Company
Copper	Merck KGaA
Dipotassium phosphate	VWR International AS
EDTA	Merck KGaA
Ethanol, 98% (v/v)	VWR International AS
Glycerol, 85 % (v/v)	Merck KGaA
Guanine hydrochloride	Sigma-Aldrich Corporation
Hydrochloric acid, 37 %	Merck KGaA
Imidazole	PanReac AppliChem
Iodoacetamide	Sigma-Aldrich Corporation
Isopropanol	VWR International AS
Kanamycin, Gibco™	ThermoFisher Scientific
L-Arginine	Sigma-Aldrich Corporation
Methanol	Merck KGaA
MilliQ water, filter Millipak Express 40, size 0,22 µm	Merck KGaA
Oxidized glutathione	Sigma-Aldrich Corporation
Potassium dihydrogen phosphate	Sigma-Aldrich Corporation
Reduced glutathione	Sigma-Aldrich Corporation
Sodium acetate, ICS standard	Sigma-Aldrich Corporation
Sodium hydroxide, 50 % solution for ion chromatography system (ICS) analysis, Fluka™	Honeywell International
Sodium chloride	VWR International AS
Sodium dihydrogen phosphate	Merck KGaA
Sodium phosphate	Merck KGaA
Triton x-100	Sigma-Aldrich Corporation
Trizma base	Sigma-Aldrich Corporation

3.1.3. CARBOHYDRATE SUBSTRATES

In **Table 3**, carbohydrate substrates used in enzyme assays are presented.

Table 3: Table showing all carbohydrates used during the laboratory work, along with specifications of production and/or source of distribution.

Carbohydrate substrates	**Specifications and distributor**
Avicel	Sigma-Aldrich Corporation
Bacterial microcrystalline cellulose (BMCC)	A kind gift from Priit Väljamäe, Tartu university, Estonia
Phosphoric-acid swollen cellulose (PASC)	Made in-house, prepared from Avicel using the method described by Wood: (Wood, 1988)
α-chitin	Extracted from *Pandalus borealis*, Seagarden, Husøyvegen 278, Karmsund Fiskerihavn, 4262 Avaldsnes, Norway
β-chitin	Extracted from squid pen, Batch 20140101, France Chitin, Chemin de Porte Claire, F- 84100 Orange, France

3.1.4. BUFFERS, ENZYMES, MEDIA, STANDARDS, KITS

Table 4 shows a listing of all buffers, enzymes and standard solutions that were used in the laboratory work, along with the suppliers for these materials.

Table 4: Table showing all buffers, enzymes, kits and other standard solutions and mixes that were prepared by the companies which distributed it, and that was used in the laboratory work.

Buffers, enzymes, standard solutions and kits	**Distributor/Supplier**
BfuAI (10U) restriction endonuclease	New England BioLabs
BSA	New England BioLabs
BugBuster® Protein Extraction Reagent	Merck KGaA
Coomassie Brilliant Blue	Bio-Rad Laboratories, Inc.
dCTP	Roche Diagnostics Norge AS
dGTP	Roche Diagnostics Norge AS
DTT, 1 M	Invitrogen

GelGreen® Nucleic Acid Gel Stain	Biotium
Glc2	Megazyme
Glc3	Megazyme
Glycoside hydrolase 6.1	Produced according to Jensen et. al. (Jensen et al., 2018)
Lysozyme	Bio-Rad Laboratories, Inc.
NE Buffer 2.1	New England BioLabs
NucleoSpin® Plasmid purification kit	MACHEREY-NAGEL
NucleoSpin® Gel and PCR Clean-up	MACHEREY-NAGEL
Premix Ex Taq	TakaRa
Protein assay dye reagent (Bradford)	Bio-Rad Laboratories, Inc.
Q5 Hot Start HF master mix	New England BioLabs
Red taq DNA polymerase 2x	VWR International AS
SOC medium	Invitrogen
SYPRO™ Orange Protein Gel Stain	Sigma-Aldrich Corporation
T4 DNA polymerase(10U)	New England BioLabs

3.1.5. PRIMERS

Table 5 lists primers used for cloning the three genes encoding three novel proteins, as well as truncated variants of some of these proteins (see **Table 7**).

Table 5: Primer sequences used for production of DNA for protein expression. The bold part of the sequences is the part complementary to the vector. The last letter in the primer name indicates if the primer is a forward (F) or reverse (R) primer. nSS indicates that the protein contains the native signal sequence. For the LPMO, the restriction sites are indicated in parentheses following the primer name.

Primer name	**Primer sequence (5' → 3')**
InF_nSS_Sd10A_F (NdeI site)	**GAAGGAGATATACATATG**TTCGCGAAGAAA
InF_Sd10A_F (BsmI site)	**CGCAACAGGCGAATGCC**CACGGTCTGATGGTT
InF_Sd10A_R1 (HindIII site)	**CAGCCGGATCAAGCTT**TTAGTTGCACACCG

InF_Sd10A_R2 (HindIII site)	**CAGCCGGATCAAGCTT**TTACTGGCTGCTCA
InF_Sd10A_R3 (HindIII site)	**CAGCCGGATCAAGCTT**TTAACCAAAGGTAACG
pNIC_LapA_F1	**TTAAGAAGGAGATATACTATG**CAGAGCACCTGCAGC
pNIC_LapA_F2	**TTAAGAAGGAGATATACTATG**CTGGCGTATAGCCTGGA
pNIC_LapA_R	**AATGGTGGTGATGATGGTGCGC**CGGCGCCTCATAAAACA
pNIC_LapB_F1/2	**TTAAGAAGGAGATATACTATG**GCGGACCTGTGCAACGT
pNIC_LapB_F3	**TTAAGAAGGAGATATACTATG**GCGGTTTGGGAGCTGAAC
pNIC_LapB_F4	**TTAAGAAGGAGATATACTATG**GCGCCGACCAGCCTGA
pNIC_LapB_R1/4	**AATGGTGGTGATGATGGTGCGC**ACGCGCCCACGCTTTA
pNIC_LapB_R2/3	**AATGGTGGTGATGATGGTGCGC**CGCATCGAAGTCCAGAC GA

3.2. METHODS

3.2.1. GENE AND PRIMER DESIGN

Syntethic genes for *LapA, LapB,* and the LPMO were codon optimized for expression in *E. coli* and ordered from GenScript.

Primers for three versions of *Sd*LPMO10A, two versions of *LapA* and four versions of *LapB* were designed and ordered from Eurofins Genomics (see **Table 5** for the primer sequences).

3.2.2. PREPARATION OF CLONING VECTORS

A pRSET B vector containing a periplasmic signal sequence was used for cloning of *LPMO10A* (see section 3.2.5.). The pRSET B vector was isolated from *E. coli* using a NucleoSpin® Plasmid purification kit, with protocol "5.1 Isolation of high-copy plasmid DNA", and the vector was eluted using MilliQ water. The solution with purified vector was subsequently split into two tubes, and the two vector preparations were cut with different restriction enzymes, one with BsmI and one with NdeI. In addition, both vector preparations were also cut using HindIII. The restriction cutting solution consisted of 10 µL vector solution (approx. 1.1 µg/tube), 5 µL 10x New England Biolabs buffer (NE Buffer) 2.1, 29 µL MQ water, 3 µL HindIII, and 3 µL of either BsmI or NdeI. After incubation at 37 °C for 1.5 h (followed by an additional 1.5 h at 65 °C for the BsmI-containing reaction), the enzymes were inactivated by heating the tubes for 20

min at 80 °C. The linearized vectors were separated from the insert using a 1 % agarose gel (all agarose gels used in section 3.2. contained GelGreen® Nucleic Acid Gel Stain), followed by extraction of the correct DNA fragment from the gel using a NucleoSpin® Gel and PCR Clean-up kit, with protocol "5.2 DNA extraction from agarose gels".

pNIC_CH-vectors (AddGene, Cambridge, MA, USA) coding for a C-terminal His-tag were used for cloning of *LapA* and *LapB* (see section 3.2.4.). The pNIC-CH-vector was isolated from *E. coli* using the same kit as for the pRSET B vector isolation, but with protocol "5.2 Isolation of low-copy plasmids, P1 constructs or cosmos". The vector was digested using a mix of 10 µg vector, 17 µL dH_2O, 2 µl NE Buffer 2.1, 1 µl BfuA restriction endonuclease. After incubation at 50 °C for 2 hours a PCR-cleanup was performed according to protocol "5.1 PCR-clean up" from NucleoSpin® Gel and PCR Clean-up kit. Next, T4 DNA polymerase digestion was performed using a mix of 4 µl NE buffer 2.1, 4 µl 25 mM dCTP, 2 µl 100 mM dithiothreitol (DTT), 2 µl T4 DNA polymerase (10U), 2 µl 0.5 mg/ml bovine serum albumin (BSA), 0.4 pmol vector, and dH_2O to a total volume of 54 µl. The reaction mix was incubated for 60 min at 22 °C, followed by 21 min at 75 °C. Both digestions were done in a SimpliAmpTM Thermal cycler PCR machine.

3.2.3. BROTH PREPARATION

For production of vectors and proteins in *E. coli* cells, the culture medias used were lysogeny broth (LB) medium and terrific broth (TB) medium. LB medium consisted of 10 g Bacto-Tryptone, 5 g Bacto-Yeast Extract and 10 g NaCL per 1-liter finished broth. TB medium consisted of 24 g Bacto-Yeast Extract, 12 g Bacto-Tryptone, 4 ml 85 % glycerol, 2.31 g KH_2PO_4, and 12.54 g K_2HPO_4 per 1 liter finished medium (solutions of KH_2PO_4, and K_2HPO_4 were autoclaved separately before use). The LB medium and TB medium were autoclaved at 121 °C for 15 min before use. For all growth media containing antibiotics, a concentration of 50 µg/ml were used (both for Kanamycin and Ampicillin). Growth plates were made by adding 1 % (w/v) agarose to TB medium before autoclaving the medium. The autoclaved medium was cooled to about 50 °C, when the medium was placed in a sterile cabinet before 100 µg/ml antibiotics were mixed in. The medium was poured into plates before the plates were allowed to set. The plates were stored at 4 °C.

3.2.4. CLONING, PRODUCTION AND PURIFICATION OF LapA AND LapB VARIANTS

3.2.4.1. DNA amplification and ligation independent cloning

Ligation independent cloning (Aslanidis & De Jong, 1990) was performed on the genes coding for different variants of the LapA and LapB proteins. A reaction mix consisting of 0.5 pmol/µl forward primer, 0.5 pmol/µl reverse primer, 4 ng/µl template DNA, 25 µl 2x Q5 Hot Start HF master mix, and dH_2O to a total volume of 50 µl was incubated in a SimpliAmpTM Thermal cycler PCR machine with the following settings: lid temperature 105 °C, an initial denaturing step at 98 °C for 30 sec. Then a cycle consisting of denaturing for 10 sec at 98 °C, followed by annealing for 30 sec at 65 °C, and elongation for 20 sec (40 sec for two of the *LapB* variants) at 72 °C, was repeated 35 times. The last step of the PCR was a prolonged elongation reaction for 2 min at 72 °C, after which the tubes were held at 10 °C until further analysis. A 1 % agarose gel with the PCR products was run. The PCR products underwent the same PCR-cleanup protocol as described for the pNIC-CH-vector in section 3.2.2. The concentrations of DNA in these samples were measured with a 3 mm quartz cuvette in a spectrophotometer (Eppendorf BioPhotometer), measuring absorbance of light at wavelength 280 nm (A_{280}). The concentration of the DNA was used to calculate the volume of this sample needed for digestion of the genes (coding for LapA and LapB variants).

A digest was prepared for each of the genes coding for LapA and LapB protein variants. The reaction mixes contained 2 µl NE Buffer 2.1, 0.5 mg/ml BSA, 2 µl 25 mM dGTP, 1 µl 100 mM DTT, 1 µl T4 DNA polymerase (10U), 0.2 pmol/µl insert, and dH2O to a final volume of 20 µl. This mix was incubated in the PCR machine at 22 °C for 1 hour, then at 75 °C for 21 min. Predigested pNIC-CH vector (1 µl) and 2 µl of the digest was then mixed and incubated at room temperature for 1 hour, followed by addition of 2 µl 25 mM EDTA and additional 10 min of incubation. This was then used to transform the vectors into competent cells.

Transformation of vectors into *E. coli* TOP10 competent cells was performed by the heat shock method. Competent cells (50 µl) were mixed with 1.5 µl construct and incubated on ice for 10 min. Then the mix was exposed to a 42 °C heat shock in a water bath for 30 sec, followed by immediate cooling on ice for 2 min. After cooling, 100 µl SOC medium was added, before the cells were incubated for approximately 30 min at 37 °C and 200 rpm. After incubation, the cells were spread on LB/Kanamycin/Sucrose (5%) agar plates, before a final incubation at 37 °C was performed overnight. Sucrose was used in the plates as many *E. coli* strains do not grow well

on sucrose, but the pNIC-CH vector allow for sucrose growth (Lee et al., 2010)(Addgene plasmid # 26117 ; http://n2t.net/addgene:26117 ; RRID:Addgene_26117).

3.2.4.2. Colony PCR and glycerol stocks

Colonies from each of the plates with plasmids encoding a variant of LapA or LapB were used to inoculate 2 ml LB/Kanamycin medium. After incubation for three hours at 37 °C, with 200 rpm shaking, 20 µl of each culture was mixed with 80 µl dH_2O, and the rest of the cultures were put back on incubation. The cells were boiled for 10 min and then used to perform colony PCR. A reaction mix containing 5 µl boiled cells, 1 µl primer mix (1:1 forward:reverse) and 6 µl Red Taq DNA polymerase 2x was used for the colony PCR. The PCR was run by SimpliAmpTM Thermal cycler PCR machine with the following settings; lid temperature 105 °C, an initial denaturing step at 95 °C for 30 sec (2 min for *LapB*). Then a cycle consisting of denaturing for 10 sec at 95 °C (20 sec for *LapB*), followed by annealing for 30 sec at 55 °C, and elongation for 1 min at 72 °C (3 min for *LapB*), was repeated 35 times. Lastly, 10 min of annealing at 72 °C was performed. The samples were then placed on hold at 10 °C in the PCR machine. All the samples were analyzed on a 1 % agarose gel. The cultures which were put back on incubation were increased to a total volume of 8 ml (keeping the LB/Kanamycin ratio) for the cultures showing a band with the expected size on the gel. Then, these cultures were placed back for overnight incubation at 37 °C, 200 rpm shaking. Glycerol stocks of each of the clones containing a plasmid encoding a variant of LapA or LapB were made by mixing 700 µl of the overnight cultures with 300 µl 85 % glycerol in a sterile cabinet. The glycerol stocks were stored at -80 °C.

Plasmid purification was performed on the rest of each of the overnight cultures, according to the "5.2 Isolation of low-copy plasmids, P1 constructs or cosmids" protocol in the NucleoSpin® Plasmid purification kit. The concentrations of DNA in these samples were measured with a 3 mm quartz cuvette in a spectrophotometer (Eppendorf BioPhotometer), measuring absorbance of light at wavelength 280 nm (A_{280}). The measured DNA concentrations were used to calculate volume needed from these solutions to transfer 500 ng vector into sequencing sample mixes. The sequencing sample mix contained 500 ng purified vector, 2,5 µl primer solution (either forward or reverse, 10 pmol/µl) and dH_2O to a total volume of 11 µl. These sequencing sample mixes were sent for gene sequencing at Eurofins operon.

3.2.4.3. Transformation and protein production

Transformation of vectors containing *LapA* or *LapB* gene variants into competent *E. coli* BL-21 cells was performed by mixing 1 µl of purified vector with 25 µl competent cells. These

mixes were incubated on ice for 15 min, before heat shock for 30 sec at 42 °C. Immediately following the heat shock, the samples were cooled on ice for 2 min, before addition of 100 µl SOC medium. The samples were then incubated at 37 °C, 200 rpm, for 35 min. The samples were plated on LB/Kanamycin agar plates, and the plates were incubated overnight at 37 °C.

Colonies from each plate were picked and used to inoculate in 5 ml LB/Kanamycin. After incubation at 37 °C, 200 rpm overnight, glycerol stocks were made for each of the transformants as described above.

For initial assessment of protein production, 0.5 ml of an overnight culture was transferred to 50 ml LB/Kanamycin medium (three for each protein variant) and incubated until $OD_{600} \approx 0.6$. To induce protein expression, isopropyl ß-D-1-thiogalactopyranoside (IPTG) was added to a final concentration of 0,1 mM, 0.25 mM or 0.5 mM. The cultures were placed at 22°C, 200 rpm. After overnight incubation, 2 ml of each culture was centrifuged for 10 min at 8000 rpm in an Eppendorf Centrifuge 5425. The pellet was weighed, and 50 µl BugBuster® Protein Extraction Reagent was added per 0,01 g pellet to disrupt the cells. The solution was mixed by rotation for 20 min, followed by centrifugation at 16 000 x g for 20 min in an Eppendorf Centrifuge 5425, and the presence of protein in the soluble and insoluble fractions was checked by SDS-PAGE. The SDS-PAGE analysis showed that the LapB-1 and LapB-2 variants formed inclusion bodies, whereas the other two variants did not show expression (see section 3.2.4.4. for how the inclusion body issue was solved).

For large scale protein production, 5 ml overnight cultures were used to inoculate 500 ml TB/Kanamycin medium containing 55 µl antifoam solution. The cultures were incubated at 37 °C in a Harbinger system until the OD_{600} reached approximately 0.6, when 0,1 mM IPTG was added, followed by further incubation overnight at 22 °C. The cultures were harvested by centrifugation for 12 min at 4 °C, 8000 rpm in a JA10 rotor. The pellet was resuspended in 50 ml NiNTA Buffer A (5 mM imidazole, 500 mM NaCl, 50 mM Tris/HCl pH =8.0). The pellets of the LapB-1 and LapB-2 variants were used in a denaturing and refolding procedure (Section 3.2.4.4.).

In the resuspensions containing the LapA-1 variant, 600 µl 10 g/l lysozyme and 1 µl DNAse I per 10 ml solution were added, as well as 2 µl 50 mM phenylmethylsulfonyl fluoride. The cells were disrupted using a Microfluidizer® at 15 000 psi, before centrifugation at 12 000 rpm, 4 °C for 15 min in a JA14 rotor. The supernatant was filtrated using 0,45 µm syringe filter.

3.2.4.4. Solubilization of inclusion bodies, denaturation and refolding: LapB

Large scale production of LapB variants was performed as described for LapA until resuspension of the cell pellet. Since LapB-1 and LapB-2 variants formed inclusion bodies during production, a denaturing and refolding procedure was applied (Monge et al., 2018). The LapB cell pellets were resuspended in 200 mM NaCl, 50 mM Tris/HCl pH =8.0. A total of 25 ml of the LapB cell resuspensions were centrifuged for 12 min at 4 °C, 16 000 rpm in a JA14 rotor. The pellet was resuspended in 10 ml 2 M NaCl, 50 mM Tris/HCl pH =8. 200 µl 10 g/l lysozyme and 1 µl DNAseI was added, and the resuspensions were incubated on ice for 30 min. These cells were disrupted using a Microfluidizer® at 15 000 psi. After centrifugation for 12 min at 4 °C, 14 000 rpm in a JA14 rotor, the pellet was resuspended in 25 ml washing buffer (100 mM NaCl, 2% Triton x-100, 20 mM TrisHCl pH =8.0). This was repeated two times, after which the pellet was resuspended in 5 ml denaturing solution (50 mM TrisHCl, pH =8.5, 100 mM NaCl, 6 M guanidine HCl, 1 mM EDTA, 20 mM DTT). The resulting suspensions were vortexed for 1 min and rotated by inverting the tubes at 4 °C, 25 rpm overnight. The solutions with denatured protein were then slowly transferred to 250 ml refolding buffer (100 mM TrisHCl, 0,4 M L-Arginine, 0,5 mM oxidized gluthatione, 5 mM reduced gluthatione) at a rate of 1 ml per hour under intense stirring at 4 °C. After all the solution with denatured protein had been transferred into the refolding buffer, the refolding buffer solution was left to stir at 4 °C overnight.

After overnight stirring, the refolding solutions were centrifuged at 9000 rpm, 4 °C for 10 min in a JA14 rotor, before the supernatant was filtrated (0,45 µm). The filtrate was transferred to a 10 000 molecular weight cutoff Snakeskin dialysis tube. Dialysis was performed at 4 °C against 2.5 liters 50 mM Tris, 0,1 M NaCl, pH =8.0, which was changed after 7 hours, before leaving the dialysis overnight. The dialyzed samples were then filtrated using 0.45 µm filters.

3.2.4.5. Protein purification

LapA-1, LapB-1 and LapB-2 variants were purified using affinity chromatography based on the 6×His- tag encoded for in the pNIC vector, using a 5 ml HisTrap column inserted in an Äkta Pure chromatography system. Buffers designated A and B were used for binding to the column and elution by an increasing imidazole gradient, respectively. Buffer A was 5 mM imidazole, 500 mM NaCl, 50 mM TrisHCl pH =8.0, while buffer B was 500 mM imidazole, 500 mM NaCl, 50 mM TrisHCl, pH =8.0. A 50 min gradient going from 0-50 % buffer B over 50 min was used, at 2 ml per min flow rate. After the purification, solutions with LapB proteins were concentrated down to about 2 ml using 10 000 mw cutoff centrifuge filters, 4000 x g at 4 °C,

with simultaneous buffer exchange. The final solutions with purified LapB variants were stored in 50 mM TrisHCl pH =7.5 at 4 °C.

LapA-1 was further purified by ion exchange chromatography (IEX). The IEX was performed using a 5ml DEAE anion exchange column, using an Äkta Pure chromatography system. Buffers designated A and B were used for binding to the column and elution by an increasing salt gradient, respectively. Buffer A was a 50 mM TrisHCl, pH =7.5 solution, while buffer B was a 50 mM TrisHCl, pH =7.5, 500 mM NaCl solution. A 50 min gradient going from 0-50 % buffer B over 50 min was used, at 2 ml per min flow rate. After the purification, solutions with LapA-1 was concentrated down to about 2 ml using 10 000 mw cutoff centrifuge filters, 4000 x g at 4 °C, with simultaneous buffer exchange. The final solution with purified LapA-1 was stored in 50 mM TrisHCl, pH =7.5 at 4 °C.

Protein concentrations were measured using Bradford assay and A_{280} spectrophotometry. For the Bradford assay, 5 µl protein was mixed with 795 µl 50 mM TrisHCl, pH =7.5 buffer, and then mixed with 200 µl BioRad dye reagent. Blank sample consisted of 800 µl storage buffer mixed with 200 µl BioRad dye reagent. The samples were measured using a 1 ml cuvette (1 cm light path) in an Eppendorf spectrophotometer, at 595 nm wavelength. A_{280} was also measured using the Eppendorf spectrophotometer, but instead of 1 ml, a 100 µl cuvette (1 cm light path) was used. For A_{280}, dilutions of 10x, 50x and 100x were used, and an average value was calculated based on these measurements.

3.2.5. CLONING, PRODUCTION AND PURIFICATION OF *Sd*LPMO10A

3.2.5.1. DNA amplification and In-Fusion cloning

For DNA amplification of the *LPMO10A* gene, a reaction mix of 50 µl was made as described for DNA amplification of *LapA* and *LapB*, and the program of the PCR reaction was set up as described for the initial PCR for DNA amplification on *LapA*.

The PCR products of *LPMO10A* were analyzed on a 1 % agarose gel. The PCR samples containing bands around expected sizes for the different genes of the *Sd*LPMO10A variants were extracted from the gel and treated according to the protocol "5.2 DNA extraction from agarose gels" from the kit NucleoSpin® Gel and PCR Clean-up. The concentrations of DNA in these samples were measured with a 3 mm quartz cuvette in a spectrophotometer (Eppendorf BioPhotometer), measuring absorbance of light at wavelength 280 nm (A_{280}). These concentrations were used to calculate volume needed for In-Fusion cloning reaction.

In-Fusion cloning reaction mixes were made for all three variants of the *LPMO10A* gene according to In-Fusion HD cloning kit (Clontech). Each reaction mix contained 3.5 µl linearized pRSET-B vector coding for the periplasmic signal peptide, 9 ng/µl insert, 2 µl Premix Ex Taq, and dH_2O was added to a final volume of 10 µl. The reaction mixes were incubated at 50 °C for 15 min, before the mixes were on ice. A total of 90 µl TE buffer (10 mM Tris, 1 mM EDTA, pH =8.0) was added to each incubated reaction mix. These reaction mixes were then used to transform *E. coli* TOP10 competent cells as described for *LapA* and *LapB* (Section 3.2.4., third paragraph). After the transformation of the competent cells, the cells were incubated for 30 min at 37 °C, before the cells were plated on LB/Ampicillin agar plates. A final incubation of the cells at 37 °C was performed overnight.

3.2.5.2. Colony PCR and glycerol stocks

The colony PCR for *Sd*LPMO10A was started by picking colonies from the agar plates, leaving some of the colony in PCR tubes, before having the rest of the colony transferred into 2 ml LB/Ampicillin medium. The cultures were placed in an incubator at 37 °C, 200 rpm. The PCR-tubes with traces of the colonies, were microwaved at maximum power for 2,5 min followed by addition of 2 µl primer mix (1:1 forward:reverse), 8 µl dH2O and 10 µl Red taq DNA polymerase 2x. These reaction mixes were run run by SimpliAmpTM Thermal cycler PCR machine with the following settings; lid temperature 105 °C, an initial denaturing step at 95 °C for 30 sec. Then a cycle consisting of denaturing for 10 sec at 95 °C, followed by annealing for 30 sec at 55 °C, and elongation for 1,5 min at 72 °C, was repeated 35 times. 72 °C for 10 min ended the PCR, while 10 °C were used as holding temperature after that. The PCR products were analyzed on a 1 % agarose gel, and cultures having bands with the expected size were increased to 8 ml LB/Ampicillin, and incubation at 37 °C was continued overnight.

Glycerol stocks were made for each of the variants of the LPMO, as described for for *LapA* and *LapB* above. Plasmid purification was performed on the rest of the overnight cultures, according to the "5.2 Isolation of low-copy plasmids, P1 constructs or cosmids" protocol from the NucleoSpin® Plasmid purification kit. Concentration of these vector samples was measured in a 3 mm Quartz cuvette, using an Eppendorf spectrophotometer. Concentration was used to calculate volumes of the samples needed for sequencing. The sample sequencing mixes were prepared as described for *LapA* and *LapB.*

3.2.5.3. Transformation and production

The pRSETB vectors encoding the different *Sd*LPMO10A variants were transformed into competent cells of *E. coli* BL-21 (DE3) Star as described above for LapA and LapB.

Single colonies for all three *Sd*LPMO10A variants were picked and used to inoculate 500 ml LB medium supplemented with Ampicillin. The cultures were grown overnight at 37 °C and 200 rpm stirring. From these overnight cultures, periplasmic extract (PPE) was prepared using an osmotic shock method (Manoil & Beckwith, 1986). In brief, the cultures were centrifuged (12 min at 8000, rpm 4 °C), using a JA10 rotor in an AvantiTM J-25 centrifuge. The pellets from the centrifuged cultures were resuspended in 50 ml ice cold spheroplast buffer (50 mM TrisHCl, pH =8.0, 0.5 M sucrose, 100 µM EDTA), incubated on ice for 5 min, and then centrifuged for 12 min at 8000 rpm, 4 °C using a JA10 rotor in an AvantiTM J-25 centrifuge. The pellet was left in room temperature for 15 min, before being resuspended 25 ml ice cold dH_2O culture, then adding 2 ml 20 mM $MgCl_2$. The resuspensions were centrifuged for 12 min at 8000 rpm, 4 °C using a JA10 rotor in an AvantiTM J-25 centrifuge, and the PPE (being the supernatant) was filtrated using 0,45 µm filters.

3.2.5.4. Protein purification

The *Sd*LPMO10A variants were purified from the PPE using IEX chromatography. The IEX was performed using an Äkta Plus chromatography system, using a HiTrapTM DEAE 5 ml column. Buffers designated A and B were used for binding to the column and elution by an increasing salt gradient, respectively. Buffer A was a 50 mM TrisHCl, pH =8.0 solution, while buffer B was a 50 mM TrisHCl, pH =8.0, 1 M NaCl solution. A 50 min gradient going 0-50 % buffer B over 50 min, at a flow rate of 2 ml/min. After purification, the protein samples were concentrated down to about 1 ml using 10 000 mw cutoff centrifuge filters, 4000 xg at 4 °C, and the buffer was exchanged simultaneously, into SEC buffer.

The *Sd*LPMO10A was not completely pure after IEX, so it was further purified by size exclusion chromatography (SEC). The SEC was performed using an Äkta purifier chromatography system and a HiLoad 16/600 Superdex 75 pg column. The SEC buffer consisted of a 200 mM NaCl, 50 mM TrisHCl, pH =7.5 solution. After purification, the protein samples were concentrated down to about 2 ml using 10 000 mw cutoff centrifuge filters, 4000 xg at 4 °C, with simultaneous buffer exchange. The final solutions with purified *Sd*LPMO10A variants were stored in 50 mM TrisHCl pH =7.5 at 4 °C.

Protein concentration of the purified LPMO was initially measured using the Bradford Assay, while later measurements was performed using A_{280} spectrophotometry. Both methods were performed as described LapA and LapB in section 3.2.4.5.

*Sc*LPMO10C was used as a reference LPMO for the tests done on the *Sd*LPMO10A. The *Sc*LPMO10C proteins were produced and purified as described by Forsberg et. al. (Forsberg et al., 2014).

3.2.5.5. Copper saturation

*Sc*LPMO10C and *Sd*LPMO10A were copper saturated before activity tests were performed. For initial activity tests, a "quick and easy" copper saturation method was used. *Sd*LPMO10A and *Sc*LPMO10C were copper saturated by adding a solution containing oxidized copper (Cu^{2+}) into a tube containing purified *Sc*LPMO10C, in a 1:1 molar ratio. The copper- *Sc*LPMO10C mix was left to react for about 25 min before the proteins of this solution were transferred to the reactions it was used in.

For the rest of the activity assays (and binding assays), *Sd*LPMO10A and *Sc*LPMO10C were copper saturated by mixing 500 µl of the enzyme with a solution containing oxidized copper (Cu^{2+}) in a 1:3 molar ratio. The proteins were then de-salted using a PD midiTrap G-25 column.

3.2.6. VERIFICATION OF LapA-1 USING PROTEOMICS TECHNOLOGY

Samples of LapA variants were run on an SDS-PAGE gel, which was stained with Coomassie Brilliant Blue. To do so, 0,1 % Coomassie brilliant blue was mixed in a 50 % isopropanol/20 % acetic acid/dH_2O-mixture to a final concentration of 0,05% Coomassie brilliant blue, and the gel was soaked in this solution for 30 min. Next the gel was de-stained in 25 % isopropanol/10 % acetic acid/dH_2O-mixture for 10 min, before a final soak in dH_2O with small amounts of isopropanol and acetic acid (about 2 % isopropanol/1 % acetic acid) was performed overnight.

Gel bands containing the protein were cut out of the gel, and each band was divided into 1x1mm pieces using a disposable scalpel blade. The pieces for each band were transferred to an Eppendorf LowBind tube, soaked in 200 µl dH_2O and incubated for 15 min at 22 °C. The liquid was removed, before the gel pieces were incubated for 15 min at 22 °C in 200 µl 50 % acetonitrile/25 mM ammonium bicarbonate. This step was repeated once. Then, 100 µl 100 % acetonitrile was added, followed by incubation for 5 min at 22 °C. The liquid was removed and 50 µl 10 mM DTT, 100 mM ammonium bicarbonate was added, followed by incubation for 30 min at 56 °C. After cooling the samples, the liquid was removed and 50 µl of 10 mg/ml iodoacetamide, 100 mM ammonium bicarbonate was added. The gel pieces were incubated for 30 min at 22 °C in the dark, before the solution was removed and 200 µl 100 % acetonitrile was added. After 5 min incubation at 22 °C, the liquid was removed.

Trypsin digestion of the proteins was done by adding 30 µl 10 ng/µl trypsin in 25 mM ammonium bicarbonate, 10 % acetonitrile. After 30 min incubation on ice, 20 µl of 25 mM ammonium bicarbonate, 10 % acetonitrile was added to soak the gel pieces, before the samples were incubated overnight at 37 °C.

After this overnight incubation, the samples were cooled to room temperature and 40 µl 1 % TFA was added to the samples, after which they were sonicated in a water bath for 15 min. To purify the peptides, C-18 ZipTips® were calibrated with 10 µl 100 % methanol, then 10 µl 70 % acetonitrile/0,1 % trifluoroacetic acid, and lastly 10 µl 0,1 % trifluoroacetic acid. Then the sample was pipetted through the filter of the ZipTips® six times up and down, followed by washing the filter in 10 µl 0,1 % trifluoroacetic acid. Lastly, the peptides were eluted in 10 µl 70 % acetonitrile/0,1 % trifluoroacetic acid by pipetting up and down six times. The samples were dried for 15 min using a Vacfuge Concentrator, after which the peptides were resuspended in 10 µl 70 % acetonitrile/0,1 % trifluoroacetic acid.

The peptide solutions were mixed with 15 mg/ml alpha-Cyano-4-hydroxycinnamic acid matrix in a 1:1 volume ratio and applied on a stainless steel MALDI target plate (Bruker Daltonics, Billerica, MA). MS data acquisition was performed with an Ultraflextreme MALDI-TOF/TOF (Bruker Daltonics) instrument which was operated in reflectron mode with delayed extraction. Positively charged ions in the m/z range of 700-3,000 were analyzed using an acceleration voltage of 20 kV and a delayed extraction (PIE) setting of 140 ns. External calibration of the sample spectra was performed with a peptide calibration standard covering the m/z range 700–3,500 (Bruker Daltonics). MS/MS spectra of selected peptides were recorded by using the LIFT ion optics of the mass spectrometer (Suckau et al., 2003).

3.2.7. BINDING ASSAYS

Binding assays were performed for LapA-1, LapB-2, and all three variants of SdLPMO10A. The reactions, which were performed in triplicates, consisted of 50 mM sodium phosphate pH =6.0, 10 g/l Avicel, 0.1 g/l protein and dH_2O to a total volume of 600 µl. Samples of 100 µl were taken after 4, 8, 16, 32 and 64 min and immediately filtered using a 0,22 µm MilliPore filter. A_{280} was then used to measure protein concentrations in the filtrates in an Eppendorf spectrophotometer. The protein concentrations in the samples from LapB-2 and *Sd*LPMO10A-2 assays were also measured using Bradford assay (as described above).

BSA was used as a negative control and the blank sample consisted of 50 mM sodium phosphate pH =6.0. Samples for background correction contained 50 mM sodium phosphate pH =6.0 and 10 g/l Avicel in dH_2O, while zero-time samples consisted of 50 mM sodium phosphate pH =6.0 and 0.1 g/l protein.

3.2.8. ACTIVITY ASSAYS FOR *Sd*LPMO10A

3.2.8.1. Control reaction for activity of Sc*LPMO10C*

As a control reaction, an activity assay was performed with *Sc*LPMO10C, which is active on cellulose. The reaction mix contained 10 g/l Avicel, 50 mM $NaPO_4$ buffer, pH =6.0, 1 µM enzyme, 1 mM ascorbic acid. The reactions were incubated at 40 °C, with 800 rpm shaking for 72 hours in a ThermoMixer. The reaction mixture was then centrifuged for 3 min at 13 000 rpm, before 1 µl sample was mixed with 2 µl 2,5-Dihydroxybenzoic acid (DHB) on a MALDI-ToF MS target plate, followed by analysis of oligomeric reaction products using MALDI-ToF MS as previously described (Vaaje-Kolstad et al., 2010).

3.2.8.2. Assay of substrate specificity for Sd*LPMO10A*

*Sd*LPMO10A was incubated with substrates Avicel, β-chitin, α-chitin, PASC and BMCC. Avicel, β-chitin and α-chitin were added in concentrations of 10 g/l, while the last two substrates were added in concentrations of 1 g/l. The rest of the reaction mixes were composed as described in section 3.2.8.1., and the reactions were incubated overnight, as above. *Sc*LPMO10C, active on Avicel, and CBP21 (see (Vaaje-Kolstad et al., 2005) for production), active on chitin, were used as control reactions. Products were analyzed using MALDI-ToF MS as described above (Vaaje-Kolstad et al., 2010).

3.2.8.3. Temperature optimum of Sd*LPMO10A and other activity assays*

Assays at varying temperatures were performed using *Sd*LPMO10A-1 (full-length protein) in 300 µl reaction mixes that were prepared as described in section 3.2.8.1. These reactions were performed in three parallels, and the reaction mixes were pre-incubated for 10 min at the appropriate temperature before reactions were started by adding the ascorbic acid. The reactions were placed in a ThermoMixer set to 800 rpm shaking, at 10, 20, 30, 40, 50, 60 and 70 °C.

At time points 10, 30, 60 and 120 min, 70 µl samples were taken and filtrated using MilliPore filters. Thirty-five µl of the filtrate was mixed with 35 µl 2 µM glycoside hydrolase 6.1 (a cellulase; see (Jensen et al., 2018)for production method) to degrade soluble products generated by *Sd*LPMO10A to oligomers with two or three glucose units, for easier product quantification

(see section 4.4.3. for further explanation). The reactions with the cellulase were incubated overnight at 37 °C. Reactions with *Sc*LPMO10C were used as positive control, and reaction mixes without ascorbic acid used as negative controls.

Product formation was analyzed using high-performance anion exchange chromatography with pulsed amperometric detection (HPAEC-PAD) using an ICS-5000 with a disposable gold electrode, as described previously (Westereng et al., 2013). Eluent A consisted of 0,1 M NaOH. Eluent B consisted of 1 M sodium acetate and 0,1 M NaOH. 5 µL samples were injected on a CarboPac PA1 2× 250 mm analytical column (Dionex, Sun-nivale, CA, USA), with a CarboPac PA1 2× 50 mm guard column at a 0,25 ml/min flow rate and 30°C. Elution was achieved by running a stepwise gradient of eluent B: 0–10% B over 10 min; 10–14% B over 5 min; 14–30% B over 1 min; 30–100% B over 2 min. Then, reconditioning of the column was performed by a gradient of 100– 0% B over 0.1 min and then 0% B over 10.9 min. Chromatograms were recorded using Chromeleon 7.0 software.

Identical reactions were performed, using all three variants of *Sd*LPMO10A, at 50 °C only. Total reaction mix volumes were 600 µl, and samples were taken at 0.5, 1, 2, 4, 6 and 24 hours. The samples were analyzed using an ICS-3000 system (Dionex, Sunnivale, CA, USA) using the same conditions as described for the ICS-5000 system, above (and by (Westereng et al., 2013)). These chromatograms were also recorded using Chromeleon 7.0 software.

For the reactions using all three variants of *Sd*LPMO10A, the liquid remaining in the reaction mixes after all the samples had been taken were filtrated (as described for the samples) and analyzed directly on the ICS-3000 system (described above) in order to compare product profiles.

3.2.9. APPARENT MELTING TEMPERATURE

The apparent melting temperature was determined using the Protein Thermal Shift Assay kit from Sigma-Aldrich. 10 µL 1 g/l protein, 10 µl 10x buffer (500 mM Tris/HCl pH =8.0), 67,5 µl dH_2O and 12,5 µl SYPRO orange were mixed, and 20 µl of this mix was transferred into real time PCR plate-wells (4 parallels). This plate was analyzed using a StepOnePlus^{TM} Real-Time PCR machine, using a 50 min gradient from 25 to 99 °C.

3.2.10. EFFECT OF LapA AND LapB ON THE ACTIVITY OF *Sd*LPMO10A

In initial tests with LapA, reaction mixes containing 10 g/l Avicel in 50 mM sodium phosphate pH =6.0 were prepared containing different amounts of proteins, and ascorbic acid according to **Table 6**. Each reaction mix had a final volume of 300 µl. The reaction mixes were incubated at 50 °C, 800 rpm. Aliquots of 70 µl were taken after 1, 3 and 24 hours. These samples were filtrated using 0,22 µm MilliPore filters and 35 µl of the filtrate was mixed with 35 µl a glycoside hydrolase 6.1 (Jensen et al., 2018) and incubated overnight at 37 °C to degrade soluble products to short oligomers containing two or three glucose units only, for easier quantification (see section 4.4.3. for a further explanation). The samples were analyzed using the ICS-3000 set-up, as described above.

Table 6: Protein and reductants added to various reactions testing the effect of LapA on the activity of *Sd*LPMO10A.

Reaction mix	Proteins and reductant concentrations
1	1 µM *Sd*LPMO10A + 1 mM ascorbic acid
2	1 µM *Sd*LPMO10A
3	1 µM *Sd*LPMO10A + 1 µM LapA-1
4	1 µM *Sd*LPMO10A + 1 µM LapA-1 + 100 µM ascorbic acid
5	1 µM *Sd*LPMO10A + 100 µM ascorbic acid
6	1 µM LapA-1
7	1 µM LapA-1 + 100 µM ascorbic acid

This test was repeated, testing reaction mix 1, 4 and 5 in triplicates, as these were the only ones showing any product formation in the first run.

A third test was performed, this time at 30 °C (instead of 50 °C). In this test, both LapA-1 and LapB-2 were tested in reactions that were set up according to reactions 4 and 5 in **Table 6**, which means that these reactions either contained 1 µM LapA (as shown in **Table 6**), or 1 µM LapB. The samples were taken at 3, 6 and 24 hours instead of 1, 3 and 24 hours due to a slower reaction speed at lower temperature.

In all cases product formation was analyzed using the ICS-3000 set-up, as described above.

4. RESULTS

4.1. BIOINFORMATIC ANALYSIS

As outlined in section 2., two proteins from the Gram-negative bacterium *S. degradans*, LapA and LapB, have been studied because of their potential roles as redox partners for the *S. degradans* LPMO, called *Sd*LPMO10A. All three proteins contain a family 2 carbohydrate-binding module (CBM2), indicating that these proteins bind to cellulose (**Figure 10**). In addition to the AA10 domain and the CBM2, the LPMO contains a domain of unknown function. The two potential redox partners, LapA and LapB, both contain an isoprenoid quinone binding domain (YceI-like domain) that has been found to bind Coenzyme Q8 and octaprenyl pyrophosphate (Vincent et al., 2010), where Coenzyme Q8 could potentially have a role in electron transport (Nohl et al., 2001). In addition, the gene encoding LapB contains multiple C-terminal cytochrome (CYT) domains. A cytochrome domain is responsible for the electron donating ability of fungal CDHs to LPMOs, and the cytochromes found in *LapB* could potentially have similar function. Interestingly, a gene encoding a cytochrome is also located upstream of the *LapA* gene.

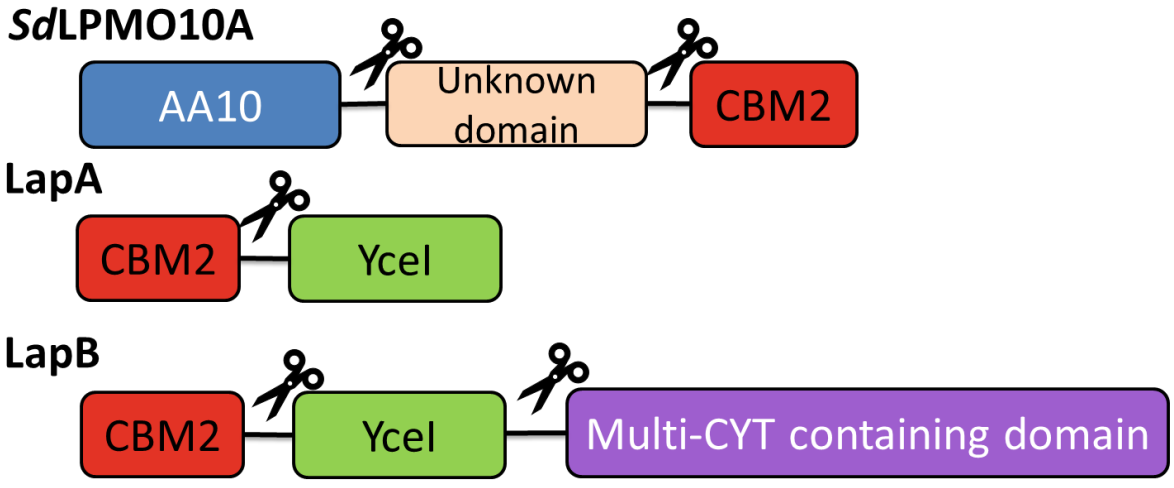

Figure 10: Domain architecture of SdLPMO10A, LapA and LapB. The scissors indicate truncation points used in this study to produce truncated versions of the three proteins. The purple box of LapB represents multiple cytochrome-domains, along with regions of low complexity.

The domain organizations of LapA and LapB are similar the domain organizations of Cbp2E and Cbp2D from *C. japonicus*, respectively. Cbp2E contains an N-terminal CBM2 and a C-terminal YceI domain, like LapA (see **Figure 10**), while Cbp2D contains an additional region of cytochromes and unknown domains that is similar to the C-terminal region of LapB. Sequence alignments were carried out using Clustal Omega to compare the sequences of LapA

and LapB with Cbp2D and Cbp2E. The alignments revealed that LapA and Cbp2E share 34 % sequence identity (**Figure 11**). Areas with lower similarities were shown to contain repeats of prolines and glutamates in LapA and serines in Cbp2E, which is typical for linker regions. For two proteins with different phylogenetic origin this identity percentage is relatively high, which makes it seem likely that these proteins have similar functions. Comparison of LapB and Cbp2D showed 41 % sequence identity (**Figure 12**). The serine linkers of Cbp2D, which may be one of the reasons why this protein is difficult to express, are not found in LapB. Considering the even larger protein size of LapB and Cbp2D, as well as the even higher sequence identity, these proteins are very likely to have similar functions.

A prediction of transmembrane helices using Transmembrane Hidden Markov Model analysis (TMHMM server v 2.0, http://www.cbs.dtu.dk/services/TMHMM/) was performed for LapA and LapB prior to codon optimization and gene synthesis, to check whether they contain transmembrane regions (**Appendix 1**). The TMHMM analysis of the full-length LapA showed internal and transmembrane regions among the first 50 residues. However, a new TMHMM was performed, this time without the first 44 residues (believed to be the signal peptide), in which the prediction showed the entire sequence as extracellular. No part of LapB showed any putative transmembrane regions and the entire protein was predicted to be an extracellular protein.

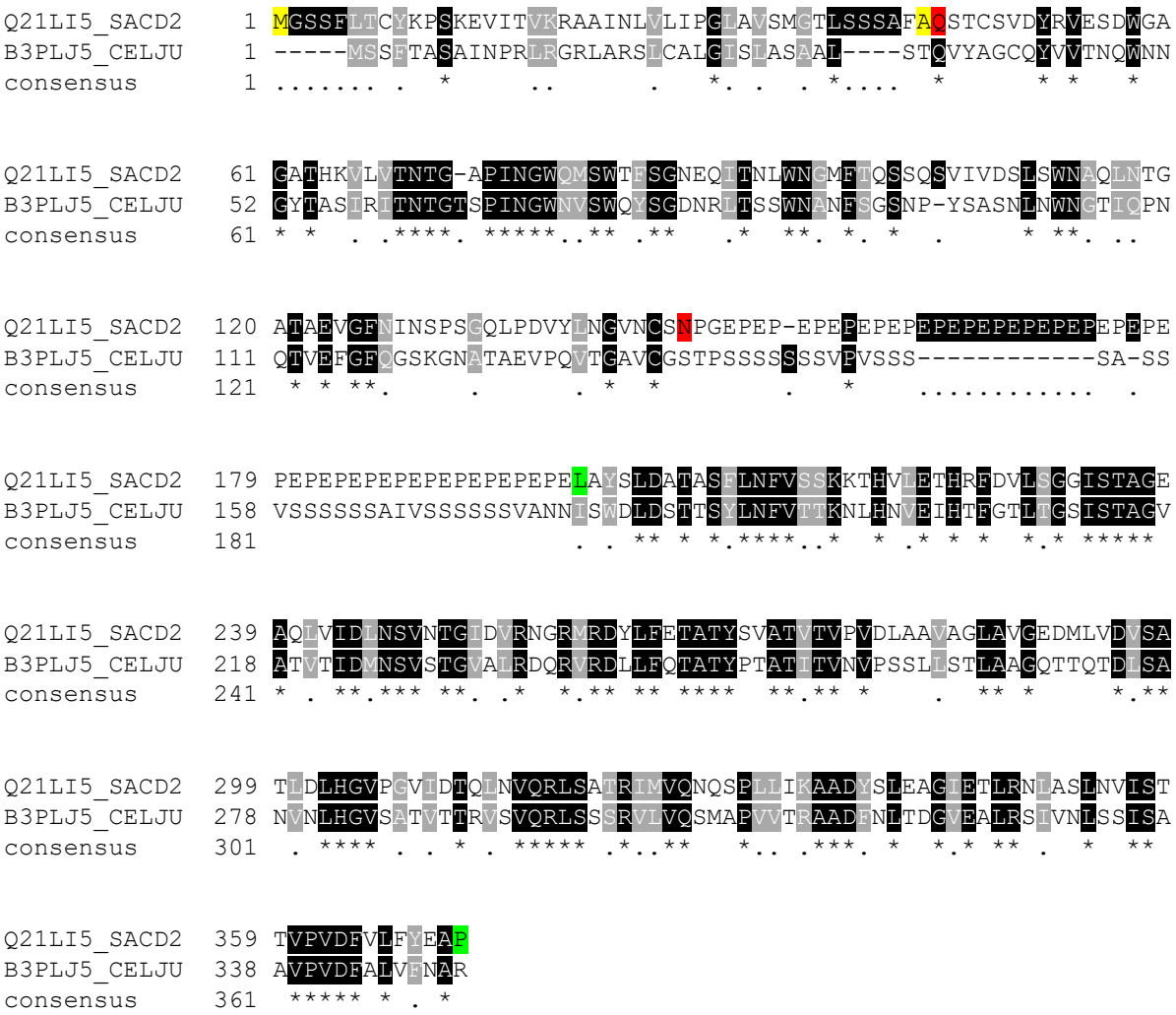

Figure 11: Multiple sequence alignment shown in PEARSON/FASTA format. Clustal Omega was used to carry out the alignments of LapA (Uniprot ID Q21L15_SACD2) and Cbp2E (Uniprot ID B3PLJ5_CELJU). The figure was made using BOXSHADE from ExPASy (https://embnet.vital-it.ch/software/BOX_form.html). The amino acids are marked according to the level of similarity; marked in black, with a * underneath indicates identical amino acids, marked in grey with a · underneath indicates amino acids with similar properties (chemical, structural) The color indicates domains, with the first and second of each color indicating the beginning and end of the domain, respectively. Yellow indicates signal peptide, red indicates CBM2 and green indicates YceI.

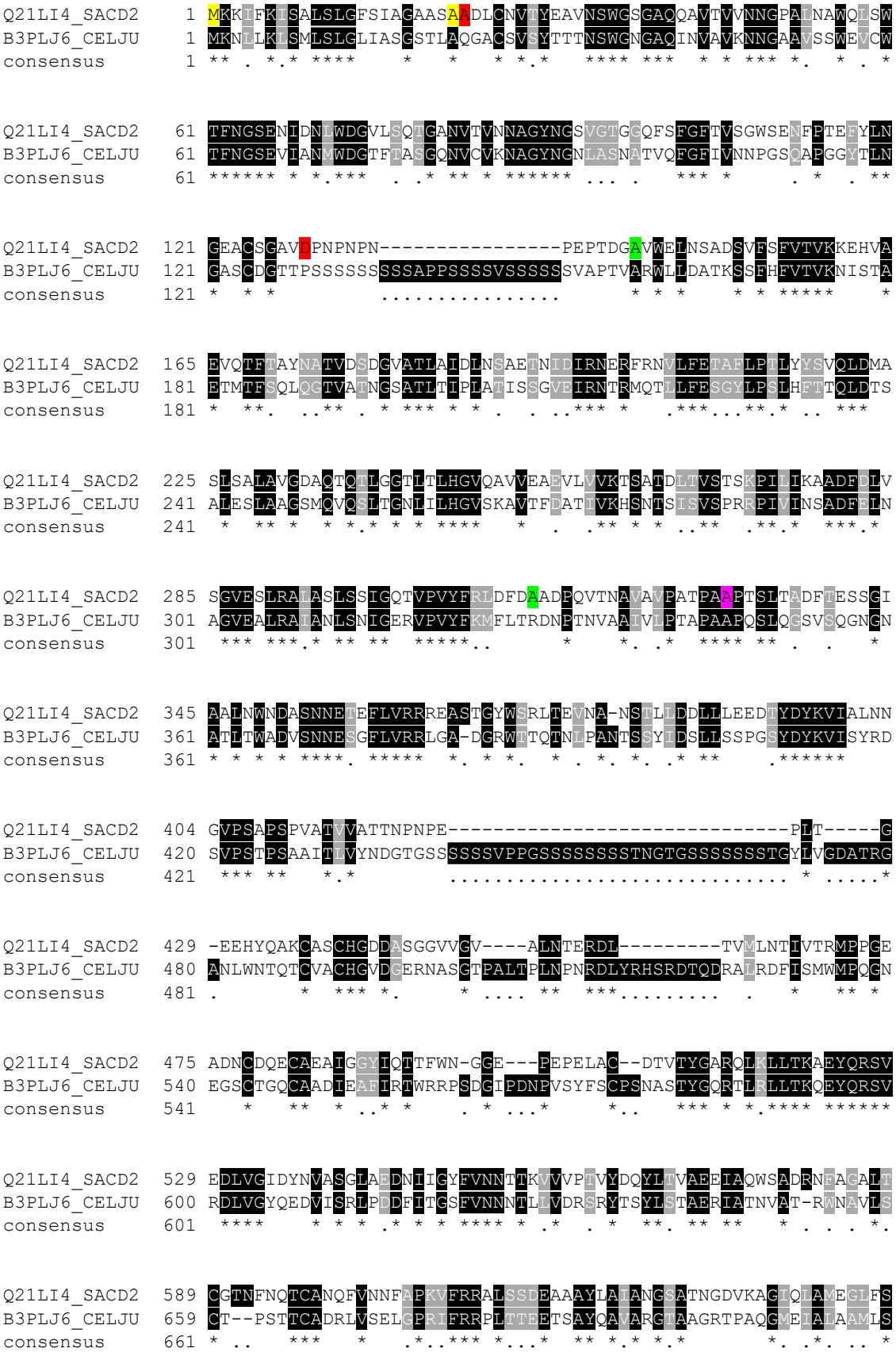

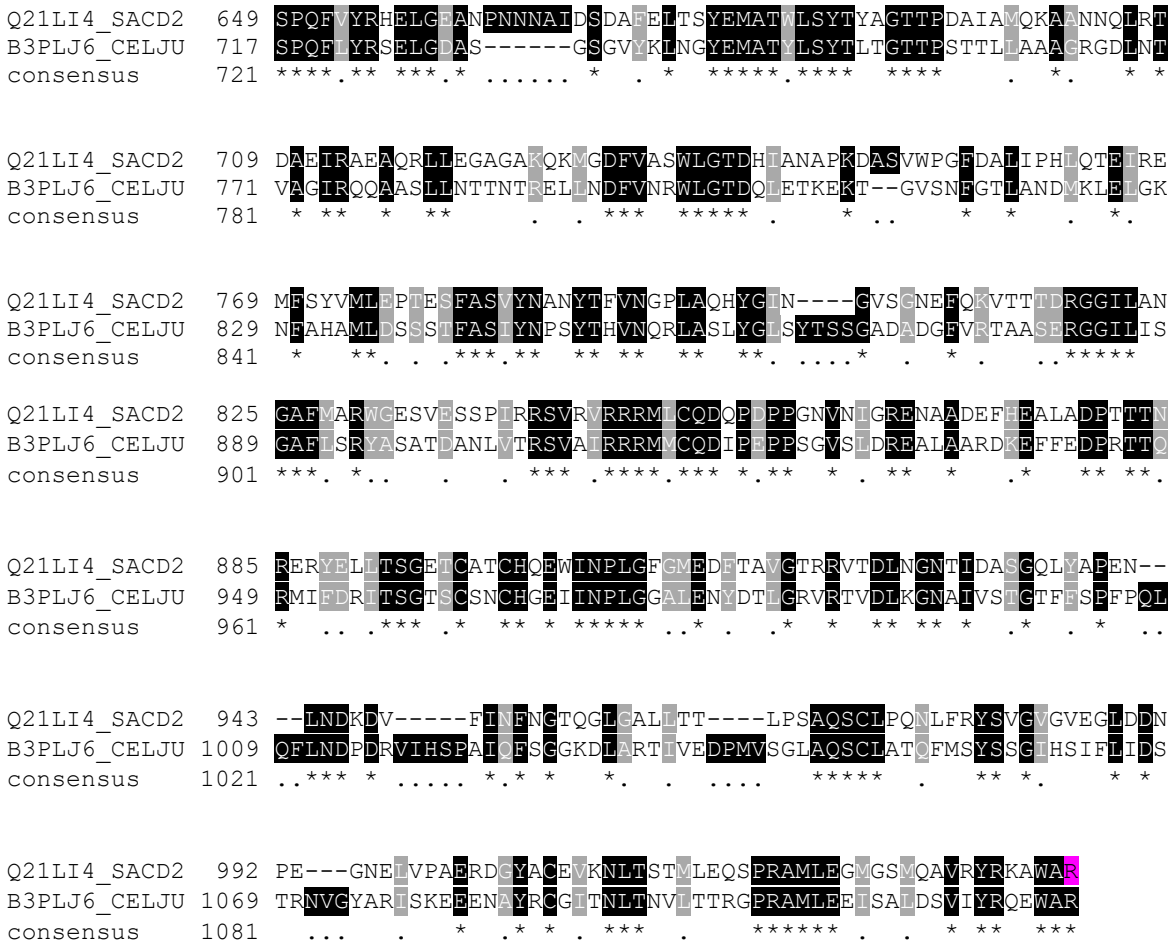

Figure 12: Multiple sequence alignment shown in PEARSON/FASTA format. Clustal Omega was used to carry out the alignments of LapB (Uniprot ID Q21L14_SACD2) and Cbp2E (Uniprot ID B3PLJ6_CELJU). The figure was made using BOXSHADE from ExPASy (https://embnet.vital-it.ch/software/BOX_form.html). The amino acids are marked according to the level of similarity; marked in black, with a * underneath indicates identical amino acids, marked in grey with a · underneath indicates amino acids with similar properties (chemical, structural). The color indicates domains, with the first and second of each color indicating the beginning and end of the domain, respectively. Yellow indicates signal peptide, red indicates CBM2, green indicates YceI and purple indicates multiple cytochrome-containing domain.

4.2. CLONING, PRODUCTION AND PURIFICATION OF PROTEINS

4.2.1. CLONING OF GENES ENCODING LPMO, LapA AND LapB FROM *S. degradans*

Linearized cloning vectors were successfully produced by PCR and purified via agarose gel electrophoresis, before being extracted from this gel (see section 3.2.2.). The PRSET B vector was cut with restriction enzyme HindIII, before being split into two fractions, one of which was cut with BsmI and one of which was cut with NdeI. pNIC-CH vector encoding a C-terminal

His-tag was linearized with BfuA restriction endonuclease, followed by a T4 DNA polymerase treatment.

Prior to cloning, the genes encoding *S. degradans* LPMO, LapA and LapB were optimized for *E. coli* expression. Cloning primers were designed to generate gene fragments in total nine protein variants, as outlined in **Table 7**. These variants were constructed to contain different domain combinations so that the function of each domain could be investigated. Using the synthetic full-length genes as templates, PCR was used to generate the nine gene fragments which were then inserted into the vector fragments, as described in sections 3.2.4. and 3.2.5. After cloning the LPMO constructs into the pRSET B vector for periplasmic expression using In-Fusion cloning and the LapA and B variants into the pNIC-CH vector for intracellular expression using a LIC protocol, the vectors were transformed into *E. coli* TOP10 competent cells. Colony PCR was performed to identify positive clones (**Figure 13**), after which vectors with inserts were purified for verification of the insert sequences. All sequencing results showed expected sequences, which means that all nine variants were successfully inserted into the expression vectors. The sequenced vectors were subsequently transformed into the *E. coli* BL21 (DE3) Star expression strain.

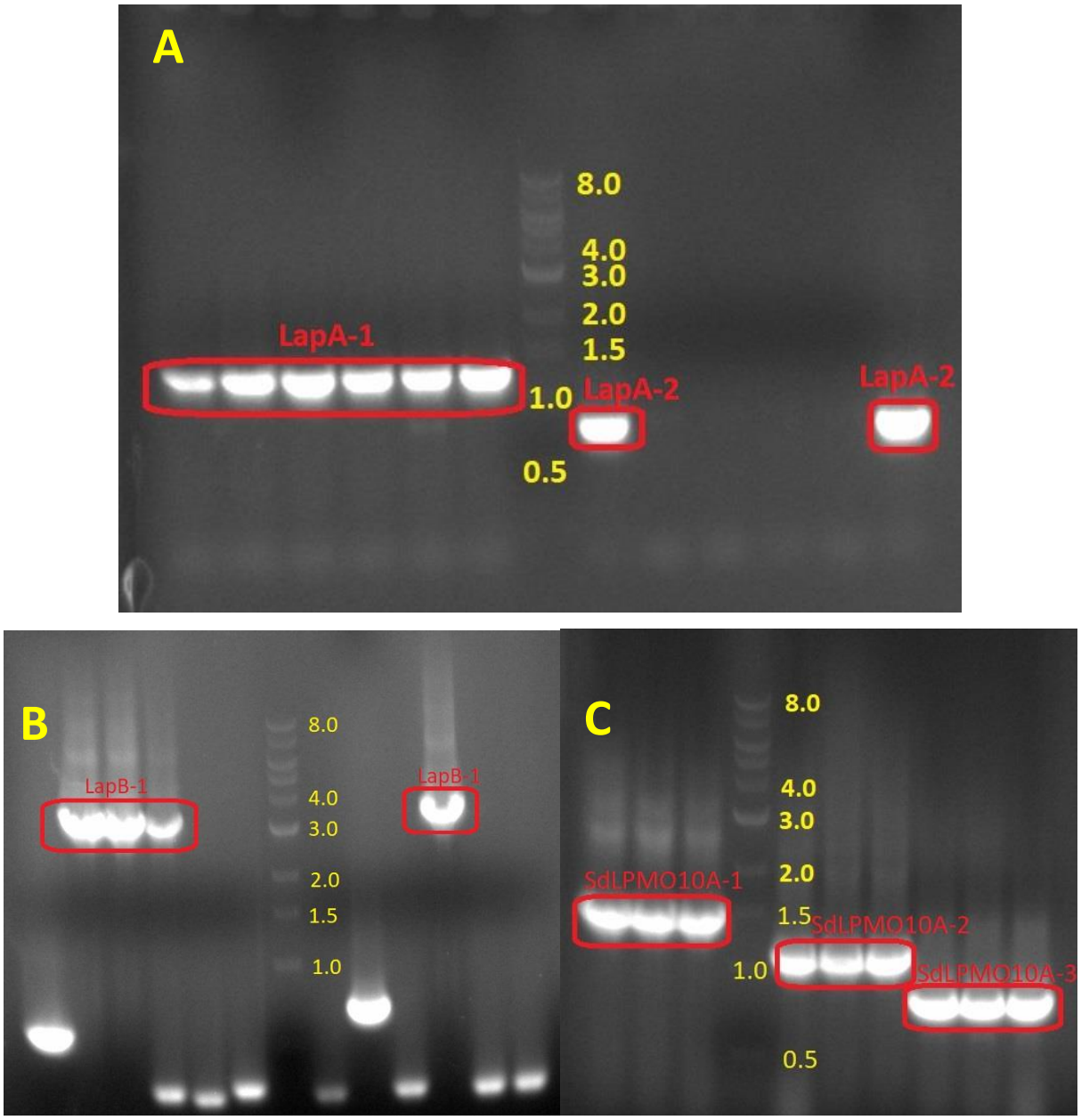

Figure 13: Agarose gel electrophoresis of products from colony PCR. Molecular weight markers were used to determine size of fragments. Band sizes for the molecular weight markers are written as kilobase-pairs (kbp) in yellow, next to the marker. Bands which represent the correct gene fragments are marked with a red box. A) LapA-1 (left, 984 bp) and LapA-2 (right, 519 bp), in which all six parallels were successful for LapA-1, but only two were successful for LapA-2. B) LapB-1 (3063 bp), in which a total of four parallels were successful. C) All three of the *Sd*LPMO10A-variants, with all three parallels successful, and showing (from the left) *Sd*LPMO10A-1 (1311 bp), *Sd*LPMO10A-2 (963 bp) and *Sd*LPMO10A-3 (669 bp).

4.2.2. PROTEIN EXPRESSION

All LPMO variants and full-length variants of LapA and LapB could be expressed successfully, along with LapB-2 (**Table 7**). The other truncated versions of LapA and B did not express under

the tested conditions. Expression of the LPMO variants was achieved using the *E. coli* BL21 (DE3) Star expression strain grown in LB/Ampicillin medium overnight at 30 °C, 200 rpm. LapA-1 as well as LapB-1 and LapB-2 were successfully expressed using the *E. coli* BL21 (DE3) Star expression strain grown in TB/Ampicillin medium in a Harbinger system at 37 °C until IPTG induction, and then overnight at 22 °C. In all cases, gene expression was induced by adding 0,1 mM IPTG (final concentration) at OD_{600}≈0,6. Thus in total, six proteins were successfully expressed.

Table 7: Overview of variants produced in this study showing the names of protein variants, the domain structures of each variant, the theoretical molecular weight, as well as expression success and methods used to purify each variant.

Protein name	Domains	Theoretical molecular weight (kDa)	Expression success	Purification methods
*Sd*LPMO10A-1 (full-length)	AA10-UKD-CBM2	43.8	Yes	IEX, SEC
*Sd*LPMO10A-2	AA10-UKD	31.8	Yes	IEX, SEC
*Sd*LPMO10A-3	AA10	22.2	Yes	IEX, SEC
LapA-1 (full-length)	CBM-YceI	35.3	Yes	IMAC, IEX
LapA-2	YceI	18.5	No	-
LapB-1 (full-length)	CBM-YceI-CYT	109.9	Yes – inclusion bodies	Denaturing/refolding, IMAC
LapB-2	CBM-YceI	30.8	Yes – inclusion bodies	Denaturing/refolding, IMAC
LapB-3	YceI	18.4	No	-
LapB-4	CYT	77.6	No	-

4.2.3. PROTEIN PRODUCTION AND PURIFICATION

4.2.3.1. Production and purification of Sd*LPMO10A*

All three variants of *Sd*LPMO10A underwent successful periplasmic extraction from *E. coli* cells performed as described in section 3.2.5.3. **Figure 14** shows an SDS-PAGE analysis of a typical periplasmic extract.

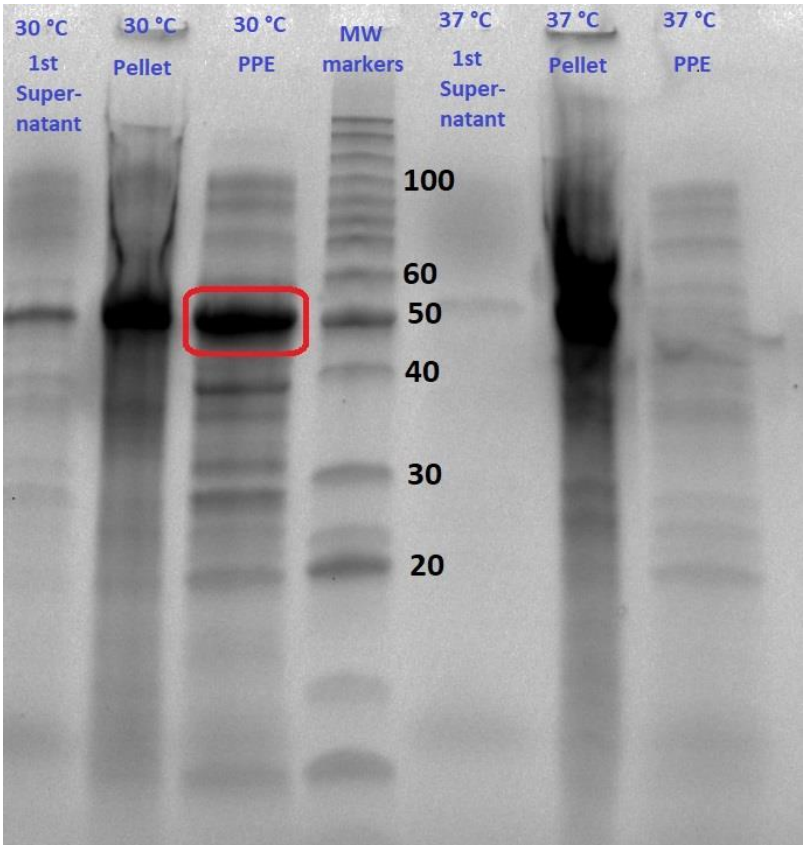

Figure 14: SDS-PAGE showing fractions obtained during production of periplasmic extract (PPE) of the full-length *Sd*LPMO10A protein tested at 30 °C (left samples) and 37 °C (right samples). In addition to the PPE (final supernatant), the supernatants from the first centrifugation as well as the pellets from the final centrifugation are also shown (see section 3.2.5.3.). Molecular weight (MW) markers were used to determine size of bands. Band sizes for the molecular weight markers are written as kiloDaltons (kDa) in black, next to the marker. The band containing *Sd*LPMO10A-1 is marked with a red box. Theoretical molecular weight of *Sd*LPMO10A-1 is 43.8 kDa.

The LPMO was purified from the PPE by IEX chromatography and SEC as described in section 3.2.5.4. IEX was performed using a HiTrap^{TM} DEAE column, with a gradient of 0-100 % buffer B (containing 1 M NaCl) over the course of 50 min for all three versions of *Sd*LPMO10A. **Appendix 2A** shows a typical ion exchange chromatogram, obtained for purification of *Sd*LPMO10A-1. Elution happened at about 30-40 % buffer B for *Sd*LPMO10A-1, about 35-40 % for *Sd*LPMO10A-2 and about 30-35 % for *Sd*LPMO10A-3. SEC was performed using HiLoad 16/600 Superdex 75 pg column, with 1 ml/min flow rate. **Appendix 2B** shows a typical size exclusion chromatogram, obtained for purification of *Sd*LPMO10A-1. Elution happened at 55-65 ml for the full-length LPMO**,** 60-65 ml for *Sd*LPMO10A-2, and 69-78 ml for *Sd*LPMO10A-3. Fractions were analyzed by SDS-PAGE gel electrophoresis as explained in section 3.2.5.4. for both chromatography methods. **Figure 15** shows the SDS-PAGE gels performed on products from IEX and SEC for the full length LPMO. The *Sd*LPMO10A full

length showed an extra band on the gels, as seen in **Figure 15B**. *Sd*LPMO10A-1 was therefore tested by band intensity comparison, which indicated that the protein was purified to 90 % purity. Neither *Sd*LPMO10A-2 or -3 showed this extra band. After the purification, all variants were concentrated down to about 2 ml, before subsequently being stored at 4 °C, in 50 mM TrisHCl, pH =8.0, as described in section 3.2.5.4.

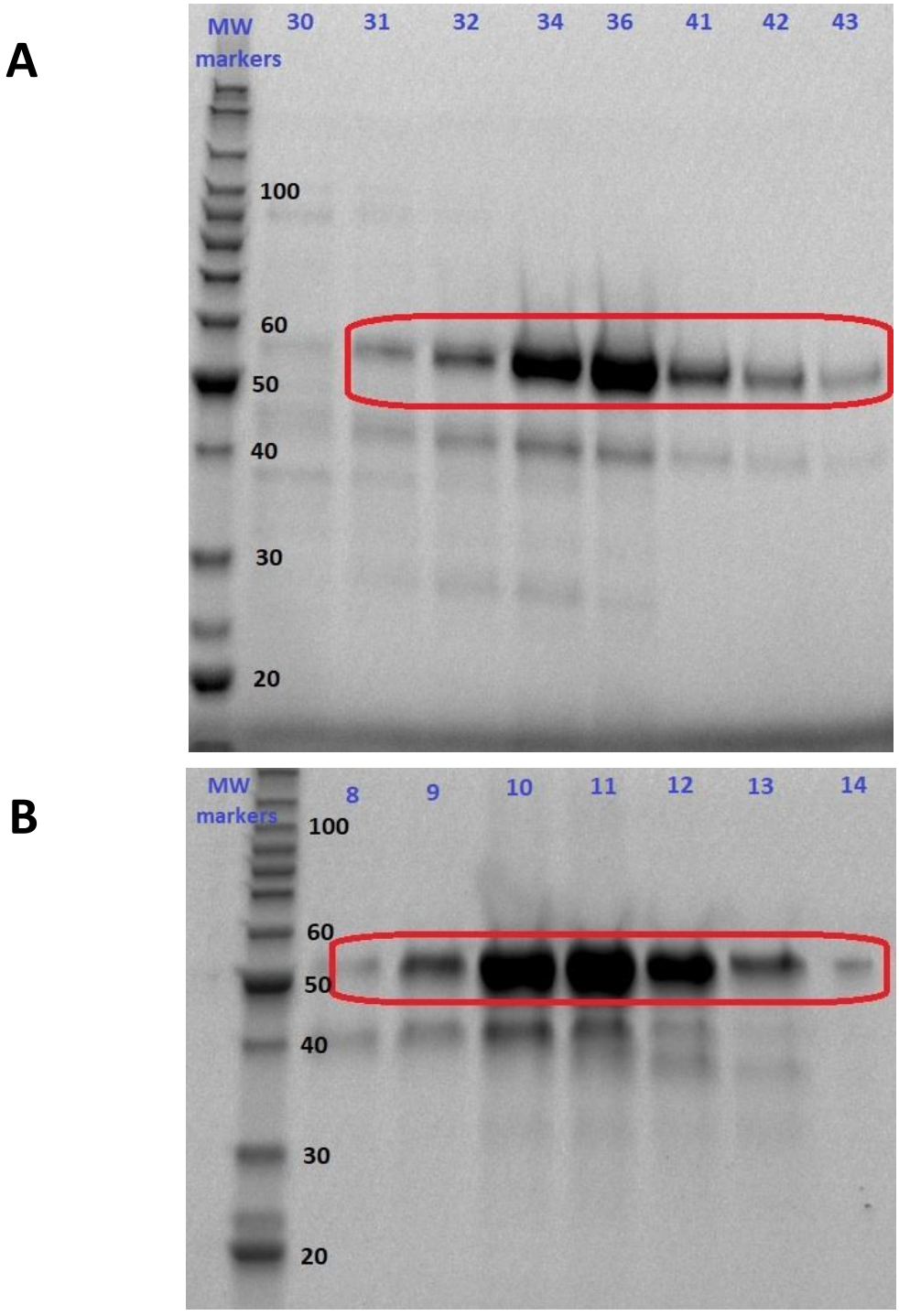

Figure 15: SDS-PAGE showing purification of *Sd*LPMO10A. Molecular weight (MW) markers were used to determine size of bands. Band sizes for the molecular weight markers are written as kiloDaltons (kDa) in black,

next to the marker. The bands containing *Sd*LPMO10A-1 are marked with a red box. Theoretical molecular weight of *Sd*LPMO10A-1 is 43.8 kDa. See **Appendix 2** for chromatograms for IEX and SEC runs of *Sd*LPMO10A-1. A) SDS-PAGE gel showing fractions from IEX of full-length *Sd*LPMO10A. The top numbers represent fraction numbers of the fraction collector for the IEX. Fraction 32-43 were pooled and further purified by SEC. B) SDS-PAGE gel showing fractions from SEC of full-length *Sd*LPMO10A. The top numbers represent fraction numbers of the fraction collector for the SEC. Fraction 8-13 were pooled and concentrated.

4.2.3.2. Production and purification of LapA-1, LapB-1 and LapB-2

The LapA and LapB variants were expressed with a C-terminal His-tag using the pNIC-CH vector for intracellular expression. To check for solubility of the proteins after cell harvest, BugBuster® lysis was performed as described in section 3.2.4.3. After SDS-PAGE analysis, LapA-1 was detected in the soluble fraction, and was successfully extracted from the *E. coli* cells by adding lysozyme, DNAse I and PMSF, followed by crushing the cells with a microfluidizer (section 3.2.4.3.). However, BugBuster® lysis and microfluidizer extraction of LapB-1 and LapB-2 did not result in soluble protein, and the proteins were only found in the insoluble fractions shown in **Figure 16**. For that reason, the proteins were denatured, refolded and dialyzed as described in section 3.2.4.4., in order to solubilize the proteins (**Figure 17**). Post-denaturing and refolding, bands were visible in the expected area. **Figure 17A** shows bands of LapB-1 and LapB-2 close to their theoretical molecular weights of 109.9 kDa, and 30.8 kDa, respectively. The bands are, however, not easily detected, and they appear smeared. **Figure 17B** shows that after dialysis, the bands were more distinguished and were still located in the expected area of the SDS-PAGE gel. This indicates that the denaturing, refolding and dialysis procedure was successful.

A

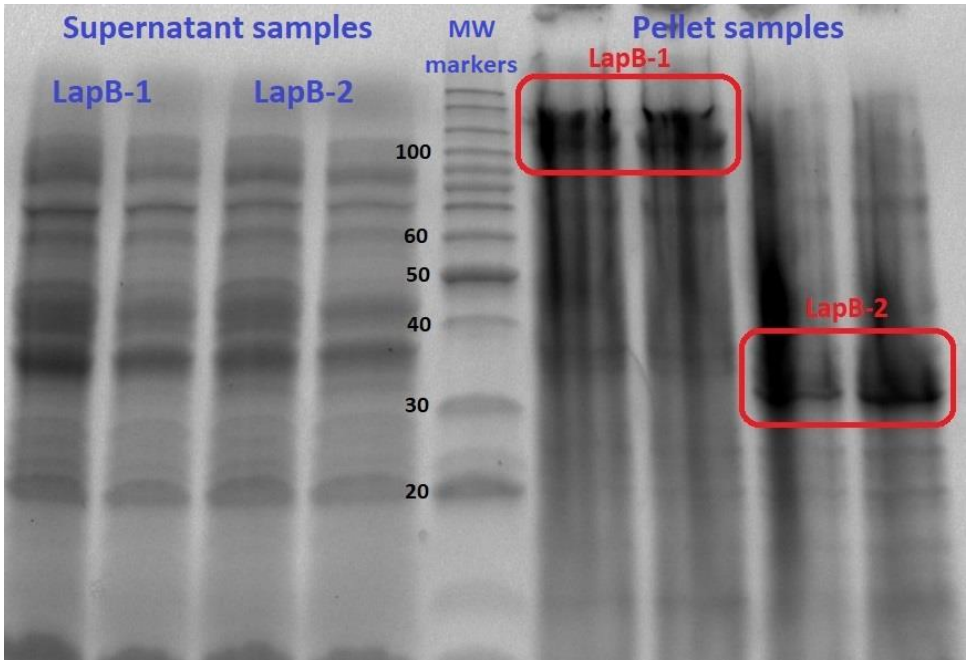

B

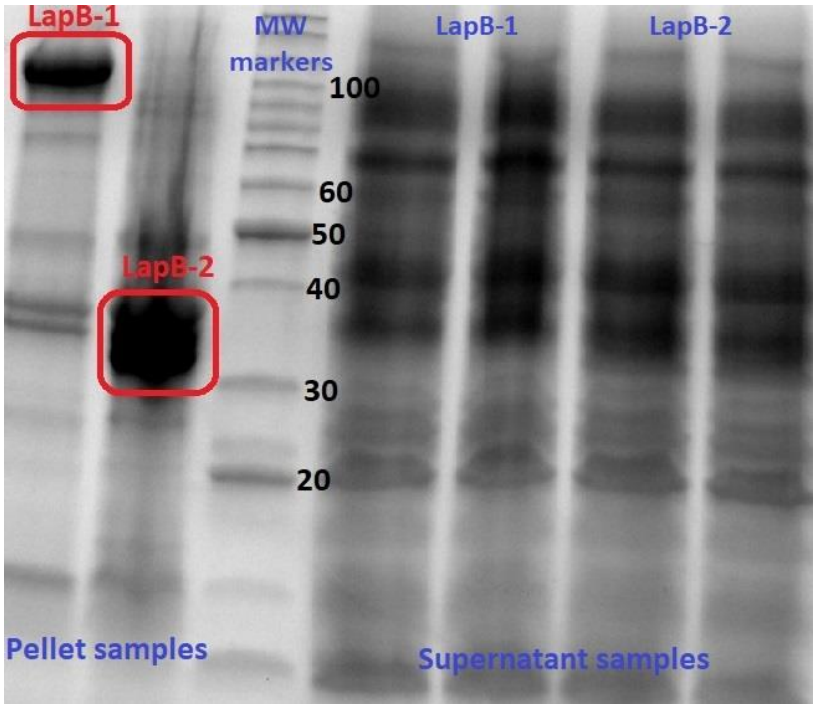

Figure 16: SDS-PAGE gels showing samples taken after solubilization analyses had been performed for LapB-1 and LapB-2. Samples were taken from both pellets and supernatants. Molecular weight (MW) markers were used to determine size of bands. Band sizes for the molecular weight markers are written as kiloDaltons (kDa) in black, next to the marker. The bands containing LapB-1 and LapB-2 are marked with red boxes. The theoretical molecular weight of LapB-1 is 109,9 kDa, while LapB-2 is 30,8 kDa. A) Pellet- and supernatant samples taken after BugBuster® lysis had been performed on *E. coli* cells containing LapB-1 and LapB-2. The soluble proteins are shown on the left-hand side of the ladder, while the insoluble proteins that remain in the pellet are shown on the right-hand side of the gel. B) SDS-PAGE of soluble and insoluble fractions after cell lysis using a microfluidizer. The insoluble proteins in the pellet are shown to the left of the benchmark ladder, while the supernatants are shown to the right.

A

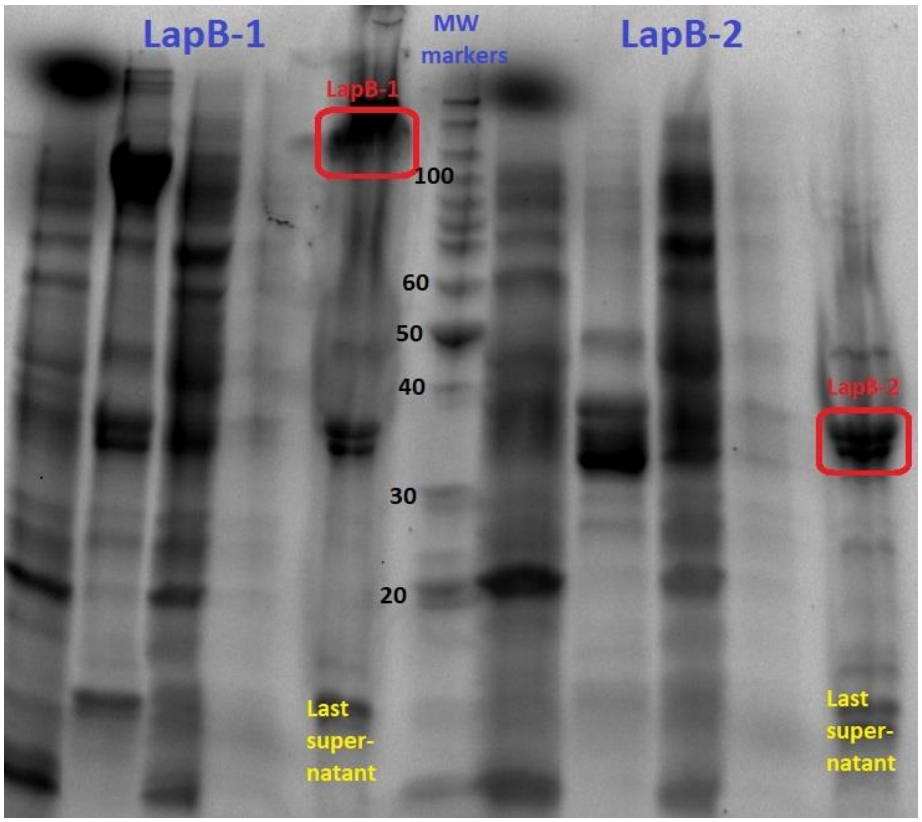

B

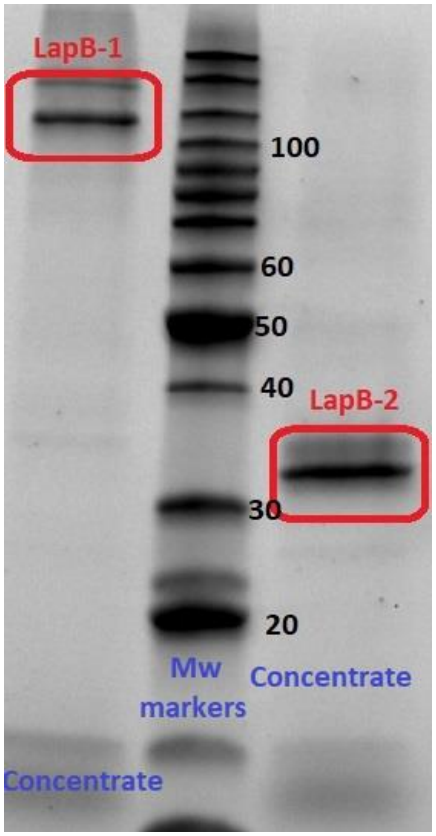

Figure 17: SDS-PAGE gels for LapB- 1 and LapB-2 in the process of denaturing and refolding the proteins. Molecular weight (MW) markers were used to determine size of bands. Band sizes for the molecular weight markers are written as kiloDaltons (kDa) in black, next to the marker. The theoretical molecular weight of LapB-1 is 109,9 kDa, while LapB-2 is 30,8 kDa. A) Post denaturing and refolding of LapB-1 and LapB-2. The protein

circled in red was the supernatant used for dialysis, for both LapB-1 (left) and LapB-2 (right). The other wells show samples taken during the denaturing and refolding process in order to control protein location. B) SDS-PAGE gel of concentrated protein-solutions for LapB-1 and LapB-2 from the dialysis (section 3.2.4.4.). Full-length LapB is shown to the left of the MW markers, and LapB-2 to the right, both circled in red.

The pNIC-CH vector was used due to its C-terminal His-tag, which means that LapA-1, LapB-1 and LapB-2 could be purified based on this His-tag. Therefore, immobilized metal affinity chromatography (IMAC) was used to purify these proteins, according to section 3.2.4.5. A gradient of 0-50 % buffer B (500 mM imidazole) over 50 min was used, with a flow rate of 1.5 ml/min. The proteins eluted at 12-28 % conductivity for LapA-1 and 30-50 % conductivity for LapB-1 and LapB-2. **Figure 18** shows an SDS-PAGE gel of the fractions collected for IMAC purification of LapA-1. The proteins were not completely pure after the IMAC purification and were therefore further purified by IEX. A gradient of 0-50 % buffer B (500 mM NaCl) over 50 min was used, with a flow rate of 2 ml/min. LapA-1 eluted at 25-32 % conductivity, while LapB-1 and LapB-2 eluted at 40-50 % conductivity. After the purification, LapA-1, LapB-1, and LapB-2 were concentrated down to about 2 ml, before subsequently being stored at 4 °C, in 50 mM TrisHCl, pH =7.5 as described in section 3.2.4.5. Purified LapA-1 and LapB-1 can be seen in **Figure 19** (section 4.2.4.).

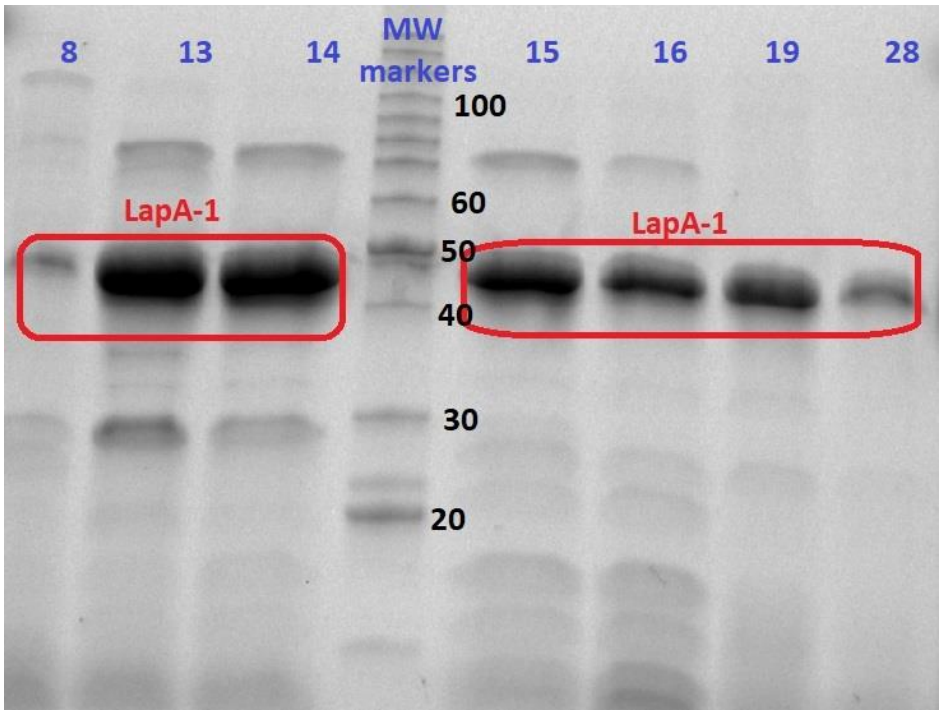

Figure 18: SDS-PAGE gel of IMAC results for LapA-1. The blue numbers represent fraction numbers of the IMAC fraction collector. Molecular weight (MW) markers were used to determine size of bands. Band sizes for the molecular weight markers are written as kiloDaltons (kDa) in black, next to the marker. Bands containing LapA-1 are marked with a red box. The theoretical molecular weight of LapA-1 is 35,3 kDa.

As mentioned in section 4.1., the YceI-domain found in LapA-1, LapB-1 and LapB-2 contains an isoprenoid ligand that can vary in type. LapA-1 and LapB-1 was therefore tested with MALDI-TOF MS (section 3.2.6.) in order to assess the presence and nature of the isoprenoid ligand. LapB-1 is a large protein of 109.9 kDa. Therefore, mass spectrometry measurements of LapB-1 was far outside the calibrated range of the MALDI-TOF MS and could not be trusted. Measurements done for LapA-1, on the other hand, was inside the calibrated range of the MS. However, the results of the MS analysis of LapA-1 assigned a higher molecular mass to the protein than the theoretical mass, regardless of which of the isoprenoid units, ubiquinone-8 or octaprenyl pyrophosphate, was used to calculate the theoretical mass.

4.2.4. MOLECULAR WEIGHT INVESTIGATION OF SdLPMO10A AND LapA-1

Figure 19 shows samples from four of the purified proteins; SdLPMO10A-1, SdLPMO10A-3, LapA-1 and LapB-1. Unexpectedly, *Sd*LPMO10A-1, -2 and -3, as well as full-length LapA showed higher molecular weight on the SDS-PAGE gel compared to the theoretical mass. All four proteins appeared to be approximately 10 kDa bigger than their theoretical mass. For example, *Sd*LPMO10A-1 seemed to be at a little over 50 kDa on the gel, while its theoretical mass is 43,8 kDa. SdLPMO10A was analyzed for oxidative activity to verify protein identity (see section 4.4.). However, since the activity of LapA is still unknown, an activity assay was not an option. For that reason, trypsination followed by mass spectrometry-based analysis of the generated protein fragments was performed as described in section 3.2.6., to verify the protein sequence of LapA-1. Trypsin was used to digest LapA-1 into peptides that could be analyzed accurately by the mass spectrometer. Trypsin cleaves C-terminal to arginine or lysine, giving characteristic theoretical peptide sizes based on protein sequence (Aebersold & Mann, 2003; Olsen et al., 2004). These theoretical peptide sizes for LapA-1 corresponded with masses

found by the mass spectrometer and MS-MS analysis of the peptides, which indicated that the protein had the correct sequence, and was indeed LapA-1.

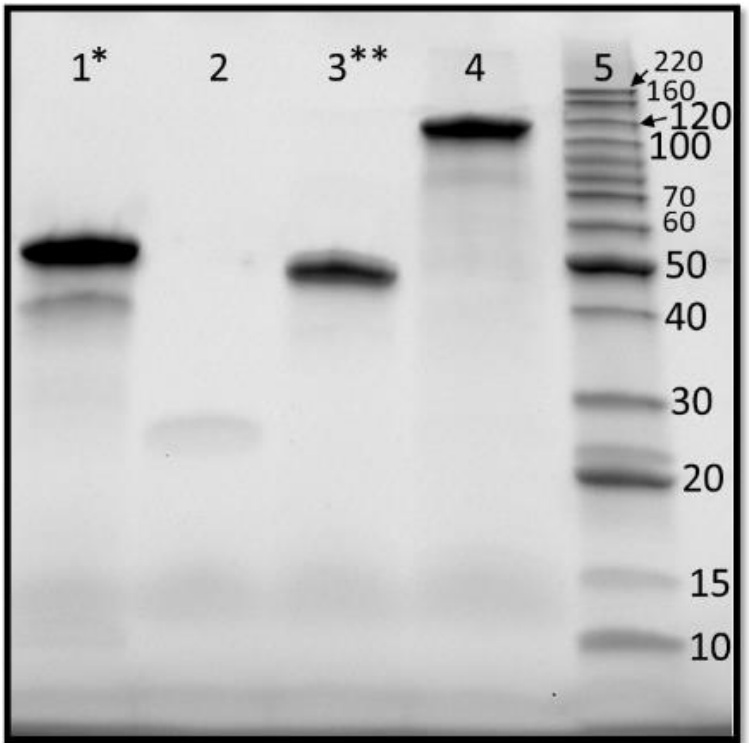

Figure 19: SDS-PAGE of purified 1) *Sd*LPMO10A-1 (43.8 kDa); 2) *Sd*LPMO10A-3 (22.2 kDa); 3) LapA-1 (35.3 kDa); 4) LapB-1 (109.9 kDa); and 5) BenchMarkTM ladder. *Sd*LPMO10A-1 was identified by analyzing for oxidative activity (section 3.2.8.1.). LapA-1 was identified by proteomics analysis (section 3.2.6.). *Sd*LPMO10A-1, *Sd*LPMO10A-3 and LapA-1 show higher than expected molecular weight.

4.3. BINDING TO CELLULOSE BY *Sd*LPMO10A, LapA-1, LapB-1 AND LapB-2

All three variants of *Sd*LPMO10A along with LapA-1, LapB-1 and LapB-2 were tested for substrate binding to Avicel. Each protein was added to sodium phosphate solutions at pH =6.0 which contained Avicel (see section 3.2.7.). Upon incubation, samples were filtrated and the protein concentration in the filtrates (= unbound protein) was determined using A_{280} spectrophotometry. **Figure 20** shows the binding assay results for all three variants of *Sd*LPMO10A, as well as for LapA-1 and LapB-2. BSA was used as a control protein as it is a well-studied protein with low binding to Avicel at this pH (Cai & Arntfield, 1997; Imeson et al., 1977). LapA-1 and *Sd*LPMO10A-1 showed significant affinity for Avicel. *Sd*LPMO10A-2 and -3 showed no binding. This indicates that the CBM2 in *Sd*LPMO10A-1 is a functional binding module, since neither of the variants without this domain showed binding. This result was as expected for type 3, as it does not have any additional domains, other than the AA10

domain. *Sd*LPMO10A-2, on the other hand, does have what seems to be an additional domain. As this protein variant did not show any binding to Avicel, it seems unlikely that this domain is a cellulose targeting CBM.

LapB-1 (not shown) and -2 (**Figure 20**) did not show Avicel binding, even though these proteins are supposed to contain a CBM2. This might be an indication that the proteins were not correctly refolded during the denature/refolding and dialysis process. Another indication that LapB was not correctly folded is that no color was observed for the full-length LapB, which is a typical feature for heme-binding proteins such as cytochrome containing proteins (**Figure 9**, section 1.6.).

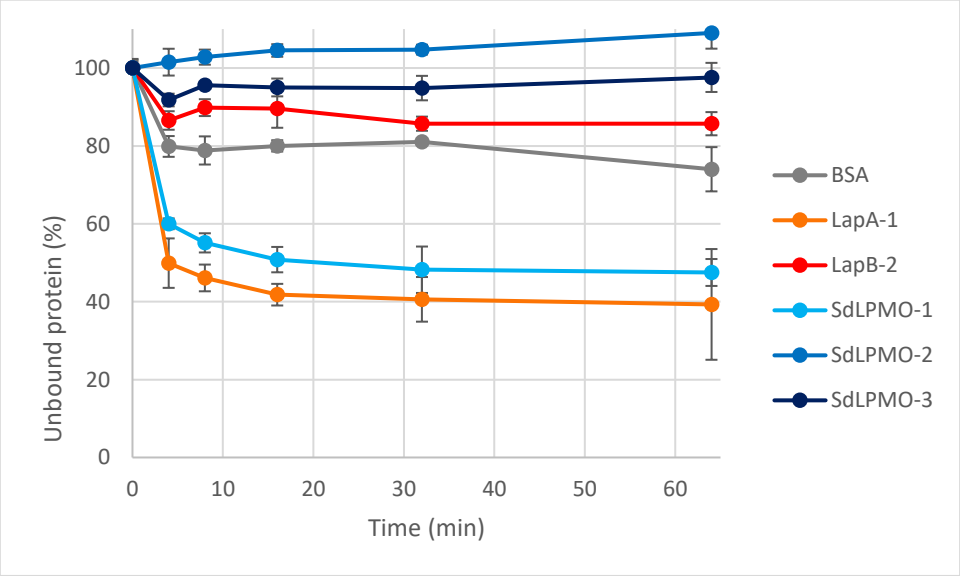

Figure 20: Binding assay for LapA (orange), LapB-2 (red) and the three versions of *Sd*LPMO10A (different shades of blue) to the substrate Avicel. BSA (grey) was used as a negative control. A_{280} measurements used to calculate average values and standard deviations used in the graph can be found in **Appendix 3**.

4.4. CHARACTERIZATION OF *Sd*LPMO10A

4.4.1. APPARENT MELTING TEMPERATURE OF *Sd*LPMO10A VARIANTS

All three versions of the SdLPMO10A were subject to melting temperature assays, as described in section 3.2.9. Each version was tested as *holo*- (i.e. bound to the Cu(II) cofactor) and as *apo*- (i.e. without the cofactor) enzyme. To chelate the copper from the enzyme, EDTA was used directly in the reaction in a concentration of 10 mM. *Sc*LPMO10C, a well-studied LPMO from *Streptomyces coelicolor* (Forsberg et al., 2011; Forsberg et al., 2014; Jensen et al., 2019) with

an apparent melting temperature (Tm) of 64 °C (based on findings by (Jensen et al., 2019)), was used as a positive control to see that the method set up worked optimally (**Figure 21A**). Apparent melting temperatures for *holo* forms of *Sd*LPMO10A-1, *Sd*LPMO10A-2 and *Sd*LPMO10A-3 were 57 °C, 55 °C and 58 °C, respectively (**Figure 21B**, **C** and **D**). However, as seen by **Figure 21A**, the control experiment with *Sc*LPMO10C showed an apparent melting temperature of 57 °C, which indicates a deviation of 7 °C from previous findings.

The results indicate that all three versions have a higher melting temperature in their *holo* forms, as has been observed for other LPMOs (Hemsworth et al., 2013) (**Figure 21B, C** and **D**). As seen in **Figure 21B**, **C** and **D**, *Sd*LPMO10A-1 showed a decrease in stability when removing the copper cofactor, from approximately 57 °C as *holo* to 47 °C as *apo*. *Sd*LPMO10A-2 decreased from 55°C to 47 °C, and *Sd*LPMO10A-3 from 58 °C to 49 °C. This indicates that the copper helps stabilize the enzymes. Copper binding in the active site usually stabilize LPMOs (Hemsworth et al., 2013), which means the stabilization effect that can be seen in this assay concur with previous findings.

Interestingly, according to the melting temperature curves shown in **Figure 21**, all three *Sd*LPMO10A-variants as well as *Sc*LPMO10C show unfolding curves with similar shapes. The apparent melting temperatures of the *Sd*LPMO10A-variants are also similar. This indicates that removal of the other two domains from the AA10-domain has little effect of the temperature stability for this protein.

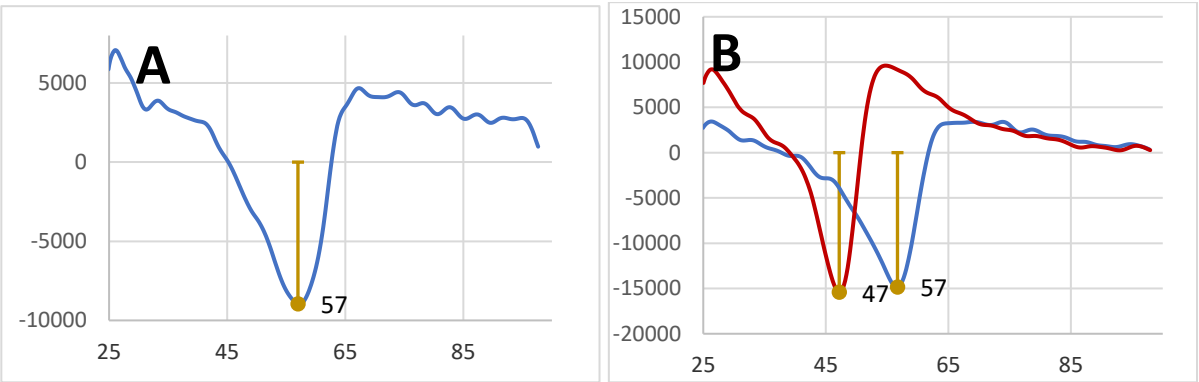

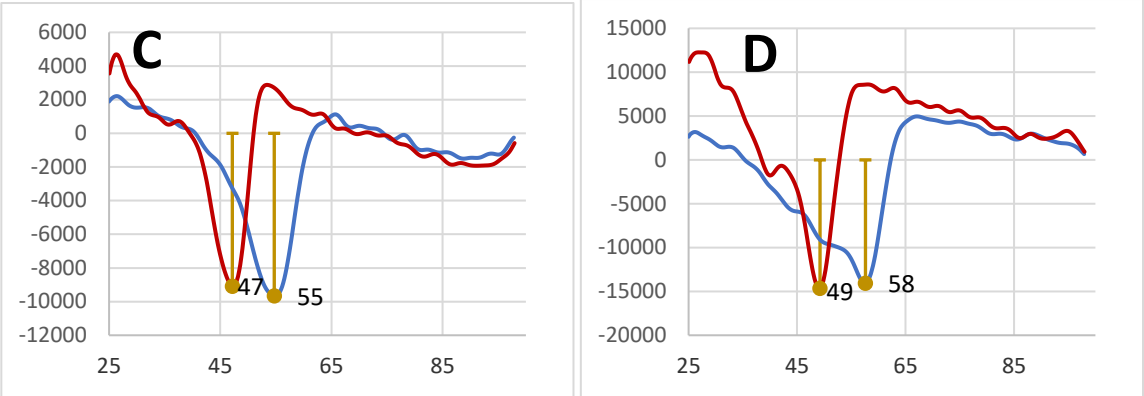

Figure 21: Melting curves for A) ScLPMO10C, B) *Sd*LPMO10A-1, C) *Sd*LPMO10A-2 and D) *Sd*LPMO10A-3. The blue graphs show the *holo* LPMOs with a bound copper ion and the red graphs show *apo* LPMOs without copper. The yellow markings indicate the apparent melting temperatures, written in °C to the right of each curve minimum. Four parallel measurements were performed, of which the average values were used to plot the graphs.

4.4.2. SUBSTRATE SPECIFICITY OF *Sd*LPMO10A

*Sd*LPMO10A-1 was tested for oxidative activity towards cellulose and chitin substrates in the presence and absence of an external electron donor (ascorbic acid). MALDI-ToF MS was used to analyze the release of oxidized products in the different LPMO reactions, as described in section 3.2.6. Only the reactions containing cellulose and ascorbic acid led to product formation. *Sd*LPMO10A-1 showed highest oxidative activity towards Avicel. *Sd*LPMO10A-1 avtivity on Avicel is shown in **Figure 22**. The MS spectrum (**Figure 22A**) shows products with a degree of polymerization (DP) of 5-8, which means products with 5-8 glucose units.

The MS shows all products as sodium adducts (complexes with sodium ions). All products also show salt signals for the sodium adducts, where one or two hydrogens of carboxyl groups have been exchanged for sodium or potassium (Coenen et al., 2007). This can be seen in the characteristic signal patterns in **Figure 22A**. The products were shown to have the molecular weight corresponding to aldonic acids. As aldonic acids have identical masses to the gemdiols with the same DP, products from C1- and C4- oxidation will have identical masses (section 1.4) (Westereng et al., 2017). However, only aldonic acids form the salts of sodium adducts (Coenen et al., 2007; Westereng et al., 2017). This means that the salts seen in the MS spectrum indicates that *Sd*LPMO10A is a C1-oxidizing LPMO.

All three *Sd*LPMO10A variants were compared based on product formation, both quantitatively (see section 4.4.4.) and qualitatively, as described in section 3.2.8.3. Qualitative HPAEC analysis was performed for the products of all three *Sd*LPMO10A variants. The product profiles are shown in **Figure 22B**. In addition to the products of 5-8 glucose units, the HPAEC analysis

also showed products of lower DP. The smaller products are, however, less frequent than the longer products (**Figure 22B**). *Sd*LPMO10A-2 and -3 showed similar product profiles as the full-length protein, although they gave lower product yields.

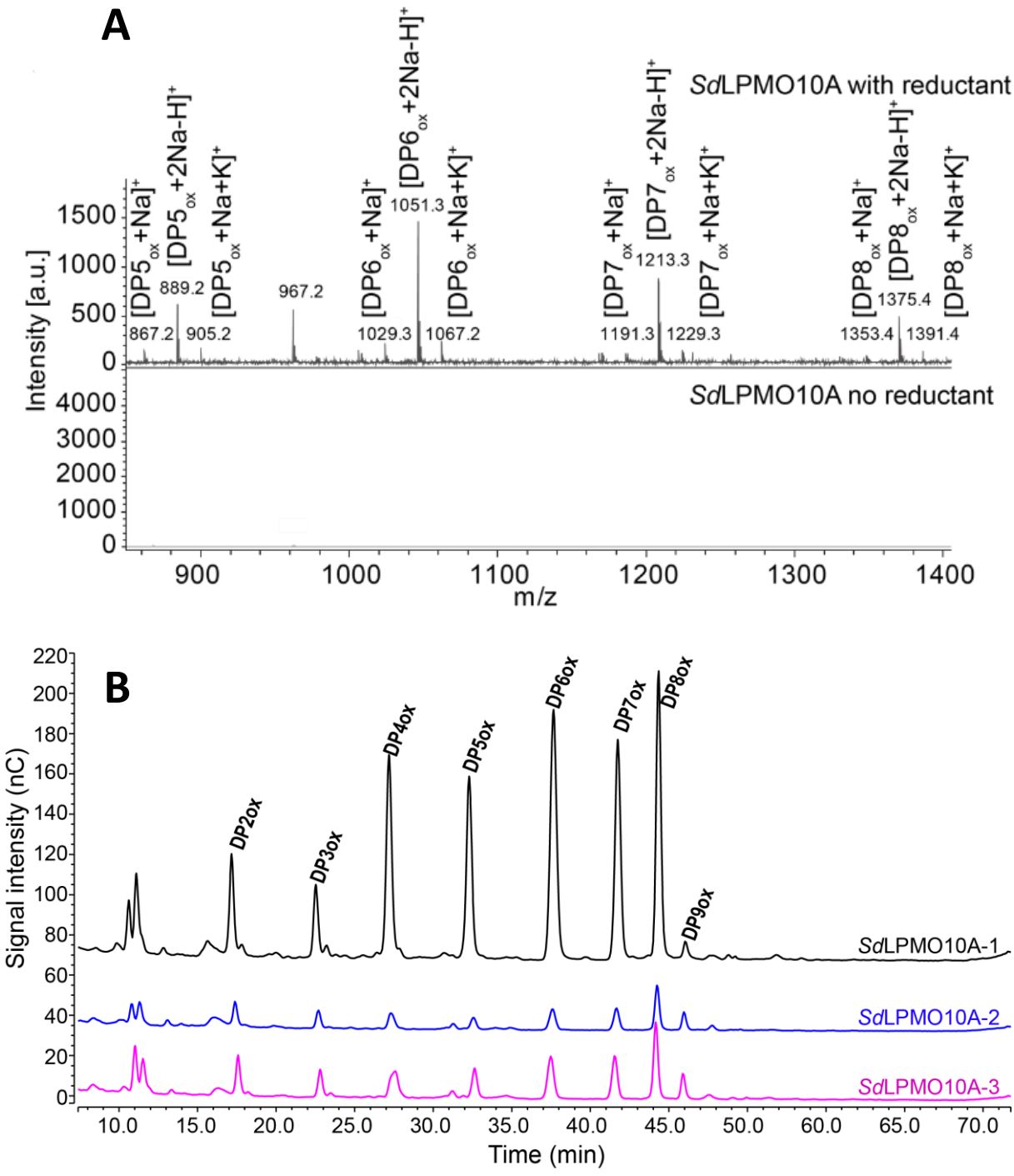

Figure 22: A) MALDI-ToF MS spectra of products generated by full-length *Sd*LPMO10A in reactions with 10 g/l Avicel, in the presence (upper spectrum) or absence (lower spectrum) of 1 mM ascorbic acid (DP = degree of polymerization). B) Overlaid HPAEC chromatograms of cello-oligosaccharides released from oxidative activity of *Sd*LPMO10A-1 (black), *Sd*LPMO10A-2 (blue) and *Sd*LPMO10A-3 (purple). The peaks are named based on

the varying sizes of the oligosaccharides they represent, e.g. DP2ox indicating a dimer of oxidized glucose. Product profile of ScLPMO10C was used for annotation of the peaks, as described by (Forsberg et al., 2014). Substrate in the reactions were 10 g/l Avicel. Concentrations of 1 mM ascorbic acid was used as reductant, and 50 mM $NaPO_4$ pH =6.0 was used as buffer.

4.4.3. OPTIMAL TEMPERATURE OF FULL-LENGTH *Sd*LPMO10A

To test the temperature-dependency of *Sd*LPMO10A activity, enzyme reactions with 10 g/l Avicel and 1 mM ascorbic acid were set up at seven different temperatures, ranging between 10 and 70 °C. Samples were taken at four time points (10, 30, 60 and 120 min) for each temperature, and these samples were filtered, after which the soluble products were degraded for 24 hours with a cellulase, glycoside hydrolase 6.1 (see section 3.2.8.3.). The glycoside hydrolase 6.1 degrades C1-oxidized cello-oligosaccharides to a mixture of C1-oxidized dimers and trimers (Jensen et al., 2018). This can be used for degradation of the products of LPMOs so that all products, also the larger chains of 4-8 units, can be quantified by measuring only two different compounds, that give large and easily quantifiable peaks in the chromatogram. The results (**Figure 23**) show that the optimal temperature for *Sd*LPMO10A is around 60 °C. At 70 °C the enzyme was almost completely inactive. This indicates that most of the enzymes are denatured at 70 °C which is in agreement with the melting temperature that was found to be 57 °C.

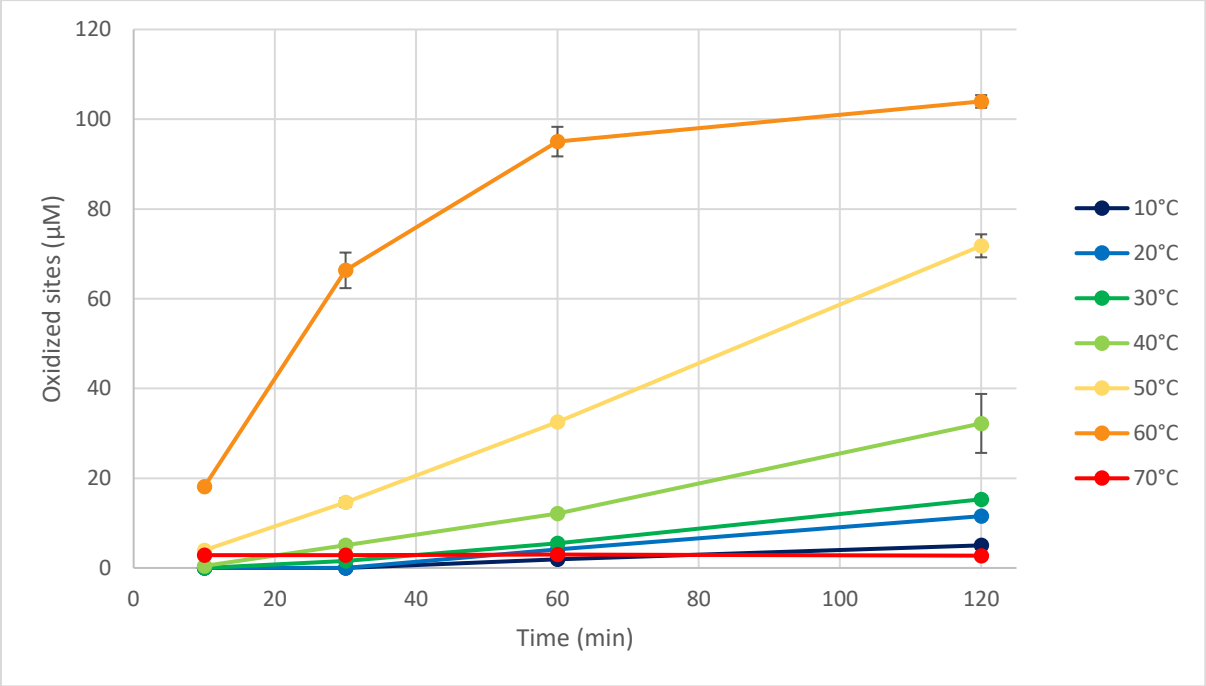

Figure 23: Product formation over time in reactions of *Sd*LPMO10A-1 (full-length) with Avicel at seven different temperatures. **Appendix 4** shows the actual product concentrations that were used to make the graph, along with standard deviations also presented in this figure. All data points are based on three parallel measurements and are

presented with standard deviations (most of which are not visible due to low variation). All reaction mixes contained 10 g/L Avicel (substrate), 1 µM enzyme, 1 mM ascorbic acid (reductant), and were performed at pH =6.0, in a ThermoMixer, at 800 rpm shaking.

4.4.4. COMPARISON OF SdLPMO10A VARIANTS

All three variants of *Sd*LPMO10A were tested for oxidizing activity on Avicel, as described in section 3.2.8.3. **Figure 24** illustrates the dimer and trimer product yields (see section 4.4.3.) of these three proteins. The samples were taken over the course of 24 hours, at time points 0.5, 1, 2, 4, ,6 and 24 hours. The full-length *Sd*LPMO10A showed the highest activity of the three variants and the product level was increasing for about four hours before ceasing and leveling out. The fully truncated version, consisting of only the AA10 domain, showed slightly higher initial activity than the full-length version, as seen from the first time point in **Figure 24**. However, this activity ceased earlier, with product amounts leveling out after only an hour. *Sd*LPMO10A-2 showed lower initial activity than the fully truncated version, and the activity completely stopped after two hours of incubation.

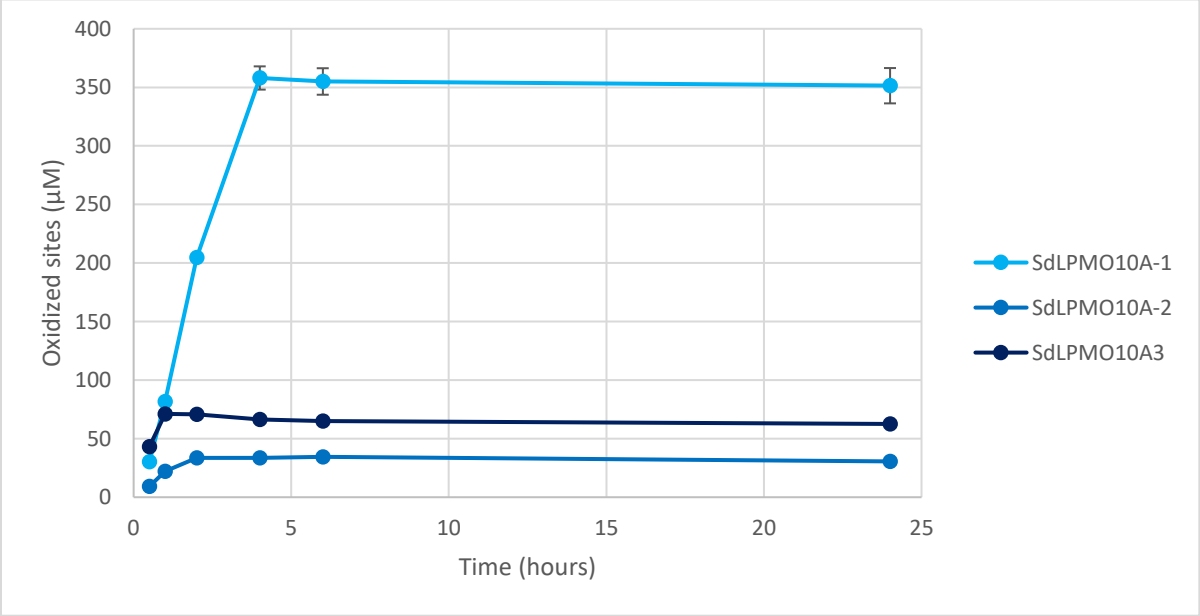

Figure 24: Oxidized product formation shown for all three variants of *Sd*LPMO10A over the course of 24 hours. **Appendix 5** shows the actual product concentrations that were used to make the graph, along with standard deviations also presented in this figure. All data points are based on three parallel measurements and are presented with standard deviations (most of which are not visible due to low variation). All reaction mixes contained 10 g/L Avicel (substrate), 1 µM enzyme, 1 mM ascorbic acid (reductant), and were performed in a 50 mM $NaPO_4$, pH =6.0 buffer. All reactions were performed at 50 °C, 800 rpm shaking in a ThermoMixer.

4.5. TESTING LapA AND B AS POTENTIAL REDOX PARTNERS FOR *Sd*LPMO10A

After testing that *Sd*LPMO10A indeed exhibited activity on cellulose, assays in combinations with LapA-1 or LapB-2 were conducted. Since LapB-1 did not show any color indication from cytochromes (see section 4.3.), it was decided to use LapB-2 instead. To see if LapA-1 or LapB-2 could reduce and/or fuel the LPMO with H_2O_2, they were added to the LPMO reaction mixtures in the presence of 100 µM ascorbic acid. This lower concentration of ascorbic acid was added in combination with LapA-1 and LapB-2 in case a priming reduction of the LPMO active site would be needed. Samples were taken for each reaction after 3, 6 and 24 hours. Product formation was quantified by HPEAC and is shown as oxidized sites in **Figure 25**. Reactions containing only the LPMO in combination with 100 µM or 1 mM ascorbic acid were used as controls.

The 1 mM ascorbic acid-containing control reaction shows a flat graph with high amounts of products already at the initial sampling time of three hours, indicating fast initial production, and subsequent inactivation of the LPMO. The reaction with lower concentration of ascorbic acid shows fewer oxidized sites at three hours, as expected. However, in this reaction the product formation was increasing throughout the experiment of 24 hours, indicating that a lower amount of ascorbic acid leads to slower inactivation of the LPMO. Therefore, the total product formation after 24 hours is higher for the reaction with 100 µM ascorbic acid, than for the reaction containing 1 mM ascorbic acid. Both reactions containing a potential redox partner, LapA-1 or LapB-2, show product formation from three to 24 hours, at a lower rate than the control reaction with the same amount of ascorbic acid. Also, the initial levels in these reactions, detected after three hours, are much lower, compared to the control reaction. This indicates that addition of LapA-1 or LapB-2 does not increase activity of *Sd*LPMO10A-1. They rather lower the product formation of the LPMO.

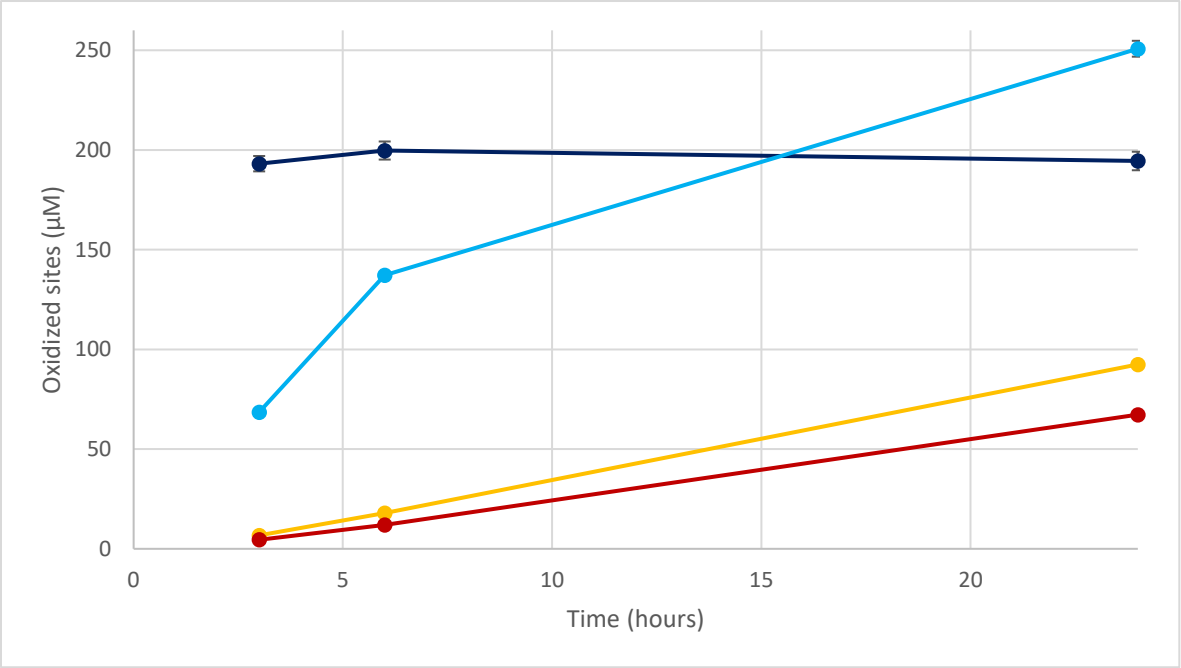

Figure 25: This figure shows oxidized products from *Sd*LPMO10A-reactions. The reaction mixes additionally contained either 1 mM ascorbic acid (dark blue), 100 µM ascorbic acid (light blue), 100 µM ascorbic acid and 1 µM LapA (yellow), or 100 µM ascorbic acid and 1 µM LapB (red). **Appendix 6** shows the actual product concentrations that were used to make the graph, along with standard deviations also presented in this figure. All data points are based on three parallel measurements and are presented with standard deviations (most of which are not visible due to low variation). All reaction mixes contained 10 g/L Avicel (substrate) and 1 µM *Sd*LPMO10A and were performed in a 50 mM $NaPO_4$, pH =6.0 buffer. All reactions were performed at 30 °C, 800 rpm shaking in a ThermoMixer.

5. DISCUSSION

The objective of this study was to clone, express and purify two proteins from the Gram-negative bacterium *S. degradans* in order to test their ability as potential bacterial redox partners for LPMOs. To maximize the chance for finding a meaningful biological interaction, the potential redox ability was to be tested using a novel LPMO from this same organism, which was expressed and characterized in this study.

5.1. CLONING AND CHARACTERIZATION OF *Sd*LPMO10A

A novel LPMO from the Gram-negative bacterium *S. degradans*, named *Sd*LPMO10A, has been successfully expressed. It is a C1 oxidizing LPMO. While some Gram-positive bacterial LPMOs have less oxidative regiospecificity, acting both on C1 and C4 (Forsberg et al., 2014; Forsberg et al., 2018), so far all characterized LPMOs from Gram-negative bacteria are C1 oxidizing. This means that C1 oxidation was the expected activity of the *S. degradans* LPMO.

The melting temperature assay indicates a Tm of approximately 57 °C for the full-length *S. degradans* LPMO, when the enzyme is temperature stabilized by copper-binding in the active site (section 4.4.1.). A Tm of 57 °C is lower than optimal temperature for *Sd*LPMO10A-1 activity, which was around 60 °C, according to the temperature dependent activity test (section 4.4.3.). An enzyme having a Tm lower than the temperature that gives optimal activity seems unlikely. One potential explanation for this is that the substrate could have a stabilizing effect on the Tm. There was no substrate available to the enzyme in the melting temperature assay, suggesting that any potential increase of Tm caused by the LPMO binding to substrate would not be shown. It might therefore be of interest to test for any possible stabilizing effect of the substrate on the LPMO to see if this would increase Tm, for instance by trying to add substrate in a new melting temperature assay.

The apparent Tm of copper stabilized *Sc*LPMO10C was previously found to be 64 °C (Forsberg et al., 2011; Forsberg et al., 2014; Jensen et al., 2019), while according to the test outlined in section 4.4.1., the *Sc*LPMO10C Tm is 57 °C. The apparent Tm that was found for the *Sd*LPMO10A is based on the same assay, implying that it is possible that these measurements of the apparent Tm are not entirely accurate. The activity assay performed at 60 °C shows a much faster increase in product levels compared to the activity assay performed at 50 °C, while enzyme activity is very low at 70 °C. However, increase in product levels stays close to constant at 50 °C for the duration of the experiment (section 4.4.3.), but is lowered over time at 60 °C. The temperature of 60 °C therefore appears to be close to the highest temperature of enzymatic

function, though the rapid inactivation could also be a result of fast substrate consumption affecting the rate due to free LPMO autocatalytic oxidative inactivation (Bissaro et al., 2017).

Currently, only one melting temperature assay has been performed for *Sd*LPMO10A, in which four parallels were run for each enzyme variant. Similarly, the optimal temperature assay was also performed once, in three parallels, for each temperature. A logical conclusion would be that further testing should be carried out before assigning both Tm and optimal temperature. Nevertheless, these tests indicate increased activity for *Sd*LPMO10A along with increased temperatures, up until the approximate denaturing temperature in the range of 60 °C. Seeing as there is little activity at 70 °C, the results indicate that the Tm is less than 70 °C for *Sd*LPMO10A.

*Sd*LPMO10A-3 show lower product levels than the full-length LPMO according to results shown in section 4.4.4. The *Sd*LPMO10A-3 variant contains only the AA10 domain, and not the CBM2 domain. The results therefore suggest lower yields due to lower binding affinity to the substrate. However, according to **Figure 24**, the initial product levels for *Sd*LPMO10A-3 is slightly higher than for *Sd*LPMO10A-1, implying that faster inactivation of the enzyme could be the cause of lower product yields. However, without the CBM, the binding equilibrium is likely changed. CBMs cause higher local concentrations of LPMOs close to the substrate (Bennati-Granier et al., 2015; Bolam et al., 1998), indicating that there would be a higher fraction of free enzymes in the reaction mix without CBMs. Previously, it has been shown that binding to substrate stabilizes LPMOs in the presence of reductant. The stabilizing effect is believed to be caused by a lowered oxidative inactivation rate when LPMOs are bound to substrate (Bissaro et al., 2017) because the active site is less exposed to oxidation. A binding equilibrium with fewer enzymes bound to substrate at any given time can therefore cause faster inactivation when the LPMO is in the presence of reductant.

There is also the possibility that the domains which are not present in the *Sd*LPMO10A-3 variant have a stabilizing effect on the full-length version. This is not obvious from the temperature assay, but it could possibly be worth exploring further. If a stabilizing effect of the other domains on the AA10 domain cannot be confirmed, then disproving this theory could strengthen the theory of self-inactivation. The only condition tested for its effect on *Sd*LPMO10A activity is temperature. Other conditions such as pH might affect the stability of the variants differently than temperature does. *Sd*LPMO10A-3 could have higher product yields at a different pH, while *Sd*LPMO10A-1 activity might be lower at this pH.

The *Sd*LPMO10A-2 enzyme has an even lower activity than *Sd*LPMO10A-1 and -3, showing a low initial yield and fast inactivation (section 4.4.4.). This could potentially mean that the domain of unknown function is a hindrance to the activity of the LPMO when the CBM2 is not attached at the C-terminal end. As seen by the binding assay (section 4.3.), it is unlikely that the region between the AA10 and the CBM2 is a cellulosic binding domain. However, further investigation is needed before making this assumption. The domain of unknown function might cause lowered binding due to steric hindrance, which could come from a change in spatial arrangement because of the removal of the CBM. The unknown domain could be a part of the protein with little or no function other than allowing for larger relative motion between the AA10 and the CBM2. This is similar to it being a particularly long linker region. What this means is that with a removed domain at the C-terminus, this region will have an even larger range of motion, and therefore be an impediment to the active site. The CBM might have a positive effect on thermostability or pH stability, as discussed for *Sd*LPMO10A-3. If this is the case, then the domain of unknown function could have the opposite effect. This means the domain could, for example, be changing the binding equilibrium so that less enzyme is bound, even compared to *Sd*LPMO10A-3. Higher exposure of the active site in the presence of reductant would cause *Sd*LPMO10A-2 to suffer even worse from oxidative inactivation. Currently, there are many uncertainties concerning the domain of unknown function, which makes it an interesting region for further analyses.

5.2. EXPRESSION OF LapA AND LapB VARIANTS

As seen from the alignments of LapA and LapB with Cbp2E and Cbp2D, respectively (section 4.1.), the linker regions were the areas of lowest identity, while the proteins otherwise seem very similar. *Gardner et al*. experienced difficulties expressing several of the proteins of *C. japonicus* in *E. coli* (Gardner et al., 2014), while both SdLPMO10A and LapA-1 seemingly expresses well in *E. coli*. This could, perhaps, be due to these differences in the linker regions.

LapB is assumed to be an extracellular protein since the very similar Cbp2D is secreted into the extracellular matrix along with the *Cj*LPMOs in *C. japonicus* (Gardner et al., 2014). Expression of LapB variants was performed intracellularly, using LIC-cloning with pNIC-CH as the production vector (section 3.2.4.). The native signal peptide of LapB was not included in the gene sequence of any of the variants. LIC cloning is a simple method which have been successfully used to produce many other proteins. However, this expression system led to LapB forming inclusion bodies (section 3.2.4.3.). Refolding of LapB was therefore attempted (3.2.4.4.). The lack of binding to cellulose shown by both LapB-1 and LapB-2 (section 4.3.)

indicates incorrect refolding, since both protein variants are supposed to contain an N-terminal CBM2, similar to that of Cbp2D **(Figure 12**, section 4.1.) which has been predicted to bind cellulose (Gardner et al., 2014). If the native signal peptide of LapB had been used, along with an expression system expected to secrete the protein, for example a system similar to the one used for *Sd*LPMO10A, this could potentially lead to LapB being released into the extracellular matrix. Since LapB did not contain the native signal peptide, the protein was not transported to the extracellular matrix by intracellular and transmembrane shuttling. If LapB is indeed an extracellular protein, it might have missed important steps in the folding process which are necessary for complete and correct folding, since it was not transported out of the cell. The path from intracellular to extracellular protein may be essential for LapB to fold correctly, which means the CBM (and potentially the rest of the protein) would depend on the native signal peptide to be correctly folded. This is certainly worth investigating in the future.

LapB-1 is expected to contain two cytochrome domains, according to alignments with Cbp2D (**Figure 12**, section 4.1.). However, unlike Cbp2D (**Figure 9**, section 1.6.), LapB-1 does not show any color indicative of the presence of functional (heme containing) cytochromes. Neither the pellet from Bug-Buster® or microfluidizer has any red or orange color-variations, but both are supposed to contain the protein variants with the cytochormes, according to the SDS-PAGE gels (**Figure 16**, section 4.2.3.2.). There is also no red or orange color shown in the refolding- and dialysis product. The lack of red color indicates a lack of a functional heme group. A functional heme group is the part of the cytochrome domain in CDHs which accept electrons from the FAD-domain and donates the electron to the LPMOs (section 1.5.1.). It is therefore believed that a functional heme-group is important for the possibility of LapB functioning as a redox partner.

Gardner et al. used a different expression system when they produced Cbp2D that indeed had a red color (Gardner et al., 2014), which means perhaps a different enzyme system is needed for the heme group to be functional in LapB-1. They also believed Cbp2D to be membrane-bound, based on the results using this expression system, while the expression system used for LapB-1 and LapB-2 led to inclusion bodies. LapB-1 might need to be membrane-bound for it to have a functional cytochrome-domain, or at least a functional heme group. Additionally, as suggested above, perhaps the signal peptide of LapB should be included, and extracellular expression should be attempted, in order for this protein to be folded properly. Transportation across the cell membrane and into the periplasmic extract might be essential for LapB to achieve correct folding. Correct folding is usually very important for protein domains to retain their

proper function and might be essential in order for the heme group and the cytochrome to work in LapB. Many potential routes of investigation are still waiting to be explored.

The cytochrome domain is important for redox partners in fungi, as seen from CDHs and PDHs (section 1.5.). This might also be the case for bacterial redox partners, and it is worth considering for LapA. Despite this protein not containing a cytochrome domain in its structure, a gene encoding a cytochrome domain is located directly upstream of the *lapA* gene, on the *S. degradans* chromosome. This means that the cytochrome and LapA are likely to be co-expressed in *S. degradans* in Nature. It may therefore be worth testing LapA in the presence of a separate cytochrome domain, to see if this affects its redox partner potential.

It might also be of interest to see if the LapA and the cytochrome encoded directly upstream of the *lapA* gene in *S. degradans* are, indeed, co-expressed. Testing co-expression of these proteins might be performed by testing whether cellulose degradation in *S. degradans* is affected by knock-outs of different genes, as performed by *Gardner et al*. on Cbp2D and Cbp2E in relation to the *C. japonicus* LPMOs (Gardner et al., 2014). Knock-outs of the gene encoding LapA or the gene for the cytochrome encoded for upstream of the *lapA* gene could be tested. It would also be interesting to see if knock-outs of the *lapB* gene has the same effect on cellulose degradation for *S. degradans*, as *Gardner et al*. showed that the knock-out of Cbp2D had on cellulose degradation for *C. japonicus* (Gardner et al., 2014). Another way of testing co-expression for the cytochrome and LapA is by analyzing likelihood of co-expression bioinformatically, as performed by *Tuveng et al*. on Cbp2D in relation to both of the LPMOs in *C. japonicus* (Tuveng et al., 2016). Additionally, this bioinformatic approach could also be used to test if LapA and LapB are co-expressed with *Sd*LPMO10A in *S. degradans.* Some transcriptomics data exist for cellulose-active enzymes found in S. degradans (Zhang & Hutcheson, 2011), although information on the cellulose binding proteins, which means LapA and potentially LapB, seems somewhat lacking.

5.3. USE OF LapA AND LapB IN LPMO REACTIONS

LPMO reactions containing LapA-1 or LapB-2 in addition to sub-stochiometric amounts of ascorbic acid both show lower product yields than reactions with only sub-stochiometric amounts of ascorbic acid (section 4.5.). However, even though the results seem to indicate that the proteins have a negative effect on *Sd*LPMO10A activity, a conclusion concerning the redox partner potential of these proteins cannot yet be drawn, due to many uncertainties. One of these uncertainties is that LapA-1 or LapB-2 might be reacting with ascorbic acid and consume it,

e.g. by oxidizing it. Considering that LapA-1 has what seems to be a functional CBM2 (section 4.3.), the protein might also be a competitor with the LPMO for the available binding sites on the cellulose surface. However, as LapB-2 does not show binding to cellulose, but still has a negative effect on the product yield, it seems unlikely that competition for binding sites is the cause of the inhibitory effect of LapA-1 on LPMO activity. Nevertheless, without further testing, competitive binding cannot be excluded as a potential interference.

Another reason that LapA-1 and LapB-2 slow down the LPMO reaction could be that their isoprenoid ligand affects the redox reactions. LapA has been shown to have an isoprenoid ligand bound in the YceI domain (Vincent et al., 2010). The type of isoprenoid ligand will likely affect the proteins' redox abilities. **Figure 26** shows two illustrations of the YceI domain of LapA bound to different isoprenoid ligands; ubiquinone-8 and octaprenyl pyrophosphate. While ubiquinone-8 is expected to behave as a reductant and might make LapA and LapB potential redox partners of *Sd*LPMO20A, octaprenyl pyrophosphate is not expected to have this effect.

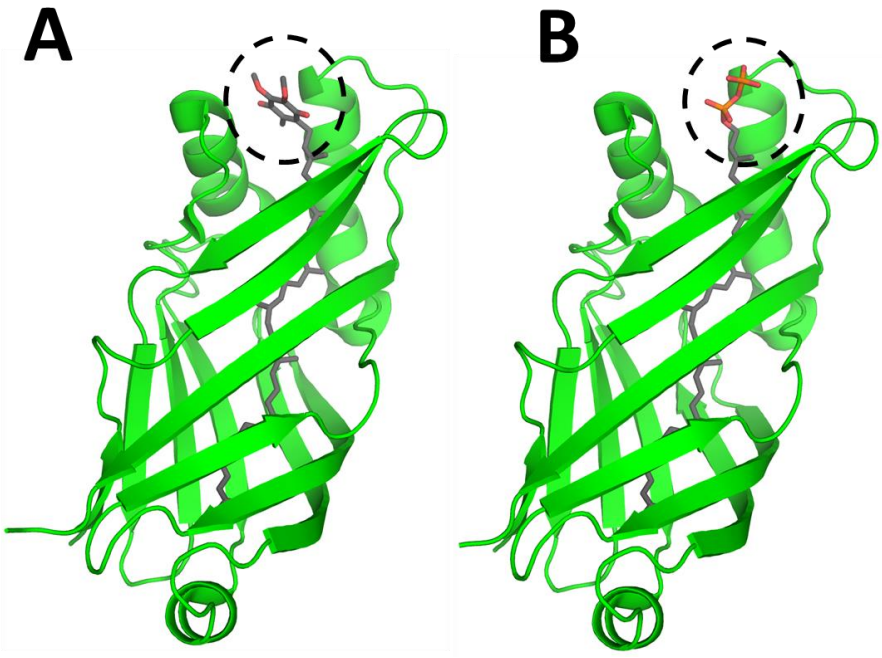

Figure 26: Panels A) and B) show the three-dimensional structure of the YceI domain of LapA (Vincent et al., 2010). bound to two types of ligands (grey), ubiquinone-8 A) and octaprenyl pyrophosphate B). Illustration made by Zarah Forsberg (not published).

The production of LapA-1, LapB-1 and LapB-2 was performed using TB-medium, which is a rich medium. According to Vincent et. al., a rich medium is expected to give ubiquinone-8 as an isoprenoid ligand, while octaprenyl pyrophosphate is more likely to bind when using a less energy-rich medium (Vincent et al., 2010). Using a rich medium such as TB-medium should therefore make LapA-1 and LapB-2 more likely to function as redox partners for LPMOs. However, Vincent et al. performed analyses using a different type of rich medium than TB-medium, which was a medium called 2YT medium (Vincent et al., 2010). For cells grown in TB-medium, the YceI-domains of the proteins could contain a different ligand than ubiquinone-8. This different ligand could be octaprenyl pyrophosphate, similar to when a less energy-rich medium was used (as seen by Vincent et al.), or it could be an entirely different type of isoprenoid ligand.

LapA-1 and LapB-1 was tested with MALDI-TOF MS (section 3.2.6.) in order to assess the presence and nature of the isoprenoid ligand. Results for LapB-1 was outside of the calibrated range of the MALDI-TOF MS and could not be used, but LapA-1 was inside the calibrated range (section 4.2.3.2.). However, the gap between the theoretical and the measured mass for LapA-1 was too big to be the mass of either ubiquinone-8 or octaprenyl pyrophosphate. This gap indicates that LapA-1 of these analyses could have bound a different ligand than the ones already described, or there are other, unknown factors, which are affecting the measured mass of LapA-1. Additionally, the accuracy of the method used in the MALDI-TOF MS instrument was not optimal for such small variations in mass. Since ubiquinone-8 has a molecular mass of 727,1 g/mol, while the mass of octaprenyl pyrophosphate is 722,9 g/mol, only 4,2 g/mol separates them. In conclusion, no isoprenoid unit could be determined for LapA-1. A different method would have to be applied, in order to analyze the isoprenoid ligand in the YceI-domain of LapA and LapB.

Mass spectrometry should be the preferred analysis to determine the isoprenoid unit, based on previous studies (see (Handa et al., 2005; Sisinni et al., 2010) or supplementary data of (Vincent et al., 2010)). However, modifications to the mass spectrometry method are needed, as the method described here (section 3.2.6.) was not adequate for this analysis. If the method is developed so that the isoprenoid unit can be determined, expression of the YceI-domain with different ligands should be attempted. The current LapA-1 and LapB-2 do not function as redox partners for LPMOs, but using protein variants with different isoprenoid ligands for testing might be more successful. The proteins' potentials as redox partners for LPMOs might change. The isoprenoid ligand of the YceI-domain is believed to be of importance for the redox

chemistry of this domain, and by testing isoprenoid ligands which could be used as reductants, LapA and LapB might function as redox partners.

There are multiple opportunities for testing expression with other ligands. If growth conditions do affect the isoprenoid ligand, as believed by Vincent et al., trying to change these conditions might result in other isoprenoid units; units that are more likely to help the protein achieve redox partner abilities. There are many options for broth-variations, temperature, and pH variations that can be tested for varying the ligands. Ubiquinone-8, for instance, is also available for purchase, which means the ligands can possibly be exchanged in proteins that are already produced. Exchanging isoprenoid ligand without having to produce proteins using multiple different methods would both be both time and cost efficient and would be the preferable method. However, the isoprenoid ligand in the YceI- domain might not use ubiquinone-8, even if it is available during production, due to the non-native signal peptide of both LapA and LapB. If the non-native signal peptide changes the folding process, the YceI-domain might use different types of ligands. Therefore, it might be necessary to make some changes in the production process, e.g. trying to produce the protein using the native signal peptide.

5.4. CONCLUSIONS AND FUTURE PERSPECTIVES

In conclusion, three novel full-length proteins from S. degradans have successfully been expressed. All three full-lengt proteins have also been purified, in addition to *Sd*LPMO10A-2, *Sd*LPMO10A-3 and LapB-2. *Sd*LPMO10A is a tri-modular cellulose-oxidizing enzyme with optimal activity at around 60°C, i.e. a temperature close to its apparent melting temperature. The AA10-domain of this enzyme is temperature stabilized when containing an oxidized copper ion. The C-terminal module was shown to bind cellulose, but its internal domain is still of unknown function and awaits further characterization. LapA-1 was also shown to bind cellulose, but its potential redox activity has not yet been shown, possibly due to the absence of correct ligand and/or the lack of an interacting cytochrome domain, where the latter could imply that the hypothesis that LapA alone can drive LPMO reactions is incorrect. Future work should include studying the ligands in LapA and LapB. LapA with characterized isoprenoid ligand could potentially be tested for redox partner activity in the presence of an external cytochrome. LapB should be attempted to be refolded again, as it is seemingly incorrectly folded. Additionally, other production methods should be tested in order to see if production of extracellular LapB can be achieved. If correctly refolded and/or production of extracellular

LapB can be achieved, testing LapB as a redox partner for SdLPMO10A should also be attempted, as this protein contains cytochrome domains and is thus more promising as a redox partner for LPMOs.

6. REFERENCES

Abdel-Hamid, A. M., Solbiati, J. O. & Cann, I. K. (2013). Insights into lignin degradation and its potential industrial applications. In vol. 82 *Advances in Applied Microbiology*, pp. 1-28: Elsevier.

Aebersold, R. & Mann, M. (2003). Mass spectrometry-based proteomics. *Nature*, 422 (6928): 198-207.

Aslanidis, C. & De Jong, P. J. (1990). Ligation-independent cloning of PCR products (LIC-PCR). *Nucleic Acids Research*, 18 (20): 6069-6074.

Bacic, A., Harris, P. J. & Stone, B. A. (1988). Structure and function of plant cell walls. *The Biochemistry of Plants*, 14: 297-371.

Barikani, M., Oliaei, E., Seddiqi, H. & Honarkar, H. (2014). Preparation and application of chitin and its derivatives: a review. *Iranian Polymer Journal*, 23 (4): 307-326.

Beeson, W. T., Phillips, C. M., Cate, J. H. & Marletta, M. A. (2012). Oxidative cleavage of cellulose by fungal copper-dependent polysaccharide monooxygenases. *Journal of the American Chemical Society*, 134 (2): 890-892.

Bennati-Granier, C., Garajova, S., Champion, C., Grisel, S., Haon, M., Zhou, S., Fanuel, M., Ropartz, D., Rogniaux, H. & Gimbert, I. (2015). Substrate specificity and regioselectivity of fungal AA9 lytic polysaccharide monooxygenases secreted by Podospora anserina. *Biotechnology for Biofuels*, 8 (1): 90.

Berg, B., Hofsten, B. v. & Pettersson, G. (1972a). Electronmicroscopic observations on the degradation of cellulose fibres by Cellvibrio fulvus and Sporocytophaga myxococcoides. *Journal of Applied Bacteriology*, 35 (2): 215-219.

Berg, B., Hofsten, B. v. & Pettersson, G. (1972b). Growth and cellulase formation by Cellvibrio fulvus. *Journal of Applied Bacteriology*, 35 (2): 201-214.

Bisaria, V. S. & Ghose, T. K. (1981). Biodegradation of cellulosic materials: substrates, microorganisms, enzymes and products. *Enzyme and Microbial Technology*, 3 (2): 90-104.

Bissaro, B., Røhr, Å. K., Müller, G., Chylenski, P., Skaugen, M., Forsberg, Z., Horn, S. J., Vaaje-Kolstad, G. & Eijsink, V. G. (2017). Oxidative cleavage of polysaccharides by monocopper enzymes depends on H 2 O 2. *Nature Chemical Biology*, 13 (10): 1123.

Bissaro, B., Varnai, A., Røhr, Å. K. & Eijsink, V. G. (2018). Oxidoreductases and reactive oxygen species in conversion of lignocellulosic biomass. *Microbiol. Mol. Biol. Rev.*, 82 (4): e00029-18.

Black, G., Hazlewood, G., Millward-Sadler, S., Laurie, J. & Gilbert, H. (1995). A modular xylanase containing a novel non-catalytic xylan-specific binding domain. *Biochemical Journal*, 307 (1): 191-195.

Black, G. W., Rixon, J. E., Clarke, J. H., Hazlewood, G. P., Theodorou, M. K., Morris, P. & Gilbert, H. J. (1996). Evidence that linker sequences and cellulose-binding domains enhance the activity of hemicellulases against complex substrates. *Biochemical Journal*, 319 (2): 515-520.

Bolam, D. N., CIRUELA, A., McQUEEN-MASON, S., SIMPSON, P., WILLIAMSON, M. P., RIXON, J. E., BORASTON, A., HAZLEWOOD, G. P. & GILBERT, H. J. (1998). Pseudomonas cellulose-binding domains mediate their effects by increasing enzyme substrate proximity. *Biochemical Journal*, 331 (3): 775-781.

Breslmayr, E., Laurent, C. V., Scheiblbrandner, S., Jerkovic, A., Heyes, D. J., Oostenbrink, C., Ludwig, R., Hedison, T. M., Scrutton, N. S. & Kracher, D. (2020). Protein Conformational Change Is Essential for Reductive Activation of Lytic Polysaccharide Monooxygenase by Cellobiose Dehydrogenase. *ACS Catalysis*, 10 (9): 4842-4853.

Brodin, M., Vallejos, M., Opedal, M. T., Area, M. C. & Chinga-Carrasco, G. (2017). Lignocellulosics as sustainable resources for production of bioplastics–A review. *Journal of Cleaner Production*, 162: 646-664.

Cai, R. & Arntfield, S. (1997). Thermal gelation in relation to binding of bovine serum albumin-polysaccharide systems. *Journal of Food Science*, 62 (6): 1129-1134.
Cannella, D., Chia-wen, C. H., Felby, C. & Jørgensen, H. (2012). Production and effect of aldonic acids during enzymatic hydrolysis of lignocellulose at high dry matter content. *Biotechnology for Biofuels*, 5 (1): 26.
Cannella, D., Möllers, K. B., Frigaard, N.-U., Jensen, P. E., Bjerrum, M. J., Johansen, K. S. & Felby, C. (2016). Light-driven oxidation of polysaccharides by photosynthetic pigments and a metalloenzyme. *Nature Communications*, 7 (1): 1-8.
Cardoso, L., Cacciaguerra, T., Gaveau, P., Heux, L., Belamie, E. & Alonso, B. (2017). Synthesis of textured polysaccharide–silica nanocomposites: a comparison between cellulose and chitin nanorod precursors. *New Journal of Chemistry*, 41 (13): 6014-6024.
Carpita, N. C. & Gibeaut, D. M. (1993). Structural models of primary cell walls in flowering plants: consistency of molecular structure with the physical properties of the walls during growth. *The Plant Journal*, 3 (1): 1-30.
Chandra, R. P., Chu, Q., Hu, J., Zhong, N., Lin, M., Lee, J.-S. & Saddler, J. (2016). The influence of lignin on steam pretreatment and mechanical pulping of poplar to achieve high sugar recovery and ease of enzymatic hydrolysis. *Bioresource Technology*, 199: 135-141.
Cheng, J. (2017). *Biomass to renewable energy processes*: CRC Press.
Cherubini, F. (2010). The biorefinery concept: using biomass instead of oil for producing energy and chemicals. *Energy Conversion and Management*, 51 (7): 1412-1421.
Coenen, G., Bakx, E., Verhoef, R., Schols, H. & Voragen, A. (2007). Identification of the connecting linkage between homo-or xylogalacturonan and rhamnogalacturonan type I. *Carbohydrate Polymers*, 70 (2): 224-235.
Courtade, G., Wimmer, R., Røhr, Å. K., Preims, M., Felice, A. K., Dimarogona, M., Vaaje-Kolstad, G., Sørlie, M., Sandgren, M. & Ludwig, R. (2016). Interactions of a fungal lytic polysaccharide monooxygenase with β-glucan substrates and cellobiose dehydrogenase. *Proceedings of the National Academy of Sciences*, 113 (21): 5922-5927.
Couturier, M., Ladeveze, S., Sulzenbacher, G., Ciano, L., Fanuel, M., Moreau, C., Villares, A., Cathala, B., Chaspoul, F. & Frandsen, K. E. (2018). Lytic xylan oxidases from wood-decay fungi unlock biomass degradation. *Nature Chemical Biology*, 14 (3): 306.
de Souza, W. R. (2013). Microbial degradation of lignocellulosic biomass. *Sustainable Degradation of Lignocellulosic Biomass-techniques, Applications and Commercialization*: 207-247.
Dimarogona, M., Topakas, E., Olsson, L. & Christakopoulos, P. (2012). Lignin boosts the cellulase performance of a GH-61 enzyme from Sporotrichum thermophile. *Bioresource Technology*, 110: 480-487.
Eijsink, V. G., Petrovic, D., Forsberg, Z., Mekasha, S., Røhr, Å. K., Várnai, A., Bissaro, B. & Vaaje-Kolstad, G. (2019). On the functional characterization of lytic polysaccharide monooxygenases (LPMOs). *Biotechnology for Biofuels*, 12 (1): 58.
Ferreira, L., Wood, T. M., Williamson, G., Faulds, C., Hazlewood, G. P., Black, G. W. & Gilbert, H. J. (1993). A modular esterase from Pseudomonas fluorescens subsp. cellulosa contains a non-catalytic cellulose-binding domain. *Biochemical Journal*, 294 (2): 349-355.
Fierobe, H. P., BAGNARA-TARDIF, C., GAUDIN, C., GUERLESQUIN, F., SAUVE, P., BELAICH, A. & BELAICH, J. P. (1993). Purification and characterization of endoglucanase C from Clostridium cellulolyticum: Catalytic comparison with endoglucanase A. *European Journal of Biochemistry*, 217 (2): 557-565.
Filiatrault-Chastel, C., Navarro, D., Haon, M., Grisel, S., Herpoël-Gimbert, I., Chevret, D., Fanuel, M., Henrissat, B., Heiss-Blanquet, S. & Margeot, A. (2019). AA16, a new lytic polysaccharide monooxygenase family identified in fungal secretomes. *Biotechnology for Biofuels*, 12 (1): 55.
Forsberg, Z., Vaaje-Kolstad, G., Westereng, B., Bunæs, A. C., Stenstrøm, Y., MacKenzie, A., Sørlie, M., Horn, S. J. & Eijsink, V. G. (2011). Cleavage of cellulose by a CBM33 protein. *Protein Science*, 20 (9): 1479-1483.

Forsberg, Z., Mackenzie, A. K., Sørlie, M., Røhr, Å. K., Helland, R., Arvai, A. S., Vaaje-Kolstad, G. & Eijsink, V. G. (2014). Structural and functional characterization of a conserved pair of bacterial cellulose-oxidizing lytic polysaccharide monooxygenases. *Proceedings of the National Academy of Sciences*, 111 (23): 8446-8451.

Forsberg, Z., Nelson, C. E., Dalhus, B., Mekasha, S., Loose, J. S., Crouch, L. I., Røhr, Å. K., Gardner, J. G., Eijsink, V. G. & Vaaje-Kolstad, G. (2016). Structural and functional analysis of a lytic polysaccharide monooxygenase important for efficient utilization of chitin in Cellvibrio japonicus. *Journal of Biological Chemistry*, 291 (14): 7300-7312.

Forsberg, Z., Bissaro, B., Gullesen, J., Dalhus, B., Vaaje-Kolstad, G. & Eijsink, V. G. (2018). Structural determinants of bacterial lytic polysaccharide monooxygenase functionality. *Journal of Biological Chemistry*, 293 (4): 1397-1412.

Forsberg, Z., Stepnov, Anton A., Nærdal, Guro Kruge, Klinkenberg, Geir, Eijsink, Vincent G. H. . (2020). Engineering lytic polysaccharide monooxygenases (LPMOs). *Elsevier*.

Frandsen, K. E., Simmons, T. J., Dupree, P., Poulsen, J.-C. N., Hemsworth, G. R., Ciano, L., Johnston, E. M., Tovborg, M., Johansen, K. S. & von Freiesleben, P. (2016). The molecular basis of polysaccharide cleavage by lytic polysaccharide monooxygenases. *Nature Chemical Biology*, 12 (4): 298.

Frommhagen, M., Koetsier, M. J., Westphal, A. H., Visser, J., Hinz, S. W., Vincken, J.-P., Van Berkel, W. J., Kabel, M. A. & Gruppen, H. (2016). Lytic polysaccharide monooxygenases from Myceliophthora thermophila C1 differ in substrate preference and reducing agent specificity. *Biotechnology for Biofuels*, 9 (1): 186.

Gardner, J. G., Crouch, L., Labourel, A., Forsberg, Z., Bukhman, Y. V., Vaaje-Kolstad, G., Gilbert, H. J. & Keating, D. H. (2014). Systems biology defines the biological significance of redox-active proteins during cellulose degradation in an aerobic bacterium. *Molecular Microbiology*, 94 (5): 1121-1133.

Garvey, M., Klose, H., Fischer, R., Lambertz, C. & Commandeur, U. (2013). Cellulases for biomass degradation: comparing recombinant cellulase expression platforms. *Trends in Biotechnology*, 31 (10): 581-593.

Gilkes, N., Warren, R., Miller, R. & Kilburn, D. G. (1988). Precise excision of the cellulose binding domains from two Cellulomonas fimi cellulases by a homologous protease and the effect on catalysis. *Journal of Biological Chemistry*, 263 (21): 10401-10407.

Handa, N., Terada, T., Doi-Katayama, Y., Hirota, H., Tame, J. R., Park, S. Y., Kuramitsu, S., Shirouzu, M. & Yokoyama, S. (2005). Crystal structure of a novel polyisoprenoid-binding protein from Thermus thermophilus HB8. *Protein Science*, 14 (4): 1004-1010.

Hemsworth, G. R., Taylor, E. J., Kim, R. Q., Gregory, R. C., Lewis, S. J., Turkenburg, J. P., Parkin, A., Davies, G. J. & Walton, P. H. (2013). The copper active site of CBM33 polysaccharide oxygenases. *Journal of the American Chemical Society*, 135 (16): 6069-6077.

Hemsworth, G. R., Henrissat, B., Davies, G. J. & Walton, P. H. (2014). Discovery and characterization of a new family of lytic polysaccharide monooxygenases. *Nature Chemical Biology*, 10 (2): 122.

Hori, C., Gaskell, J., Igarashi, K., Samejima, M., Hibbett, D., Henrissat, B. & Cullen, D. (2013). Genomewide analysis of polysaccharides degrading enzymes in 11 white-and brown-rot Polyporales provides insight into mechanisms of wood decay. *Mycologia*, 105 (6): 1412-1427.

Igarashi, K., Momohara, I., Nishino, T. & Samejima, M. (2002). Kinetics of inter-domain electron transfer in flavocytochrome cellobiose dehydrogenase from the white-rot fungus Phanerochaete chrysosporium. *Biochemical Journal*, 365 (2): 521-526.

Imeson, A. P., Ledward, D. A. & Mitchell, J. R. (1977). On the nature of the interaction between some anionic polysaccharides and proteins. *Journal of the Science of Food and Agriculture*, 28 (8): 661-668.

Isaksen, T., Westereng, B., Aachmann, F. L., Agger, J. W., Kracher, D., Kittl, R., Ludwig, R., Haltrich, D., Eijsink, V. G. & Horn, S. J. (2014). A C4-oxidizing lytic polysaccharide monooxygenase cleaving both cellulose and cello-oligosaccharides. *Journal of Biological Chemistry*, 289 (5): 2632-2642.

Jensen, M. S., Fredriksen, L., MacKenzie, A. K., Pope, P. B., Leiros, I., Chylenski, P., Williamson, A. K., Christopeit, T., Østby, H. & Vaaje-Kolstad, G. (2018). Discovery and characterization of a thermostable two-domain GH6 endoglucanase from a compost metagenome. *PloS One*, 13 (5).

Jensen, M. S., Klinkenberg, G., Bissaro, B., Chylenski, P., Vaaje-Kolstad, G., Kvitvang, H. F., Nærdal, G. K., Sletta, H., Forsberg, Z. & Eijsink, V. G. (2019). Engineering chitinolytic activity into a cellulose-active lytic polysaccharide monooxygenase provides insights into substrate specificity. *Journal of Biological Chemistry*, 294 (50): 19349-19364.

Kim, S., Ståhlberg, J., Sandgren, M., Paton, R. S. & Beckham, G. T. (2014). Quantum mechanical calculations suggest that lytic polysaccharide monooxygenases use a copper-oxyl, oxygen-rebound mechanism. *Proceedings of the National Academy of Sciences*, 111 (1): 149-154.

Kittl, R., Kracher, D., Burgstaller, D., Haltrich, D. & Ludwig, R. (2012). Production of four Neurospora crassa lytic polysaccharide monooxygenases in Pichia pastoris monitored by a fluorimetric assay. *Biotechnology for Biofuels*, 5 (1): 79.

Kjaergaard, C. H., Qayyum, M. F., Wong, S. D., Xu, F., Hemsworth, G. R., Walton, D. J., Young, N. A., Davies, G. J., Walton, P. H. & Johansen, K. S. (2014). Spectroscopic and computational insight into the activation of O2 by the mononuclear Cu center in polysaccharide monooxygenases. *Proceedings of the National Academy of Sciences*, 111 (24): 8797-8802.

Kracher, D., Scheiblbrandner, S., Felice, A. K., Breslmayr, E., Preims, M., Ludwicka, K., Haltrich, D., Eijsink, V. G. & Ludwig, R. (2016). Extracellular electron transfer systems fuel cellulose oxidative degradation. *Science*, 352 (6289): 1098-1101.

Kracher, D., Forsberg, Z., Bissaro, B., Gangl, S., Preims, M., Sygmund, C., Eijsink, V. G. & Ludwig, R. (2019). Polysaccharide oxidation by lytic polysaccharide monooxygenase is enhanced by engineered cellobiose dehydrogenase. *The Federation of European Biochemical Societies Journal*.

Langston, J. A., Shaghasi, T., Abbate, E., Xu, F., Vlasenko, E. & Sweeney, M. D. (2011). Oxidoreductive cellulose depolymerization by the enzymes cellobiose dehydrogenase and glycoside hydrolase 61. *Appl. Environ. Microbiol.*, 77 (19): 7007-7015.

Leahy, S. (2004). *Drowning in an ocean of Plastic*. Wired. Available at: https://www.wired.com/2004/06/drowning-in-an-ocean-of-plastic/.

Lee, J. W., Choi, S., Park, J. H., Vickers, C. E., Nielsen, L. K. & Lee, S. Y. (2010). Development of sucrose-utilizing Escherichia coli K-12 strain by cloning β-fructofuranosidases and its application for L-threonine production. *Applied Microbiology and Biotechnology*, 88 (4): 905-913.

Levasseur, A., Drula, E., Lombard, V., Coutinho, P. M. & Henrissat, B. (2013). Expansion of the enzymatic repertoire of the CAZy database to integrate auxiliary redox enzymes. *Biotechnology for Biofuels*, 6 (1): 41.

Li, X., Beeson IV, W. T., Phillips, C. M., Marletta, M. A. & Cate, J. H. (2012). Structural basis for substrate targeting and catalysis by fungal polysaccharide monooxygenases. *Structure*, 20 (6): 1051-1061.

Lo Leggio, L., Simmons, T. J., Poulsen, J.-C. N., Frandsen, K. E., Hemsworth, G. R., Stringer, M. A., Von Freiesleben, P., Tovborg, M., Johansen, K. S. & De Maria, L. (2015). Structure and boosting activity of a starch-degrading lytic polysaccharide monooxygenase. *Nature Communications*, 6 (1): 1-9.

Loix, C., Huybrechts, M., Vangronsveld, J., Gielen, M., Keunen, E. & Cuypers, A. (2017). Reciprocal interactions between cadmium-induced cell wall responses and oxidative stress in plants. *Frontiers in Plant Science*, 8: 1867.

Loose, J. S., Forsberg, Z., Kracher, D., Scheiblbrandner, S., Ludwig, R., Eijsink, V. G. & Vaaje-Kolstad, G. (2016). Activation of bacterial lytic polysaccharide monooxygenases with cellobiose dehydrogenase. *Protein Science*, 25 (12): 2175-2186.

Lopes, A., Ferreira Filho, E. & Moreira, L. (2018). An update on enzymatic cocktails for lignocellulose breakdown. *Journal of Applied Microbiology*, 125 (3): 632-645.

Luyt, A. S. & Malik, S. S. (2019). Can biodegradable plastics solve plastic solid waste accumulation? In *Plastics to Energy*, pp. 403-423: Elsevier.
Lynd, L. R., Cushman, J. H., Nichols, R. J. & Wyman, C. E. (1991). Fuel ethanol from cellulosic biomass. *Science*, 251 (4999): 1318-1323.
Malherbe, S. & Cloete, T. E. (2002). Lignocellulose biodegradation: fundamentals and applications. *Reviews in Environmental Science and Biotechnology*, 1 (2): 105-114.
Manoil, C. & Beckwith, J. (1986). A genetic approach to analyzing membrane protein topology. *Science*, 233 (4771): 1403-1408.
Mansfield, S. D., Mooney, C. & Saddler, J. N. (1999). Substrate and enzyme characteristics that limit cellulose hydrolysis. *Biotechnology Progress*, 15 (5): 804-816.
Matsumura, H., Umezawa, K., Takeda, K., Sugimoto, N., Ishida, T., Samejima, M., Ohno, H., Yoshida, M., Igarashi, K. & Nakamura, N. (2014). Discovery of a eukaryotic pyrroloquinoline quinone-dependent oxidoreductase belonging to a new auxiliary activity family in the database of carbohydrate-active enzymes. *PloS One*, 9 (8).
Mewis, K., Lenfant, N., Lombard, V. & Henrissat, B. (2016). Dividing the large glycoside hydrolase family 43 into subfamilies: a motivation for detailed enzyme characterization. *Appl. Environ. Microbiol.*, 82 (6): 1686-1692.
Monge, E. C., Tuveng, T. R., Vaaje-Kolstad, G., Eijsink, V. G. & Gardner, J. G. (2018). Systems analysis of the glycoside hydrolase family 18 enzymes from Cellvibrio japonicus characterizes essential chitin degradation functions. *Journal of Biological Chemistry*, 293 (10): 3849-3859.
Müller, G., Chylenski, P., Bissaro, B., Eijsink, V. G. & Horn, S. J. (2018). The impact of hydrogen peroxide supply on LPMO activity and overall saccharification efficiency of a commercial cellulase cocktail. *Biotechnology for Biofuels*, 11 (1): 209.
Nakamura, T., Mine, S., Hagihara, Y., Ishikawa, K., Ikegami, T. & Uegaki, K. (2008). Tertiary structure and carbohydrate recognition by the chitin-binding domain of a hyperthermophilic chitinase from Pyrococcus furiosus. *Journal of Molecular Biology*, 381 (3): 670-680.
Nohl, H., Kozlov, A. V., Staniek, K. & Gille, L. (2001). The multiple functions of coenzyme Q. *Bioorganic Chemistry*, 29 (1): 1-13.
Öhgren, K., Galbe, M. & Zacchi, G. (2005). Optimization of steam pretreatment of SO 2-impregnated corn stover for fuel ethanol production. *Applied Biochemistry and Biotechnology*, 124 (1-3): 1055-1067.
Olsen, J. V., Ong, S.-E. & Mann, M. (2004). Trypsin cleaves exclusively C-terminal to arginine and lysine residues. *Molecular & Cellular Proteomics*, 3 (6): 608-614.
Phillips, C. M., Beeson IV, W. T., Cate, J. H. & Marletta, M. A. (2011). Cellobiose dehydrogenase and a copper-dependent polysaccharide monooxygenase potentiate cellulose degradation by Neurospora crassa. *ACS Chemical Biology*, 6 (12): 1399-1406.
Pierce, K. E., Harris, R. J., Larned, L. S. & Pokras, M. A. (2004). Obstruction and starvation associated with plastic ingestion in a Northern Gannet Morus bassanus and a Greater Shearwater Puffinus gravis. *Marine Ornithology*, 32: 187-189.
Quinlan, R. J., Sweeney, M. D., Leggio, L. L., Otten, H., Poulsen, J.-C. N., Johansen, K. S., Krogh, K. B., Jørgensen, C. I., Tovborg, M. & Anthonsen, A. (2011). Insights into the oxidative degradation of cellulose by a copper metalloenzyme that exploits biomass components. *Proceedings of the National Academy of Sciences*, 108 (37): 15079-15084.
Rojas, O. J. (2016). *Cellulose chemistry and properties: fibers, nanocelluloses and advanced materials*, vol. 271: Springer.
Sabbadin, F., Hemsworth, G. R., Ciano, L., Henrissat, B., Dupree, P., Tryfona, T., Marques, R. D., Sweeney, S. T., Besser, K. & Elias, L. (2018). An ancient family of lytic polysaccharide monooxygenases with roles in arthropod development and biomass digestion. *Nature Communications*, 9 (1): 1-12.
Saloheimo, M., Nakari-SetäLä, T., Tenkanen, M. & Penttilä, M. (1997). cDNA cloning of a Trichoderma reesei cellulase and demonstration of endoglucanase activity by expression in yeast. *European Journal of Biochemistry*, 249 (2): 584-591.

Sánchez, C. (2009). Lignocellulosic residues: biodegradation and bioconversion by fungi. *Biotechnology Advances*, 27 (2): 185-194.
Schwarz, W. (2001). The cellulosome and cellulose degradation by anaerobic bacteria. *Applied Microbiology and Biotechnology*, 56 (5-6): 634-649.
Shafiee, S. & Topal, E. (2009). When will fossil fuel reserves be diminished? *Energy Policy*, 37 (1): 181-189.
Shi, Z., Zhang, Y., Phillips, G. O. & Yang, G. (2014). Utilization of bacterial cellulose in food. *Food Hydrocolloids*, 35: 539-545.
Shokri, J. & Adibkia, K. (2013). Application of cellulose and cellulose derivatives in pharmaceutical industries. In *Cellulose-medical, Pharmaceutical and Electronic Applications*: IntechOpen.
Sisinni, L., Cendron, L., Favaro, G. & Zanotti, G. (2010). Helicobacter pylori acidic stress response factor HP1286 is a YceI homolog with new binding specificity. *The Federation of European Biochemical Societies journal*, 277 (8): 1896-1905.
Sørensen, I., Domozych, D. & Willats, W. G. (2010). How have plant cell walls evolved? *Plant Physiology*, 153 (2): 366-372.
Suckau, D., Resemann, A., Schuerenberg, M., Hufnagel, P., Franzen, J. & Holle, A. (2003). A novel MALDI LIFT-TOF/TOF mass spectrometer for proteomics. *Analytical and Bioanalytical Chemistry*, 376 (7): 952-965.
Tan, T.-C., Kracher, D., Gandini, R., Sygmund, C., Kittl, R., Haltrich, D., Hällberg, B. M., Ludwig, R. & Divne, C. (2015). Structural basis for cellobiose dehydrogenase action during oxidative cellulose degradation. *Nature Communications*, 6: 7542.
Tandrup, T., Frandsen, K. E., Johansen, K. S., Berrin, J.-G. & Lo Leggio, L. (2018). Recent insights into lytic polysaccharide monooxygenases (LPMOs). *Biochemical Society Transactions*, 46 (6): 1431-1447.
Taylor, L. E., Henrissat, B., Coutinho, P. M., Ekborg, N. A., Hutcheson, S. W. & Weiner, R. M. (2006). Complete cellulase system in the marine bacterium Saccharophagus degradans strain 2-40T. *Journal of Bacteriology*, 188 (11): 3849-3861.
Tuveng, T. R., Arntzen, M. Ø., Bengtsson, O., Gardner, J. G., Vaaje-Kolstad, G. & Eijsink, V. G. (2016). Proteomic investigation of the secretome of Cellvibrio japonicus during growth on chitin. *Proteomics*, 16 (13): 1904-1914.
UNESCO. (2017). *Facts and figures on marine pollution*: UNESCO. Available at: http://www.unesco.org/new/en/natural-sciences/ioc-oceans/focus-areas/rio-20-ocean/blueprint-for-the-future-we-want/marine-pollution/facts-and-figures-on-marine-pollution/.
Vaaje-Kolstad, G., Horn, S. J., van Aalten, D. M., Synstad, B. & Eijsink, V. G. (2005). The non-catalytic chitin-binding protein CBP21 from Serratia marcescens is essential for chitin degradation. *Journal of Biological Chemistry*, 280 (31): 28492-28497.
Vaaje-Kolstad, G., Westereng, B., Horn, S. J., Liu, Z., Zhai, H., Sørlie, M. & Eijsink, V. G. (2010). An oxidative enzyme boosting the enzymatic conversion of recalcitrant polysaccharides. *Science*, 330 (6001): 219-222.
Vaaje-Kolstad, G., Forsberg, Z., Loose, J. S., Bissaro, B. & Eijsink, V. G. (2017). Structural diversity of lytic polysaccharide monooxygenases. *Current Opinion in Structural Biology*, 44: 67-76.
Valderrama, B., Ayala, M. & Vazquez-Duhalt, R. (2002). Suicide inactivation of peroxidases and the challenge of engineering more robust enzymes. *Chemistry & Biology*, 9 (5): 555-565.
Van Dyk, J. & Pletschke, B. (2012). A review of lignocellulose bioconversion using enzymatic hydrolysis and synergistic cooperation between enzymes—factors affecting enzymes, conversion and synergy. *Biotechnology Advances*, 30 (6): 1458-1480.
Várnai, A., Umezawa, K., Yoshida, M. & Eijsink, V. G. (2018). The pyrroloquinoline-quinone-dependent pyranose dehydrogenase from Coprinopsis cinerea drives lytic polysaccharide monooxygenase action. *Appl. Environ. Microbiol.*, 84 (11): e00156-18.

Vincent, F., Dal Molin, D., Weiner, R. M., Bourne, Y. & Henrissat, B. (2010). Structure of a polyisoprenoid binding domain from Saccharophagus degradans implicated in plant cell wall breakdown. *Federation of European Biochemical Societies letters*, 584 (8): 1577-1584.

Walton, P. H. & Davies, G. J. (2016). On the catalytic mechanisms of lytic polysaccharide monooxygenases. *Current Opinion in Chemical Biology*, 31: 195-207.

Westereng, B., Agger, J. W., Horn, S. J., Vaaje-Kolstad, G., Aachmann, F. L., Stenstrøm, Y. H. & Eijsink, V. G. (2013). Efficient separation of oxidized cello-oligosaccharides generated by cellulose degrading lytic polysaccharide monooxygenases. *Journal of Chromatography A*, 1271 (1): 144-152.

Westereng, B., Arntzen, M. Ø., Aachmann, F. L., Várnai, A., Eijsink, V. G. & Agger, J. W. (2016). Simultaneous analysis of C1 and C4 oxidized oligosaccharides, the products of lytic polysaccharide monooxygenases acting on cellulose. *Journal of Chromatography A*, 1445: 46-54.

Westereng, B., Arntzen, M. Ø., Agger, J. W., Vaaje-Kolstad, G. & Eijsink, V. G. (2017). Analyzing activities of lytic polysaccharide monooxygenases by liquid chromatography and mass spectrometry. In *Protein-Carbohydrate Interactions*, pp. 71-92: Springer.

Wilson, D. B. (2004). Studies of Thermobifida fusca plant cell wall degrading enzymes. *The Chemical Record*, 4 (2): 72-82.

Wood, T. M. (1988). Preparation of crystalline, amorphous, and dyed cellulase substrates. *Methods Enzymol.*, 160: 19-25.

Wu, M., Beckham, G. T., Larsson, A. M., Ishida, T., Kim, S., Payne, C. M., Himmel, M. E., Crowley, M. F., Horn, S. J. & Westereng, B. (2013). Crystal structure and computational characterization of the lytic polysaccharide monooxygenase GH61D from the Basidiomycota fungus Phanerochaete chrysosporium. *Journal of Biological Chemistry*, 288 (18): 12828-12839.

Wymelenberg, A. V., Gaskell, J., Mozuch, M., BonDurant, S. S., Sabat, G., Ralph, J., Skyba, O., Mansfield, S. D., Blanchette, R. A. & Grigoriev, I. V. (2011). Significant alteration of gene expression in wood decay fungi Postia placenta and Phanerochaete chrysosporium by plant species. *Appl. Environ. Microbiol.*, 77 (13): 4499-4507.

Zámocký, M., Hallberg, M., Ludwig, R., Divne, C. & Haltrich, D. (2004). Ancestral gene fusion in cellobiose dehydrogenases reflects a specific evolution of GMC oxidoreductases in fungi. *Gene*, 338 (1): 1-14.

Zhang, H. & Hutcheson, S. W. (2011). Complex expression of the cellulolytic transcriptome of Saccharophagus degradans. *Appl. Environ. Microbiol.*, 77 (16): 5591-5596.

Zhao, X., Zhang, L. & Liu, D. (2012). Biomass recalcitrance. Part I: the chemical compositions and physical structures affecting the enzymatic hydrolysis of lignocellulose. *Biofuels, Bioproducts and Biorefining*, 6 (4): 465-482.

Zhou, X., Qi, X., Huang, H. & Zhu, H. (2019). Sequence and Structural Analysis of AA9 and AA10 LPMOs: An Insight into the Basis of Substrate Specificity and Regioselectivity. *International Journal of Molecular Sciences*, 20 (18): 4594.

SUPPLEMENTARY INFORMATION

APPENDIX 1

Transmembrane Hidden Markov Model prediction, as explained in section 4.1., for A) LapA full-length, B) LabA without signal peptide and C) LapB full-length.

A

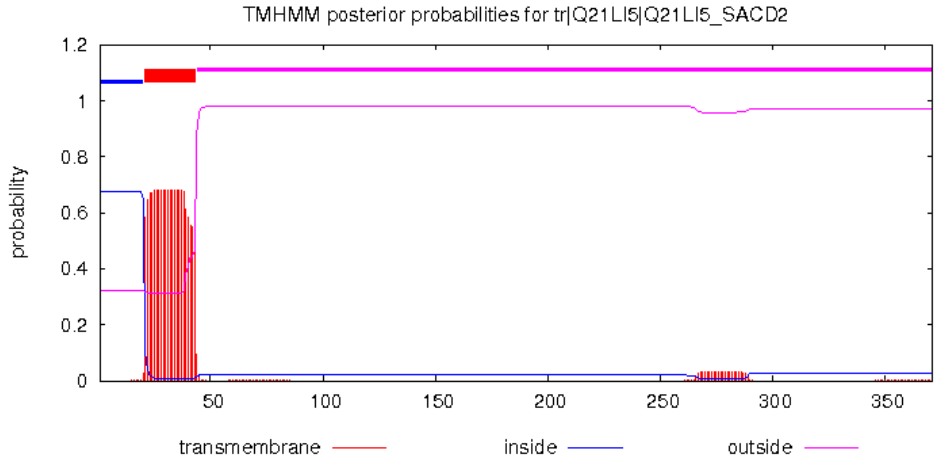

B

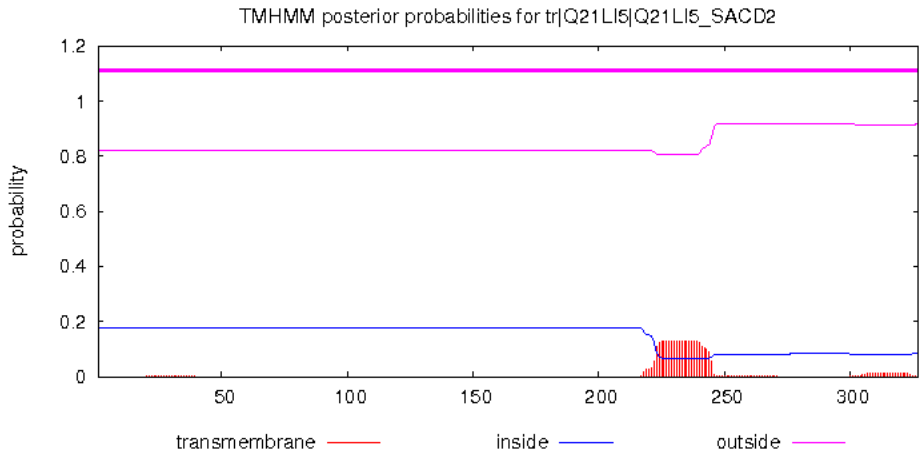

C

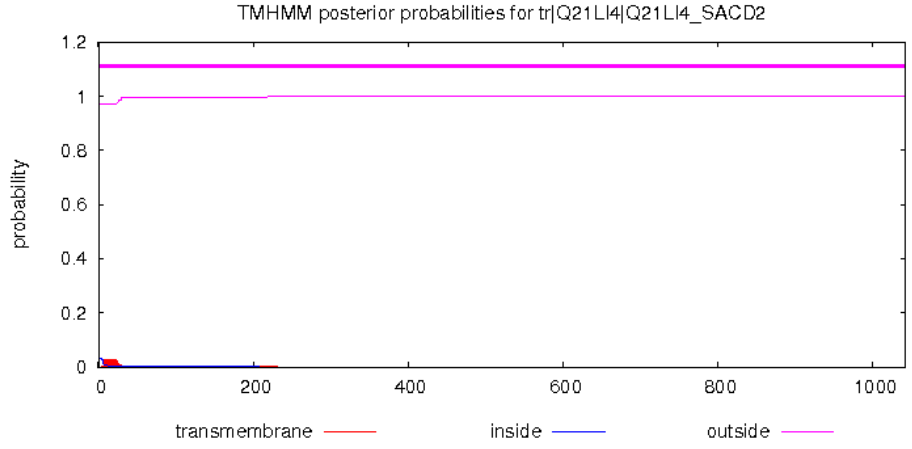

APPENDIX 2

Chromatograms of A) ion exchange chromatography (IEX) and B) size exclusion chromatography (SEC) runs for *Sd*LPMO10A-1 (full-length). The peak between the arrows in panel A contained the LPMO and was subjected to SEC. Fraction 8-13 were collected from the SEC run and analyzed by SDS- PAGE(see corresponding fraction numbers in **Figure 14**).

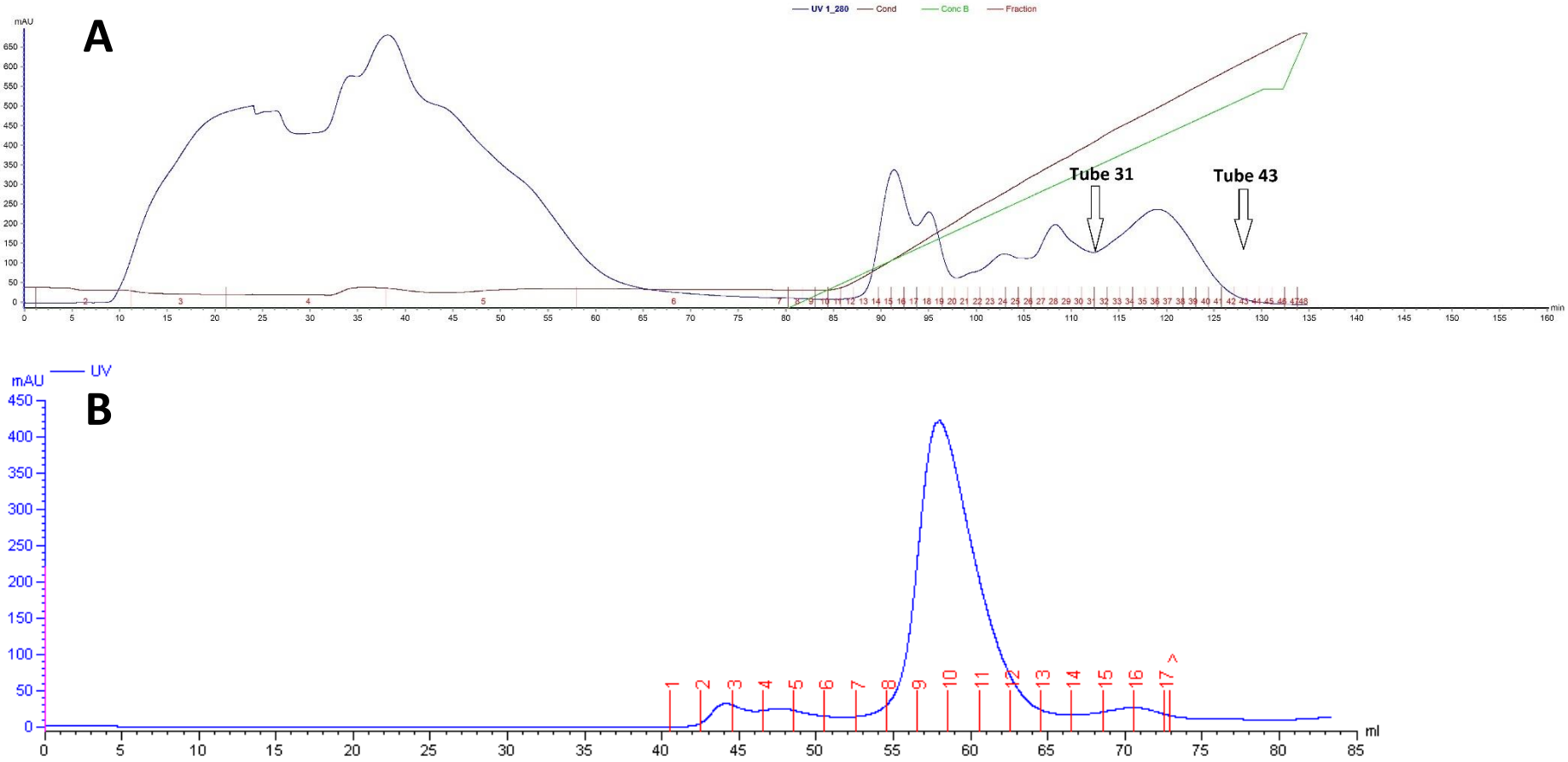

APPENDIX 3

Data for the binding assays with various proteins. The average has been calculated based on the average of the three parallels, and then a background noise value of 0.008 was subtracted. This background noise was based on measurements performed on a reaction mix containing only 10 g/l Avicel in 50 mM $NaPO_4$ pH =6.0, which underwent the same procedure all the enzyme-containing reaction mixes did. The % average and % standard deviation (Std. dev. (%)) were used to make the graph in **Figure 20**. % average was calculated based on 100 % being measurements done for each sample at time =0, which means measurements performed on a sample containing protein and buffer in the same concentrations as for parallel 1, 2, and 3, but not containing any substrate. * =deviant value and therefore not used in calculating average and Std. dev.

Time (min)		0	4	8	16	32	64
LapA	1	0.108	0.061	0.059	0.052	0.049	0.045
	2	0.109	0.067	0.060	0.055	0.055	0.095*
	3	0.105	0.059	0.056	0.054	0.053	0.057
	Average	0.099	0.054	0.050	0.045	0.044	0.042
	Std. dev.	0.002	0.003	0.002	0.001	0.002	0.006
	% average	100	54	50	46	44	43
	Std. dev (%)	1.7	6.4	3.4	2.8	5.7	14.2
LapB	1	0.134	0.111	0.116	0.111	0.110	0.110
	2	0.128	0.113	0.121	0.117	0.114	0.111
	3	0.128	0.117	0.116	0.124	0.114	0.117
	Average	0.121	0.105	0.109	0.109	0.104	0.104
	Std. dev.	0.003	0.002	0.002	0.005	0.002	0.003
	% average	100	87	90	90	86	86
	Std. dev (%)	2.3	2.4	2.2	4.9	1.8	3.0
*Sd*LPMO10A-1	1	0.226	0.147	0.136	0.122	0.118	0.113
	2	0.229	0.143	0.130	0.122	0.111	0.116
	3	0.229	0.147	0.137	0.13	0.127	0.122
	Average	0.219	0.137	0.126	0.116	0.110	0.108
	Std. dev.	0.001	0.002	0.003	0.004	0.007	0.004
	% average	100	60	55	51	48	48
	Std. dev (%)	0.6	1.4	2.5	3.3	6.0	3.4

*Sd*LPMO10A-2	1	0.163	0.174	0.173	0.175	0.174	0.188
	2	0.166	0.161	0.167	0.170	0.172	0.174
	3	0.164	0.165	0.166	0.169	0.169	0.173
	Average	0.156	0.158	0.160	0.163	0.163	0.170
	Std. dev.	0.001	0.005	0.003	0.003	0.002	0.007
	% average	100	102	103	105	105	109.0
	Std. dev (%)	0.8	3.4	1.9	1.6	1.3	4.0
*Sd*LPMO10A-3	1	0.216	0.197	0.205	0.200	0.204	0.216
	2	0.215	0.203	0.295*	0.211	0.213	0.216
	3	0.216	0.196	0.208	0.205	0.198	0.200
	Average	0.207	0.190	0.198	0.197	0.196	0.202
	Std. dev.	0.000	0.003	0.002	0.004	0.006	0.008
	% average	100	91.8	95.6	95.0	94.8	97.6
	Std. dev (%)	0.228	1.628	0.759	2.288	3.142	3.736
BSA	% average	100	80	79	80	81	74
	Std. dev (%)	2.2	2.7	3.6	1.4	0.8	5.7

APPENDIX 4

Data from activity assay done to determine the temperature optimum of *Sd*LPMO10A-1 (full-length), as presented in **Figure 23**. 2-oxidized and 3-oxidized products indicates length of product, which means 2-oxidized products are dimeric products, and 3-oxidized products are trimeric products. Oxidized product sum is the combined amount of 2- and 3-oxidized products.

Temperature (°C)	Time (min)	2-oxidized product (µM)	Standard deviation	3-oxidized product (µM)	Standard deviation	Oxidized product sum (µM)	Standard deviation
10	10	0.000	0.000	0.000	0.000	0.000	0.000
	30	0.000	0.000	0.000	0.000	0.000	0.000
	60	1.164	0.256	0.740	0.202	1.904	0.458
	120	2.829	0.425	2.200	0.349	5.029	0.774
20	10	0.000	0.000	0.000	0.000	0.000	0.000
	30	0.000	0.000	0.000	0.000	0.000	0.000
	60	2.509	0.082	1.590	0.098	4.099	0.179
	120	6.184	0.108	5.355	0.193	11.539	0.300
30	10	0.000	0.000	0.000	0.000	0.000	0.000
	30	1.109	0.058	0.480	0.012	1.589	0.069
	60	3.315	0.241	2.141	0.150	5.457	0.391
	120	8.136	0.347	7.153	0.445	15.289	0.790
40	10	0.448	0.030	0.000	0.000	0.448	0.030
	30	2.532	0.392	2.489	0.556	5.022	0.848
	60	6.281	0.318	5.856	0.355	12.137	0.624
	120	16.848	3.921	15.352	2.649	32.201	6.569
50	10	3.196	0.444	0.751	0.051	3.947	0.393
	30	8.959	0.762	5.627	0.241	14.586	0.946
	60	18.046	0.519	14.483	0.253	32.529	0.662
	120	40.385	1.427	31.395	1.140	71.780	2.566
60	10	9.396	0.198	8.699	0.472	18.095	0.670
	30	35.397	2.068	30.917	2.074	66.314	3.966
	60	53.640	2.626	41.367	0.721	95.007	3.293
	120	58.823	0.945	45.145	0.465	103.968	1.398
70	10	1.382	0.129	1.456	0.128	2.838	0.245
	30	1.424	0.298	1.442	0.338	2.866	0.634

	60	1.551	0.220	1.432	0.155	2.983	0.369
	120	1.410	0.103	1.322	0.144	2.732	0.225

APPENDIX 5

Data for the activity assay of the three *Sd*LPMO10A variants performed at 50 °C, used to make graph in **Figure 24**. Values are given in µM. Standard deviations belong to the values given in the colum to their left. 2-oxidized and 3-oxidized products indicates length of product, which means 2-oxidized products are dimeric products, and 3-oxidized products are trimeric products. Oxidized product sum is the combined amount of 2- and 3-oxidized products.

Time (hours)	*Sd*LPMO variant	2-oxidized product (µM)	Standard deviation	3-oxidized product (µM)	Standard deviation	Oxidized product sum (µM)	Standard deviation
0.5	1	16.394	0.585	13.967	0.093	30.362	0.499
	2	5.987	0.313	3.270	0.303	9.257	0.609
	3	23.360	1.525	19.800	0.370	43.160	1.890
1	1	41.736	0.493	39.898	1.041	81.633	1.264
	2	11.443	0.958	10.555	0.508	21.998	1.462
	3	35.800	0.610	35.362	0.510	71.162	1.119
2	1	105.471	1.598	99.143	0.316	204.614	1.811
	2	16.850	0.383	16.637	0.393	33.487	0.763
	3	35.585	0.294	35.255	0.265	70.840	0.546
4	1	193.593	4.998	164.407	4.914	358.001	9.913
	2	16.320	0.460	17.282	0.292	33.602	0.746
	3	33.021	0.551	33.290	0.616	66.311	1.059
6	1	191.461	5.592	163.552	5.712	355.013	11.304
	2	16.383	0.228	18.113	0.477	34.497	0.704
	3	32.443	0.540	32.595	0.434	65.038	0.924
24	1	189.705	8.644	161.704	6.474	351.409	15.083
	2	14.402	0.515	16.075	0.147	30.477	0.641
	3	31.092	0.795	31.625	0.566	62.717	1.348

APPENDIX 6

Values used for the graph in **Figure 25**. All values are average values based on three independent parallels. All reaction mixes also contained 1 µM *Sd*LPMO10A-1.

Reaction mix	Time (hours)	Oxidized products (µM)	Standard deviation
1mM Ascorbic acid	3	193	3.9
	6	200	4.5
	24	195	4.6
100 µM Ascorbic acid	3	68.5	0.5
	6	137.2	0.5
	24	251	4.0
100 µM Ascorbic acid + 1 µM LapA	3	6.8	0.2
	6	17.9	0.5
	24	92	1.2
100 µM Ascorbic acid + 1 µM LapB	3	4.5	0.3
	6	12	1.2
	24	67	1.3

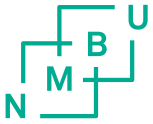

Norges miljø- og biovitenskapelige universitet
Noregs miljø- og biovitskapelege universitet
Norwegian University of Life Sciences

Postboks 5003
NO-1432 Ås
Norway